



**Eastern Nile Technical Regional Office (ENTRO)**

**Eastern Nile Climate Assessment: Rainfall Analysis**

**7<sup>th</sup> NCCR Internship Batch**

## **Theme I: Eastern Nile River Basin Rainfall Trend Analysis**

(Final Report)

Prepared By:



Rayan Hamza Elhaj



Asirat Teshome Tolosa



Lieb Gatnor Tap



Dagmawit Aman Disaso

February 13<sup>th</sup> 2024

## Contents

List of Figures .....	4
List of Tables.....	5
Executive Summary.....	6
1 Introduction .....	7
1.1 General Overview.....	7
1.2 Objectives.....	7
1.2.1 Specific Objectives .....	7
1.3 Study Area (the Eastern Nile Basin).....	8
1.3.1 Hydrology .....	8
1.3.2 Climate .....	9
1.3.3 Water Resources .....	9
1.3.4 Socio-economic indicators .....	10
2 Literature Review .....	11
2.1 Climate change impact on rainfall patterns .....	11
2.2 Rainfall Trends Analysis in the Eastern Nile Basin .....	12
2.3 Rainfall Data Types .....	13
2.3.1 Rain Gauges Stations.....	13
2.3.2 Satellite Observations .....	14
2.4 Rainfall data products.....	14
2.5 Validation and evaluation of Satellite-based rainfall products .....	20
2.5.1 Performance of satellite precipitation products in a global scale .....	20
2.5.2 Performance of satellite precipitation products in Africa (continental scale) .....	20
2.5.3 Performance of satellite precipitation products in East Africa (regional scale).....	22
2.5.4 Performance of satellite precipitation products in Eastern Nile Basin Countries....	24
2.6 Data Quality.....	26
2.6.1 Possible problems in the collected rainfall data .....	26
2.6.2 Rainfall data quality check mechanisms .....	27
2.6.3 Erroneous data correction mechanisms .....	28
3 Material and Methods .....	29
3.1 General description .....	29
3.2 Data acquisition and preprocessing .....	31

3.3	Tools and software packages.....	32
3.3.1	Q/ArcGIS .....	32
3.3.2	Climate Data Tool (CDT) .....	32
3.3.3	Programming languages .....	33
3.3.4	Easy Fit Software .....	33
3.4	Rainfall analysis steps.....	33
3.4.1	Spatial distribution .....	34
3.4.2	Box plots.....	34
3.4.3	Scatter plots .....	34
3.4.4	Rainfall trend.....	35
3.4.5	Rainfall anomalies .....	35
3.4.6	Standardized Precipitation Index (SPI).....	36
3.4.7	Rainfall distribution.....	37
3.4.8	Seasonality of rainfall.....	37
4	Results and Analysis .....	39
4.1	General description .....	39
4.1.1	Rainfall spatial distribution .....	39
4.2	Baro-Akobo-Sobat (BAS).....	40
4.2.1	Box Plots.....	40
4.2.2	Scatter Plots .....	41
4.2.3	Rainfall Trend .....	42
4.2.4	Rainfall anomalies .....	43
4.2.5	Standardized Precipitation Index (SPI).....	44
4.2.6	Rainfall frequency distribution.....	45
4.2.7	Seasonality of rainfall.....	46
4.3	Blue Nile (BN) .....	47
4.3.1	Box Plots.....	47
4.3.2	Scatter Plots .....	47
4.3.3	Rainfall Trend .....	49
4.3.4	Rainfall anomalies .....	50
4.3.5	Standardized Precipitation Index (SPI).....	51
4.3.6	Rainfall frequency distribution.....	52

4.3.7	Seasonality of rainfall.....	53
4.4	Tekeze-Setit-Atbara.....	54
4.4.1	Box Plots.....	54
4.4.2	Scatter Plots .....	54
4.4.3	Rainfall Trend .....	56
4.4.4	Rainfall anomalies.....	57
4.4.5	Standardized Precipitation Index (SPI).....	58
4.4.6	Rainfall frequency distribution.....	59
4.4.7	Seasonality of rainfall.....	60
4.5	Upper Main Nile .....	61
4.5.1	Box Plots.....	61
4.5.2	Scatter Plots .....	61
4.5.3	Rainfall Trend .....	63
4.5.4	Rainfall anomalies.....	64
4.5.5	Standardized Precipitation Index (SPI).....	65
4.5.6	Rainfall frequency distribution.....	65
4.5.7	Seasonality of rainfall.....	66
4.6	Lower Main Nile .....	67
4.6.1	Box Plots.....	67
4.6.2	Scatter Plots .....	67
4.6.3	Rainfall Trend .....	69
4.6.4	Rainfall anomalies.....	69
4.6.5	Standardized Precipitation Index (SPI).....	71
4.6.6	Rainfall frequency distribution.....	71
4.6.7	Seasonality of rainfall.....	72
5	Conclusions .....	74
6	Recommendations .....	77
7	References List .....	78

## List of Figures

Figure 1. 1 Eastern Nile Basin Subbasins (authors).....	8
Figure 3.1 Methodology flowchart	38
Figure 4.1 Spatial distribution of rainfall over the Eastern Nile Basin.....	40
Figure 4.2 Box plots of BAS subbasin .....	41
Figure 4.3 Scatter plots of BAS subbasin.....	42
Figure 4.4 Rainfall trends - BAS.....	43
Figure 4.5 Rainfall anomalies - BAS.....	44
Figure 4.6 Standardized Precipitation Index (SPI) - BAS.....	45
Figure 4.7 Rainfall distribution - BAS.....	46
Figure 4.8 Monthly rainfall - BAS .....	47
Figure 4.9 Box plots - BN.....	47
Figure 4.10 Scatter plots - BN.....	48
Figure 4.11 Rainfall trends - BN .....	50
Figure 4.12 Rainfall anomalies - BN .....	51
Figure 4.13 Standardized Precipitation Index (SPI) - BN .....	52
Figure 4.14 Rainfall distribution - BN .....	53
Figure 4.15 Monthly rainfall - BN .....	54
Figure 4.16 Box plots - TSA.....	54
Figure 4.17 Scatter plots - TSA .....	55
Figure 4.18 Rainfall trends - TSA .....	57
Figure 4.19 Rainfall anomalies - TSA.....	58
Figure 4.20 Standardized precipitation Index (SPI) - TSA.....	59
Figure 4.21 Rainfall distribution - TSA.....	60
Figure 4.22 Monthly rainfall - TSA.....	61
Figure 4.23 Box plots of Upper Main Nile subbasin .....	61
Figure 4.24 Scatter plots of UMN subbasin .....	62
Figure 4.25 Rainfall trends - UMN.....	63
Figure 4.26 Rainfall anomalies - UMN .....	64
Figure 4.27 Standardized Precipitation Index (SPI) - UMN .....	65
Figure 4.28 Rainfall distribution - UMN .....	66
Figure 4.29 Monthly rainfall - UMN .....	67
Figure 4.30 Box plots - LMN.....	67
Figure 4.31 Scatter plots - LMN.....	68
Figure 4.32 Rainfall trends – LMN.....	69
Figure 4.33 Rainfall anomalies - LMN .....	70
Figure 4.34 Standardized Precipitation Index (SPI) - LMN .....	71
Figure 4.35 Rainfall distribution - LMN .....	72
Figure 4.36 Monthly rainfall - LMN.....	73

## List of Tables

Table 2. 1 Summary of the commonly used precipitation products.....	16
Table 2. 2 Summary of the performance of satellite precipitation products in Africa .....	22
Table 2. 3 Summary of the performance satellite precipitation products in East Africa .....	23
Table 2. 4 Summary of the performance of satellite precipitation products in Countries .....	26
Table 3. 1 Summary of selected satellites characteristics.....	31
Table 3. 2 Classification of drought based on the distribution of the SPI index.....	36
Table 4.1 BAS rainfall products performance tests.....	42
Table 4. 2 BN rainfall products performance tests.....	49
Table 4. 3 TSA rainfall products performance tests .....	56
Table 4. 4 UMN rainfall products performance tests.....	63
Table 4. 5 LMN rainfall products performance tests.....	69

## Executive Summary

The Eastern Nile Basin is characterized by high variability in rainfall, and climate change is expected to increase the uncertainty, which will impact the water resources availability especially with the increasing demand. This study was designed to discuss the variation of rainfall over the Eastern Nile Basin, aiming to statistically and spatially analyzing historical rainfall data to assess the rainfall trends, considering the main subbasins of the Eastern Nile Basin; Blue Nile, Baro-Akobo-Sobat, Tekeze-Setit-Atbara, and the Main Nile.

To overcome the challenge of the scarcity of the rainfall ground observations, rainfall data was acquired from five satellite-based products; namely, CHIRPS, ARC2, PERSIANN-CDR, TAMSAT, as well as GPCC. Those products were selected according to their performance, coverage, and resolution. The historical rainfall analysis consisted of number of steps, including the data quality check and correction, spatio-temporal analysis, statistical analysis and performance testing, and rainfall trends analysis in different time scales. The analysis was conducted using a wide range of techniques, tools, and software depending on the type of the analysis and the required outcome. The main four subbasins of the eastern Nile basin were considered, with dividing the Main Nile into upper and lower subbasins as they have totally different rainfall patterns. CHIRPS was taken as a reference for comparison as it is blended with stations data and showed the best performance compared to ground observations over East Africa.

The basin was found to receive amounts of annual rainfall ranging between 0 mm rainfall at the northern part of the basin to around 1500 mm at its south-eastern area (the highlands of Ethiopia and parts of South Sudan), with differences in the spatial and temporal variations among the different rainfall products. The results of the study indicated that CHIRPS followed by TAMSAT demonstrated the best performance over the Blue Nile, Baro-Akobo-Sobat, Tekeze-Setit-Atbara, and the Upper Main Nile compared to other products. While in the Lower Main Nile, CHIRPS and GPCC can be considered the best, however, high uncertainty is observed. Results also showed that the Eastern Nile Basin have shown an increasing rainfall trend with different rates over the period 1990 – 2020.

The results of this study provide crucial information for water resources management, which directly have impacts on human socio-economic life, and environment. It can be used by different stakeholders, researchers, and policy makers to inform decision-making process.

# Introduction

## 1.1 General Overview

Climate is one of the key components in the earth's system. Many variables such as temperature, rainfall, atmospheric pressure, and humidity constitute weather and climate. Climate is usually defined as the average weather (*Panda, 2019*). In a broad sense, it is the statistical description in terms of the mean and variability of relevant quantities over a period ranging from months to thousands or millions of years. The analysis of long-term changes in climatic variables is a fundamental task in studies on climate change detection. The climate trend is the general movement of a series over an extended period, or it is the change in the dependent variable over a long period. Generally, it is determined by the relationship between the two variables and their temporal resolution, using spatial and statistical methods (*Webber and Hawkins, 1980*). Rainfall trends are considered a key factor in climate, which plays a crucial role in the water cycle that influences the availability of fresh water.

Focusing on the Eastern Nile Basin, the rainfall has a very high variability in terms of the amounts and distribution, and climate change is adding extra pressure, leading to changes in seasonal patterns, as well as the spatial and temporal distributions. This will produce higher uncertainties in the water resources management and development, as rainfall is considered an essential input for the water resources availability and distribution. On the other hand, water demand is increasing continuously in the Eastern Nile Basin as a result of the human behavior, as well as the changes in economic and social activities. This has a direct and indirect impact on water security, agriculture and food production, energy, and environment. Therefore, the need for understanding the general trends and projections of rainfall in the Eastern Nile basin is becoming more crucial, and is of paramount importance for sustainable management of water resource.

For the above-mentioned reasons, this study focuses in conducting rainfall trend analysis, to understand the historical changes in rainfall patterns and distribution, considering the Eastern Nile Basin with its four subbasins; Blue Nile, Baro-Akobo-Sobat, Tekeze-Setit-Atbara, and the Main Nile.

## 1.2 Objectives

The general objective of this report is to produce important information about rainfall trends in the Eastern Nile Basin by statistically and spatially analyzing historical rainfall data from different sources.

### 1.2.1 Specific Objectives

1. To collect and organize historical rainfall data for the Eastern Nile Basin from multiple satellite observations and country sources.
2. To conduct statistical and spatial analysis for the data showing the trends of historical rainfall over the Eastern Nile Basin.

### 1.3 Study Area (the Eastern Nile Basin)

#### 1.3.1 Hydrology

The Eastern Nile Basin (ENB) extends from 3° N to 33° N, and 26° E to 40 ° E covering an area of 1.8 million km<sup>2</sup>. It is divided into 4 subbasins in four countries; Ethiopia, Sudan, South Sudan, and Egypt. The main Nile - from the confluence of Blue Nile and White Nile in Khartoum to the Nile delta - is the largest subbasin with an area of 789,140 km<sup>2</sup> (44 % total ENB area). The second subbasin is the Baro-Akobo-Sobat-White Nile in the west, that covers an area of 460,000 km<sup>2</sup> (26 % total ENB area), with two main tributaries originating from the Ethiopian hills and the Sudd wetlands. The third subbasin with the largest contribution is the Abbay-Blue Nile on the east that originates from the highlands of Ethiopia and extends from Lake Tana until it joints the White Nile in Khartoum, covering an area of 310,000 km<sup>2</sup> (17 % total ENB area). Lastly the smallest subbasin is the Tekeze-Atbara subbasin on the east originating from the high lands of Ethiopia and covering an area of about 230,000 km<sup>2</sup> (13 % total ENB area) (*El-sheikh et al., 2017; Mersha, 2014; NBI, 2018*).

Most of the ENB is a water scarce region, with most of the Nile water generating from the Ethiopian highlands. The main Nile has a total yearly runoff of about 83.8 BCM, with contributions of about 64% (53 BCM per year) and 28% (23.6 BCM per year) by the Abbay-Blue Nile and Tekeze-Atbara subbasin respectively, which both show clear wet and dry spells as a direct response to the seasonal rain patterns (*Yitayew & Melesse, 2011*).

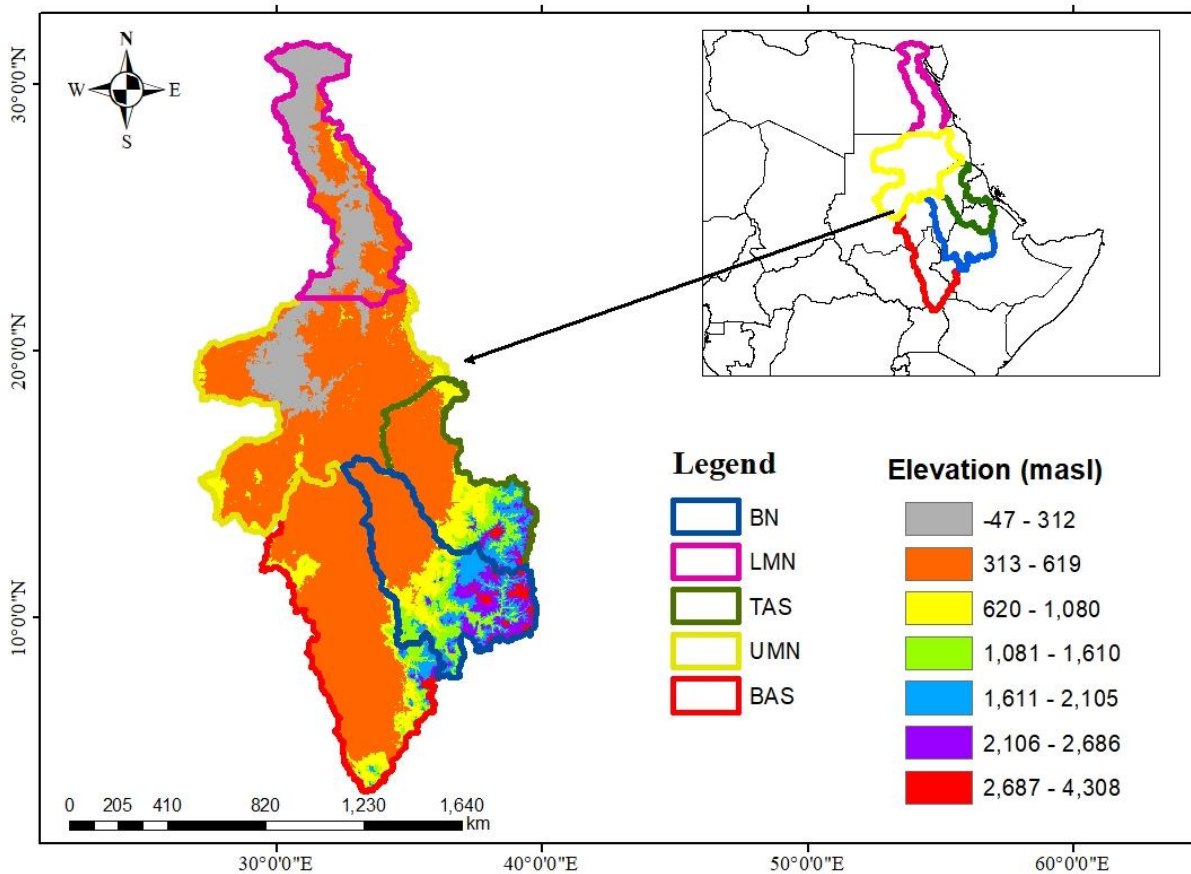


Figure 1.1 Eastern Nile Basin Subbasins (authors).

### 1.3.2 Climate

The ENB has different climates as it extends through large latitudes, with wide range of elevations. It is host of extremities, ranging from the rugged highlands of Ethiopia in the east, to the wetland areas of South Sudan and Southern Ethiopia, to the deserts of Sudan and Egypt in the north. The main Nile subbasin has a mild land slope, and a hot and arid climate with mean annual rainfall less than 200 mm in Khartoum, reducing to the north direction until reaching about 25 mm at Cairo crossing the Saharan desert, and increasing again to 200 mm at the coastal line with the Mediterranean Sea. Moreover, the subbasin is subjected to high rates of evaporation (2.6 m/year at Aswan dam), and high potential evapotranspiration (ranging between 7.8 m to 1.8 m). The Baro-Akobo-Sobat subbasin is characterized by a humid climate, and intense rainfall with spatial variation because of the elevation differences. Wet season is from May to October with the highest rainfall from June to October. The mean annual precipitation is between 3000 mm at the highlands and to 600 mm at low lands, and evapotranspiration is about 809 mm/year. Climate of the Tekeze-Atbara subbasin varies with altitude, with rainfall ranging between 1000 mm near the source at the Ethiopian highlands, to about 40 mm at the dry climate region near Atbara, Sudan. Evapotranspiration is estimated at 295 mm/year. Lastly, the Blue Nile subbasin climate ranges from temperate cool at the Ethiopian highlands to semiarid at Khartoum. The wet season (June to September) has the most rainfall, with smaller amounts occurring in the dry (October to January) and mild seasons (February to May). Rainfall ranges from 1600 mm/year to 2100 mm/year. Wide range of evaporation rates are observed in the Blue Nile basin (1500 mm/year at highlands to 6800 mm/year near Khartoum) (*Hamouda et al., 2009; Mersha, 2014*).

### 1.3.3 Water Resources

The water resources appear to be sufficient in terms of quantity and quality looking at the great potential opportunities of water, however, the Eastern Nile Basin faces many water availability and accessibility challenges, and climate change is imposing additional burden. In Ethiopia and Sudan, people suffer from the high variability of rainfall spatially and temporally, which cause drought and floods in different parts. Water accessibility is also a major problem (*Arsano & Tamrat, 2005; Hamad & El-Battahani, 2005*). Moreover, Egypt also faces challenges and limitations regarding fresh water availability with the increasing water demand, land use changes, and environmental requirements (*Abd Ellah, 2020*). Similarly, water insecurity is an existential threat in South Sudan, with a core concern of lack of access to safe drinking water supply (*Edoardo, 2023*).

In terms of water quality, the surface waters generally have acceptable chemical quality, with poor physical condition (turbidity and color) due to soil erosion, especially for the rivers originating at the Ethiopian highlands. Abbay basin is generally suitable for most uses, however, in Sudan, surveys were conducted in Khartoum area to recognize sources of pollution in the Blue and White Nile and discovered that Sudan has used pesticides in agriculture since the 1930's along with some 600 agro-chemicals, and organic pollutants are expected to be present. Exceptional high EC values were recorded near Tekeze river at Tigray region. In Egypt, water quality is one of the country most important environmental problems due to intensive agricultural and industrial activities. Number of physical and chemical characteristics of water were found to exceed acceptable range. Poor water quality was also attributed

to domestic waste and low flow conditions in parts of the subbasin (*NBI, 2005; Hydrosult et al., 2007; Merfid, 2005*).

#### 1.3.4 Socio-economic indicators

Most of the population of the Eastern Nile Basin countries fall within the basin with different percent coverage (94% for Egypt, 99% for South Sudan, 87% for Sudan, and 38% for Ethiopia). Population figures are growing rapidly and expected to reach about 305 million in 2033, which will cause tension on water supply and affect food security level. All ENB countries except Egypt are categorized as poor developing countries. Majority of population are below poverty line, and people are totally dependent on natural resources for their livelihood. Agriculture, domestic water supply, and hydropower are the main uses of EN water in the four countries, with lower uses for fisheries and industries. In Sudan and South Sudan, most of the agricultural lands fall within the ENB; 75% and 98% respectively. The percentage is around 30% in Ethiopia and Egypt. More than 5 million hectares are equipped for irrigation in Eastern Nile Basin (*ENTRO, 2018*). The high variability of rainfall poses challenges for the upstream and midstream countries of Ethiopia, South Sudan, and Sudan, as they mainly practice rain-fed agriculture. The basin has potential for the production of different crops, pastoralism, forestry, and fisheries, which can contribute to poverty reduction. Access to electricity is low in the region which hinders the economic growth. countries of the Eastern Nile basin except Egypt suffer from the non-sufficient and expensive energy supply despite of the available potential of hydropower. Only 8% of the hydropower potential is utilized, and biomass is being used instead. The population growth, urbanization, industrialization, and expansion in agriculture are exacerbating the water stress. Moreover, other political factors also have impact on the water resources development of the area (*Hamouda et al., 2009; ENTRO, 2018*).

## 2 Literature Review

### 2.1 Climate change impact on rainfall patterns

Climate change has a great impact on temperature and precipitation, which are the most important climate variables, with a direct and indirect impact on hydrology, and thus the environment and human life. Africa is one of the most vulnerable continents to climate change and climate variability, a situation aggravated by the interaction of 'multiple stresses', occurring at various levels, and low adaptive capacity (*Belay zerga, Getaneh, 2016*). Several studies on precipitation and temperature change indicated that the African continent is now warmer than it was 100 years ago, and the rainfall exhibited higher inter-annual and intra-seasonal variability. According to the Intergovernmental Panel on Climate Change (IPCC), the increase in greenhouse gases results in climate change, which in turn, leads to heavy rainfall, extreme drought, and sea level rise (*Cooper & Coe, 2011*). In the recent years the significant trend of annual rainfall increases in the Eastern Nile Basin countries more than previous years from June to September, while from March to May the rainfall trend is significantly decreasing (*Mohamed et al., 2022*).

In the Eastern Nile part of Ethiopia, the flood vulnerable areas are the flood plains at Lake Tana, the Gambella plain, and the Humera area of the Tekeze basin, as well as flash floods at different locations. In the Eastern Nile part of Republic of South Sudan, riverine floods as well as flash floods regularly affect residential area in the Akobo County and Sobat River plains. Most people there live and work in settlements in flood prone areas because their livelihoods depend mainly on farming in flood plains, fishing, and/or livestock. The Malakal town at nearby convergence of the Sobat and the White Nile River is also affected. Most floods occur annually. Estimates indicate that flash floods affect about one million people regularly. In Sudan, flood prone areas are along the Blue Nile from El Diem to Khartoum, and Gash River around Kassala City, as well as areas along the White Nile. Flash floods happen more often than riverine floods. In the previous years the flood increased in residential area along the Blue Nile, Dinder, Al-Rahad, Al-Gash and Tekeze-Atbara-Setit. The houses are in floodplains that are more defenseless to high flood impacts as well as highly vulnerable to economic, physical/ infrastructural, and attitudinal dimensions (*ENTRO, 2006*).

On the other hand, many areas of the Eastern Nile basin countries suffer from droughts. The Eastern Nile Basin part of Sudan is shifting progressively to semi-desert which located between latitude 10 – 18 N, with a low rainfall savannah in Kassala and River Nile States (Atbara River) and high rainfall savannah towards the south in Blue Nile, Senar and Gazira States, with rainfall varies from north to south about 25-700 mm between June and October, with temperatures ranging from 30-40°C in summer and 10-25°C in winter. Those areas are seriously affected by drought which affects the economic, social and environmental aspects (*National Council for Combating Desertification, 2018*). In South Sudan, the drought can be attributed to regional climate change. As the country is one of the most rapidly warming countries in the world, with temperatures increasing two and half times more than average global warming, that cause high evaporation and dry for small streams depression area and form a scarcity of water in some villages of Upper Nile State which have been wreaking to livelihoods, food security and sustainable development. (*World Bank Group.org, 2023*). In the Eastern Nile Basin part of Ethiopia, the

climate contains three seasons Short rainy season (Belg) Long rainy season (Kiremt) And dry season (Bega), In the recent years some studies identified that the annual of (Belg), and (Kiremt) precipitation over the whole of Abbay-Blue Nile Basin is significantly decreasing except (Bega) season, drought events are occurring frequently in different parts and being worsened by the anthropogenic activities that will affect the economic system and livelihood (*El-Sayed et al., 2022*).

Studies agreed on the projected increase of temperature over the Nile basin in the next century, but still the impact of climate change on precipitation anticipations is arguable. The precipitation in the Eastern Nile including Blue Nile and Tekeze-Atbara is uncertain, with possibility for reduced runoff with the increase of temperature. On the other hand, White Nile is expected to witness climate change impact on the spatial variability of water, increase of runoff due to the increase of rainfall at Lake region, effect on lake level, and moderate effect on downstream flows (*Beyene et al., 2010; Conway, 2005; Soliman et al., 2009*). Different researchers used Global Circulation Models GCMs to predict climate change. Study of *Kim & Kaluarachchi, (2009)* suggests increasing of rainfall over the mid of century at the Blue Nile. On the other hand, (*Elshamy et al., 2009*) suggests less rainfall over the Blue Nile. The projected increase in temperature and thus evaporation, is expected to decrease runoff (*Melesse, 2011*), however, High uncertainties and significant changes were found when estimating the runoff, evapotranspiration, and soil moisture based on downscaling different GCMs temperature and precipitation predictions for the Eastern Nile Basin (*Setegn et al., 2011*). Generally, the Eastern Nile basin is expected to be wetter in coming decades, with greater frequency and magnitude of extreme and localized climatic events (heavy rain events and droughts) (*Melesse, 2011*). The seasonal and spatial distribution of those climatic factors also needs to be considered to assess the risks and benefits (for example, higher precipitation in the winter at the Blue Nile have lower value as rainfed agriculture is practiced). *Soliman, (2009)* suggests similar future annual flow for the Blue Nile with changes in seasonality and spatial variability (higher discharge at wet season and reduced discharge through the dry season).

The above-mentioned changes may have potential benefits in some parts of the basin; however, it causes higher uncertainties on water availability, which negatively affects agricultural production and food security, threatens the environment, biodiversity, and health, affect energy production, and results in a socioeconomic problem (*Asfaw et al., 2018; IPCC, 2008*).

## 2.2 Rainfall Trends Analysis in the Eastern Nile Basin

According to *Onyutha et al., (2016)*, the precipitation trends in 39 locations in the Nile River Basin (NRB) were carried out, so in the equatorial region, the annual precipitation trend was found mainly positive with a significant level of  $\alpha = 5\%$  in 4 of the 7 stations. This study reveals that the annual trend analysis for Sudan, Ethiopia and Egypt was negative with a significant level of  $\alpha = 5\%$  in 69% of the 32 stations. The monthly, seasonal, and annual rainfall intensities were considered for trend analysis and the missing values were filled using the IDW interpolation techniques. Moreover, FAOCLIM contains monthly worldwide agro-climatic data for 28,100 stations with up to 14 observed and computed agro-climatic variables. In the Blue Nile basin, previous trend analyses based on short-term annual rainfall from a few

meteorological stations have been mostly limited to sub-basins. The form of trend analyzed in the rainfall of the study area seems to have mostly been rather decadal or multi-decadal variability than a long-term trend (*Taye & Willems, 2012*).

In addition to climate factors, land use land cover changes in water abstraction and watershed management practices alter the hydrological characteristics of a river basin and consequently the extreme flows. According to *Melese et al. (2010)*, the upper Blue Nile basin has experienced environmental and natural resource degradation attributed to both anthropogenic and climatic factors. To understand the influence of these factors on extreme river flows, it is important to go back to historical records and evaluate the temporal variability of extreme flows. Studying the temporal variability of extreme flows will also be useful to understand whether extreme events have become more frequent or more intense in recent years. The limitation of the study conducted by *Onyutha & Willems, (2015); Taye & Willems, (2012)* in the Nile basin analyzed the trend and variability using MK test and quantile disturbance method (QPM). The study did not cover enough locations of all the Nile Basin Riparian countries because they analyzed variability using QPM which directly takes into account rainfall intensity (without rescaling), thus making the method susceptible to possible exaggeration of anomalies in the event of the existence of an outlier. *Onyutha et al., (2016)* analyzed the variability in all countries bordering the Nile basin using the nonparametric anomaly indicator method (NAIM). The difference between QPM and NAIM is that QPM analyses variability in terms of frequency of extreme events and extreme precipitation disturbance, while NAIM calculates anomalies in the series after applying temporal convolution to the non-parametrically resized dataset.

### 2.3 Rainfall Data Types

As precipitation trends analysis is essential ranging from climate monitoring to water resources management, agriculture, and hydrological forecasting, especially with the high spatial and temporal variability, long records of data are required. Precipitation data can be acquired either from ground stations, spatial measure of precipitation through weather radars, or from satellite observations (*Kidd & Huffman, 2011; Sarojini et al., 2016*).

#### 2.3.1 Rain Gauges Stations

The rainfall direct measurements that can be obtained from surface gauge networks have limitations regarding the coverage of land and oceans areas. Point precipitation in the form of depth overtime is directly assessed using different gauges such as accumulation gauges, tipping-bucket gauges, weighing gauges, and optical gauges. Each of these types has its strengths and weaknesses (*Sun et al., 2018*). Generally, the ground stations gauges are highly affected by environmental complications and different sources of error, namely; evaporation, wind, gauge location, instrument reading error, and the spatiotemporal variation in drop-size distribution (*Michelson, 2004*). More sophisticated weather radars have been developed and used to improve the measurements of precipitation, its composition, and the potential physical processes underlying its formation. The radars can detect real-time raindrops as well as measuring the drop-size distribution, which means providing a three-dimensional structure of rainfall. Similar to rain gauges, weather radars are also limited in extent and number. The lack of accessibility and

funding has limited the development of a global radar network (*Habib, Haile, et al., 2012; Kidd & Huffman, 2011*). Quantifying rainfall represents a major challenge especially in Africa, where rain-gauge networks are poorly distributed (*Awange et al., 2016*).

### 2.3.2 Satellite Observations

On the other hand, the satellite observations provide unparalleled advantage of detecting precipitation on a global scale in the shape of temporal and spatial samples which correspond with precipitation characteristics. In recent decades, a wide range of satellite-based precipitation datasets with good spatial and temporal resolutions have become accessible (*Awange et al., 2016*). These satellite-related data sets have inherent uncertainties and limitations of their short length of record, but they still provide valuable and important information for the weather process, drought, and hydrological monitoring. Precipitation products are either IR based; i.e., derived from the geostationary satellites using Thermal Infrared (IR) sensors, with high temporal resolution, or MW based, i.e., derived from the low earth orbiting satellite using passive and active Microwave (MW) sensors, with better accuracy. Some products use both techniques to combine the advantages (*Kidd & Huffman, 2011; Sun et al., 2018*).

Different types of global precipitation data sets are available, including the gauge-based, the satellite-based, and the reanalysis data sets. Some data sets, especially the gauge-based data sets and reanalysis, are generally provided long-term records of precipitation, which are suitable for climate studies. The description of these types is as follows:

## 2.4 Rainfall data products

### I. Gauge-based products

These products were established through transformation of ground stations data into grid based. several gridded data were developed and used. For example, the Global Precipitation Climatology Centre (GPCC) developed a strong dataset based on the National Meteorological Organizations from 158 nations and 31 regional suppliers (*Becker et al., 2013*). Another dataset is the Climatic Research Unit gridded Time Series (CRU TS) that considered observations from 1961 to 2018, and provides a monthly grid with high resolution (*Harris et al., 2020*). Moreover, the Climate Prediction Center (CPC) launched different gauge-based products which consist of observations from 30,000 ground stations (*Sun et al., 2018*). Description of number of these products is illustrated in Table 2. 1 below.

### II. Satellite-based products

These products depend mainly on the Thermal Infrared sensors or the Micro-wave sensors in detecting the precipitation. Large number products were established and widely used. As example for number of the widely used products, the TRMM datasets (TRMM 3B42 and TRMM 3B43) which include estimates from different satellites, are the most extensively used products. It investigates the climatological distribution of rainfall and its frequency and intensity. However, there is inhomogeneity in the temporal records exist, with underestimation of precipitation in regions of intense convection overland and high latitudes (*Liu et al., 2012*). As continuation for TRMM, the Global Precipitation Measurement (GPM) products were developed. The last product of GPM is IMERG6, that merge rainfall data of different satellite based and gauge calibrated products (*Nasa, 2022*).

Number of satellite rainfall products were then established and widely used such as PERSIANN, CMAP 20, CPCP and CPCP 1dd (*Huffman et al., 2001*). PERSIANN-CDR is one of the important products that have been commonly used globally as it has high resolution and consistency in long-term records (*Ashouri, 2015*). Moreover, the Climate Hazards Group developed the CHIRPS satellite datasets that have become widely used. It creates gridded rainfall time series for trend analysis and seasonal monitoring high resolution (*Katsanos et al., 2016*). Additionally, the Africa Rainfall Climatology established an algorithm (ARC2 RFE2.0) that provide daily precipitation estimations over Africa at high spatial resolution (*Novella & Thiaw, 2013*). Overview and description of number satellite rainfall products that have been used in the Eastern Nile Basin area is illustrated in Table 2. 1 below.

### III. Reanalysis products

The reanalysis products are developed by reprocessing and merging irregular climate observations and models and models that encompass many physical and dynamical processes using modern forecasting/mathematical simulation systems in order to generate uniform gridded synthesized multidecadal datasets, and create a stable data system with spatial homogeneity and temporal continuity. Those products have limitations depending on the time period and location (*Sun et al., 2018; National center for atmospheric research, 2016*). Different reanalysis products were developed and being used with improving quality such as the NCEP1/NCEP2 and the two European Centre for Medium-Range Weather Forecasts (ECMWF) (ERA-40 and ERA-Interim) reanalysis systems (*Sun et al., 2018*). The NCEP2 was produced as an updated version of NCEP, nevertheless, almost similar performance for the two products was found by different researches (*Kanamitsu et al., 2002*). Furthermore, the performance of ERA-40 and ERA-Interim was also evaluated. ERA-40 was found to overestimate the precipitation of the tropical oceans (*Uppala et al., 2005*), while ERA-Interim showed less precipitation compared to ground observations (*Dee et al., 2011*). Other datasets were produced more recently such as the Twentieth Century Reanalysis system (20CRv2), the NCEP Climate Forecast System Reanalysis system (CFSR), the Modern-Era Retrospective Analysis for Research and Application system (MERRA), and the Japanese 55-year Reanalysis (JRA-55), with more advanced models and higher spatial resolution (*Sun et al., 2018*). Those products have limitations depending on the time period and location (*National center for atmospheric research, 2016*). The reanalysis precipitation datasets showed overestimated rainfall than the satellite-based products especially over tropical regions, and at high elevations over global lands compared to ground observations, with higher inconsistencies in arid and semiarid regions (*Pfeifroth et al., 2013; Hu et al., 2016; Cattani et al., 2016; Dinku et al., 2011*). However, CFSR because of its fine resolution, was able to reproduce the regional pattern, mean, and variability of rainfall in Africa (*Zhang et al., 2013*). Table 2. 1 below summarize the commonly used precipitation products focusing on datasets which previously used in the Eastern Nile Basin.

Table 2. 1 Summary of the commonly used precipitation products

Dataset Name		Data Provider	Data Input	Record Length	Spatial Coverage	Spatial Resolution	Temporal Resolution	Reference
	Full Name							
1	Climate Hazards Group InfraRed Precipitation with Station data	Climate Hazards Center	Satellite and gauge data	1981-present	50°S - 50°N	0.05° (5.5 km)	Daily, Monthly, and Annual	<a href="https://www.chc.ucsb.edu/data/chirps">https://www.chc.ucsb.edu/data/chirps</a> .
2	Tropical Applications of Meteorology using Satellite data	IGAD Climate Prediction and Application Centre	Satellite data	1983-present	Eastern Africa	4 km	Daily, 10-day, and monthly	<a href="https://www.icpac.net/data-center">https://www.icpac.net/data-center</a> .
3	Tropical Rainfall Measuring Mission 3B42/3B43	NASA and Japan's National Space Development Agency	Satellite data	1998-2014	50°N to 50°S	0.25° (27 km)	3-hourly and monthly	<a href="https://climatedataguide.ucar.edu/climate-data/trmm-tropical-rainfall-measuring-mission">https://climatedataguide.ucar.edu/climate-data/trmm-tropical-rainfall-measuring-mission</a> .
4	Global Precipitation Measurement	NASA	Satellite data	2014-present	60°N-60°S	0.1° (11 km) °	30-minute and monthly	<a href="https://gpm.nasa.gov/missions/GPM">https://gpm.nasa.gov/missions/GPM</a> .
5	Integrated Multi-satellite Retrievals for GPM	NASA	Multiple satellites data	2000-present	60°N-60°S	0.1° (11 km) °	30-minute and monthly	<a href="https://gpm.nasa.gov/data/imerg">https://gpm.nasa.gov/data/imerg</a> .
6	Integrated Multi-satellite Retrievals for GPM Gauge-Calibrated	NASA	Satellite and gauge data	2000-present	60°N-60°S	0.1° (11 km) °	30-minute and monthly	<a href="https://gpm.nasa.gov/data/imerg">https://gpm.nasa.gov/data/imerg</a> .
7	Global Satellite Mapping of Precipitation	JAXA (Japan Aerospace Exploration Agency)	Satellite data	2000-present	60°S to 90°N	0.1° (11 km) °	Hourly and daily	<a href="https://developers.google.com/earth-engine/datasets">https://developers.google.com/earth-engine/datasets</a> .
8	Global Satellite Mapping of Precipitation Gauge-Calibrated)	JAXA (Japan Aerospace Exploration Agency)	Satellite and gauge data	1998-to Present	60°N-90°N	0.1° (11 km) °	1 hour, but updated half-hourly	<a href="https://www.sciencedirect.com/science/article/pii/S1878029611005494">https://www.sciencedirect.com/science/article/pii/S1878029611005494</a> .

9	Climate Prediction Center Morphing technique	CMORPH	Center for Environmental Data Analysis	Satellite data	2002 - 2017	60S-60N	0.25 degrees (27 km)	30-minute and daily	<a href="https://catalogue.ceda.ac.uk/uuid/">https://catalogue.ceda.ac.uk/uuid/</a>
10	African Rainfall Climatology Version 2	ARC2	IGAD Climate Prediction and Application Centre	Satellite and gauge data	1983-Present	Eastern Africa	0.1° (11 km) °	Daily, 10 Days, and Monthly	<a href="https://www.icpac.net/data-center/arc2/">https://www.icpac.net/data-center/arc2/</a>
11	Precipitation Estimation from Remotely Sensed Information using Artificial Neural Networks	RERSIANN	Center for Hydrometeorology and Remote Sensing (CHRS), University of California, Irvine	Satellite data	2000 - Present	60°S to 60°N	0.25 degrees (27 km)	Hourly, daily, monthly & yearly	<a href="https://climatedataguide.ucar.edu/climate-data/persiann-cdr-precipitation-estimation-remotely-sensed-information-using-artificial">https://climatedataguide.ucar.edu/climate-data/persiann-cdr-precipitation-estimation-remotely-sensed-information-using-artificial</a>
12	Real-time Enhanced Regional Scale Imaging Actively Sensed Information and Numerical Weather Prediction–Climate Change Scenario	RERSIANN-CCS	Center for Hydrometeorology and Remote Sensing (CHRS), University of California, Irvine	Satellite data	2003-present	60°S to 60°N	0.25 degrees (27 km)	Hourly, 3-hourly, 6-hourly, daily, monthly, yearly	<a href="ftp://persiann.eng.uci.edu/CHRSdata/PERSIANN-CCS">ftp://persiann.eng.uci.edu/CHRSdata/PERSIANN-CCS</a>
13	Precipitation Estimation from Remotely Sensed Information using Artificial Neural Networks–Climate Data Record	PERSIANN-CDR	Center for Hydrometeorology and Remote Sensing (CHRS), University of California, Irvine	Satellite and gauge data	1983-2021	60S - 60N	0.25 degrees (27 km)	Daily, monthly, yearly	<a href="https://climatedataguide.ucar.edu/climate-data/persiann-cdr-precipitation-estimation-remotely-sensed-information-using-artificial">https://climatedataguide.ucar.edu/climate-data/persiann-cdr-precipitation-estimation-remotely-sensed-information-using-artificial</a>

14	Precipitation Estimation from Remotely Sensed Information using Artificial Neural Networks - Dynamic Infrared Rain Rate near real-time	PERSIANN-PDIR-Now	Center for Hydrometeorology and Remote Sensing (CHRS), University of California, Irvine	Satellite data	2000 - Present	60°S to 60°N	0.04° (4.5 km)	Hourly, 3,6-hourly, daily, monthly, yearly	<a href="ftp://persiann.eng.uci.edu/CHRSdata/PDIRNow">ftp://persiann.eng.uci.edu/CHRSdata/PDIRNow</a>
15	Precipitation Estimation from Remotely Sensed Information using Artificial Neural Networks-Cloud Classification System-Climate Data Record	PERSIANN-CCS-CDR	Center for Hydrometeorology and Remote Sensing (CHRS), University of California, Irvine	Satellite and gauge data	1983 - Present	60°S to 60°N	0.04° (4.5 km)	hourly, daily, monthly, yearly	<a href="https://climatedataguide.ucar.edu/climate-data/persiann-cdr-precipitation-estimation-remotely-sensed-information-using-artificial">https://climatedataguide.ucar.edu/climate-data/persiann-cdr-precipitation-estimation-remotely-sensed-information-using-artificial</a>
16	NOAA Climate Prediction Center	NOAA CPC	NOAA (Physical Science Laboratory)	Satellite Data and gauge data	1948 - 2022	20.125N-49.875N, 230.125E-304.875E	0.25° (27 km)	Daily	<a href="https://psl.noaa.gov/data/gridded/data.unified.daily.conus.html">https://psl.noaa.gov/data/gridded/data.unified.daily.conus.html</a>
17	Global Precipitation Climatology Project	NOAA GPCP	National Center for Environmental Information	Satellite and gauge data	1979-present	60 S - 60 N	2.5 degrees (310 km)	Monthly	<a href="https://www.ncdc.noaa.gov/cdr/atmospheric/precipitation-gpcp-monthly">https://www.ncdc.noaa.gov/cdr/atmospheric/precipitation-gpcp-monthly</a>
18	Global Precipitation Climatology Centre	GPCC	NOAA (Physical Science Laboratory)	Gauge data	1891-present	90.0N - 90.0S	0.25 (27) and 0.1° (11 km) °	Daily and monthly	<a href="https://psl.noaa.gov/data/gridded/data.gpcc.html">https://psl.noaa.gov/data/gridded/data.gpcc.html</a>
19	Multi-Source Weighted-Ensemble Precipitation	MSWEP v2.2, v2.8	gloh20	Satellite and reanalysis data	1979 - present	at equator	0.1° (11 km) °	Monthly	<a href="https://www.gloh2o.org/mswep">https://www.gloh2o.org/mswep</a>
20	Tropical Rainfall Measuring Mission Multi-Satellite Precipitation Analysis	TMPA	EARTHDATA GES DISC	Satellite Data	1998 - 2019	50°N to 50°S	0.25 degrees (27 km)	Daily	<a href="https://disc.gsfc.nasa.gov/datasets/TRMM_3B42_Daily_7/summary">https://disc.gsfc.nasa.gov/datasets/TRMM_3B42_Daily_7/summary</a>

21	TAMSAT African Rainfall Climatology and Time series	TARCAT		Satellite and ground Data	1983 - present	Africa	4km	Decadal	<a href="http://www.met.reading.ac.uk/~tamsat/data">http://www.met.reading.ac.uk/~tamsat/data</a> .
22	Merged Analysis of Precipitation	CMAP	NOAA (Physical Science Laboratory)	Satellite and gauge data	1979 - present	88.75N - 88.75S	2.5° (270 km)	Monthly	<a href="https://psl.noaa.gov/data/gridded/data.cmap.html">https://psl.noaa.gov/data/gridded/data.cmap.html</a>

## 2.5 Validation and evaluation of Satellite-based rainfall products

Different satellite precipitation products have been launched and widely used in numerous studies and applications in assessing climate variability and climate change (*Gehne et al., 2016; Huffman et al., 2001*). Most of these products have been evaluated to assess their limitations and uncertainties. The performance of many satellite datasets has been validated at different spatiotemporal scales. The estimated precipitation was not completely consistent, and this can be attributed to their different sources, quality control schemes, and estimation methods. With the research and development, satellite rainfall data products' accuracy and resolution are increasing, and reached a good level of maturity (*Adler et al., 2003; Feidas et al., 2005; Kidd & Huffman, 2011; Sun et al., 2018*). The following section shows overview of important previous studies that focus on evaluating the performance of satellite precipitation products at different scales.

### 2.5.1 Performance of satellite precipitation products in a global scale

Many researchers have compared global precipitation products in their studies. For example, *Kidd & Huffman, (2011)* provided an overview of the global satellite precipitation observations starting from the basis of satellite systems, the production, availability and validation of these rainfall datasets. More recently, *Gehne et al., (2016)* studied the characteristics of precipitation from 11 products (three global high-resolution precipitation products (HRPPs), four global climate data records (CDRs), and four reanalysis products) with at least daily temporal resolution. Furthermore, *Herold et al., (2017)* assessed five commonly used satellite precipitation products, namely; CHIRPS, GPCC, TRMM T3B42v7, PERSIANN-CDR, GPCP-1D. He explored the uncertainties in the daily observed precipitation extremes over 50°S–50°N. Lately, *Sun et al., (2018)* provided a comprehensive review of 30 available global precipitation products including gauge-based, satellite related, and reanalysis data sets. He evaluated 22 monthly or daily precipitation products with spatial resolutions varying from 0.04° to 2.5°. These include gauge-based products (CRU, GPCC, GPCC-daily, PRECL, UDEL, and CPC-Global), satellite-related products, (PERSIANN-CCS, PERSIANN-CDR, CMORPH, TRMM 3B43, TRMM 3B42 GPCP, GPCP 1dd, CMAP, and MSWEP), and reanalysis products (NCEP1, NCEP2, ERA-Interim, 20CRv2, JRA-55, MERRA, and CFSR). Differences and discrepancies in magnitude and variability at annual, seasonal, and daily timescales were found. Similarly, variations were also found in precipitation estimates by region. The author attributed the reliability of the different datasets to the number and the spatial coverage of the surface stations, the satellite algorithms, and the data assimilation models.

### 2.5.2 Performance of satellite precipitation products in Africa (continental scale)

Number of researchers have studied and evaluated the commonly used satellite precipitation products in Africa. For mentioning some of the finding of relatively recent products, *Awange et al., (2016)* evaluated number of six widely used satellite-based rainfall datasets (PERSIANN, ARC2, TRMM, CMORPH, TAMSAT, and GSMaP) with monthly time scales over Africa between 2003 and

2010. Global Precipitation Climatology Centre (GPCC) and RG observations over the Greater Horn of Africa (GHA) data were used for the validation. PERSIANN dataset was found to be the most suitable over most of Africa, followed by ARC2, TRMM, CMORPH, TAMSAT, and GSMaP. In terms of the spatio-temporal variability of rainfall over Africa, patterns of GPCC, TRMM, PERSIANN, and ARC2 were found to be similar but different from those of TAMSAT, CMORPH, and GSMaP. CMORPH appeared to be the most suitable product in the Great Horn of Africa, consistent with previous studies. In the same year, [Serrat-Capdevila et al., \(2016\)](#) evaluated the daily estimates of the TRMM, TMPA, PERSIANN, and CMORPH rainfall datasets over Africa for years 2001 – 2013. The author considered the Global Precipitation Climatology Project one Degree Day (GPCP-1dd) dataset as reference for the comparison. The study showed that the raw estimates of TMPA show higher efficiency. PERSIANN was successful in correctly capturing precipitation events, in agreement with the previously mentioned study. The areas that follow the position of the ITCZ oscillating seasonally over the equator showed relatively better performance demonstrating good match between satellite estimates and rainfall regime.

[Maidment et al., \(2017\)](#) conducted research that assessed the performance of the daily rainfall products; TAMSAT v2 and TAMSAT v3 between 1983 to 2017, by the disaggregation of 10-day (v2) and 5-day (v3) total rainfall estimates to a daily time-step. Ground observation from Mozambique, Niger, Nigeria, Uganda, and Zambia (different climates) were used for comparison. TAMSAT products were not able to accurately detect rainfall amounts, but they showed better reliability in capturing rainy days.

More recently, [Cattani et al., \(2021\)](#) assessed the capability of TAMSAT v3 and CHIRPS (daily satellite-based products), as well as MSWEP v2.2 (merge satellite-based, gauge, and reanalysis datasets) considering the period 1983 – 2017, without rain-gauge validation. Except the complex mountainous and coastal areas, the 3 products were found to show similar performance, with increasing agreement over time, and more stable ability to detect rainy days and daily rainfall amounts. [Macharia et al., \(2022\)](#) evaluated the performance of 3 gauge-calibrated satellite rainfall products (CHIRPS, TAMSAT, and GSMaP\_wGauge), as well as 1 satellite-only rainfall product (GSMaP) over Africa. He used 3 years of rainfall data acquired from 596 stations operated by the Trans-African Hydrometeorological Observatory (TAHMO). For the daily mean rainfall over Africa, GSMaP was found to score higher detection of events compared to CHIRPS and TAMSAT. CHIRPS produced the highest monthly biases in East Africa, TAMSAT in southern Africa, and GSMaP in West Africa. In seasonal rainfall, satellite datasets showed significant biases. GSMaP produced better results at different time scales.

Lastly, [Mekonnen et al., \(2023\)](#) conducted a recent study for evaluating the accuracy of 8 gauge\_corrected satellite rainfall datasets (RFE v2.0, ARC v2.0, MSWEP v2.8, TAMSATv3.1, PERSIANN-CDR ERA 5, and CHIRPS) across Africa at number of spatial and temporal scales. This study provides useful perceptions for selecting suitable satellite based precipitation datasets for

the regional or continental applications. Performance of the different products was compared to ground observations between 2001 to 2020. For temporal timescales, the study showed that generally all products performed poorly at daily timescale, while RFE v2.0, ARC v2.0, and MSWEP v2.8 were found to be reliable at the monthly and annual timescales. Comparatively, TAMSATv3.1, PERSIANN-CDR, and ERA 5 performed poorly in detecting in situ observations. On spatial different scales, IMERG-F v6B and RFE v2.0 showed higher reliability in capturing heavy rainfall events, while ARC v2.0 and CHIRPS v2.0 were successful in detecting the dry events (droughts). Generally, on regional scale, the performance of MSWEP v2.8, RFE v2.0, ARC v2.0, and CHIRPS v2.0 was better in Northern Africa, Western and Southern, Central Africa, and Eastern Africa respectively at monthly timescale. Table 2. 2 below summarize the findings of the above-mentioned studies.

Table 2. 2 Summary of the performance of satellite precipitation products in Africa (continental scale)

Satellites	Best Performance	Study
PERSIANN, ARCV2, TRMM, CMORPH, TAMSAT, and GSMaP, GPCC	PERSIANN: overmost Africa, CMORPH: over GHA	<a href="#">Awange et al., (2016)</a>
TRMM, TMPA, PERSIANN, and CMORPH	PERSIANN and TMPA	<a href="#">Serrat-Capdevila et al., (2016)</a>
TAMSAT v2 and TAMSAT v3	None	<a href="#">Maidment et al., (2017)</a>
TAMSAT v3 and CHIRPS (daily satellite-based products), as well as MSWEP v2.2	All are good, and better in detecting rainy days and daily amounts	<a href="#">Cattani et al., (2021)</a>
CHIRPS, TAMSAT, and GSMaP_wGauge, GSMaP	GSMaP	<a href="#">Macharia et al., (2022)</a>
RFE v2.0, ARC v2.0, MSWEP v2.8, TAMSATv3.1, PERSIANN-CDR ERA 5, and CHIRPS	Complex results, CHIRPS was good in East Africa	<a href="#">Mekonnen et al., (2023)</a>

### 2.5.3 Performance of satellite precipitation products in East Africa (regional scale)

East Africa has different climates varies from wet coastal and mountainous regions, to dry arid regions([Dinku et al., 2011](#)). Going more specifically with the study objective, the following section provides an overview for some of the researches conducted in East Africa focusing on evaluating and validating number of satellite rainfall products. Starting from [Dinku et al., \(2007\)](#), the author evaluated the performance of 3 low spatial and temporal resolution (GPCP, CMAP, and TRMM-3B43), and 5 high spatial and temporal resolution (NOAA-CPC African rainfall estimation algorithm, GPCP one degree daily 1DD, TRMM-3B42, TAMSAT, and CMORPH). Within east africa, where elevation varies from below sea level to 4620 m. TRMM-3B43 and CMAP from the first group and CMORPH, TAMSAT and TRMM-3B42 from the second group appeared to have the best performance. Moreover, [Dinku et al., \(2011\)](#) continued his work by focusing on exploring the

performance of AR2C, CMORPH, and TRMM 3B42 satellite precipitation data sets on the mountainous climate at Ethiopian highlands, and the arid region over Somalia, Djibouti, and parts of Ethiopia. The author recommended calibrating the satellite algorithms with rain-gauge observations as the results showed underestimation of rainfall over the highlands of Ethiopia, while the overestimation over the dry region. Later, [Habib, et al., \(2012\)](#) focused on comparing the performance of the TMPA 3B42 and CMORPH satellite rainfall products over the Nile Basin in Eastern Africa. The results showed the success of the two datasets in capturing some of the region-specific rainfall patterns over the Nile Basin, with substantial underestimation and overestimation by TMPA and CMORPH respectively. The performance is better over the equatorial region.

More recently, [Cattani et al., \(2016\)](#) used the Global Precipitation Climatology Centre (GPCC) climatological gauge monthly data as reference to evaluate the performance of 6 satellite rainfall products (CPC RFE, CMORPH, GSMaP, TMPA 3B42, PERSIANN, TAMSAT TARCAT) over East Africa for the years 2001– 2009. The satellites’ datasets succeeded in reproducing the seasonality, except for the mountainous regions. TMPA 3B42 showed the best performance, however, some of the products were bias corrected. Furthermore, the study of [Kimani et al., \(2017\)](#) which was conducted over East Africa considering 7 satellite rainfall datasets (TAMSAT, TARCAT, CHIRPS, CMORPH, PERSIANN-CDR, CMAP, and GPCP), for the years 1998 – 2012 at monthly and yearly timescales, revealed that the above-mentioned products are successful in replicating the rainfall patterns, except for the high rainfall amounts from the orographic types (elevation of 2500 and above). However, CMORPH, CHIRPS, and TRMM performed well, with TRMM showing the best comparatively the best performance. Table 2. 3 summarize the findings of the above-mentioned studies.

*Table 2. 3 Summary of the performance satellite precipitation products in East Africa (regional scale)*

<b>Satellites</b>	<b>Best Performance</b>	<b>Study</b>
GPCP, CMAP, and TRMM-3B43), GPCP, TRMM-3B42, TAMSAT, and CMORPH	TRMM-3B43, CMAP, CMORPH, TAMSAT and TRMM-3B42	<a href="#">Dinku et al., (2007)</a>
AR2C, CMORPH, and TRMM 3B42	None	<a href="#">Dinku et al., (2011)</a>
TMPA 3B42 and CMORPH	Both over equatorial region only	<a href="#">Habib, et al., (2012)</a>
(CPC RFE, CMORPH, GSMaP, TMPA 3B42, PERSIANN, TAMSAT TARCAT)	TMPA 3B42	<a href="#">Cattani et al., (2016)</a>
TAMSAT, TARCAT, CHIRPS, CMORPH, PERSIANN-CDR, CMAP, and GPCP	TRMM, CHIRPS, and CMORPH. TRMM is the best	<a href="#">Kimani et al., (2017)</a>

2.5.4 Performance of satellite precipitation products in Eastern Nile Basin Countries (local scale)  
Number of studies were conducted in the 4 Eastern Nile Basin countries to assess the reliability of satellite precipitation products, most of them were in Ethiopia, with fewer number in the rest 3 countries Egypt, Sudan, and South Sudan. The findings of number of them are reviewed in the following section.

### I. Egypt

In Egypt, *Nashwan et al., (2019)* explored the capability of the high resolution precipitation products, GSMaP, IMERG, and CHIRPS, in detecting and estimating the daily rainfall amounts for the period March 2014 to May 2018. The results indicated that, generally, CHIRPS succeeded in detecting the amount of rainfall, and IMERG showed the worst performance. However, IMERG was able to detect the occurrence of rainfall better, with showing the spatial variability of rainfall during flood caused by heavy rain event.

Another study was conducted by *Nashwan et al., (2020)* in which the performance of 5 high resolution satellite\_gauge calibrated rainfall datasets in the arid region evaluated, namely; ARC2, CHIRPSv2, GSMaPv6, TAMSATv3 and PERSIANN-CCS. The comparison was conducted against rain-gauge observations for the years 2003 - 2018. The results of the study showed that all datasets performed poorly in detecting rainfall, with better performance of CHIRPS in capturing dry days (rainfall < 1 mm/day) - which is similar to the previously mentioned study (*Nashwan et al., 2019*) -, and better performance of ARC and GSMaP in estimating higher intensities (rainfall  $\geq$  1 mm/day), however, high number of false detections was observed. Comparatively, TAMSAT appeared to have the worst performance among the group, while GSMaP recorded the best performance in the arid area of Egypt.

More recently, *Roushdi, (2020)* evaluated 12 satellite rainfall datasets (TRMM, ARC, RFE, Chirps, CMORPH, CPC, CRU, GPCC, GPCP\_1DD, GPCP, PERSIANN and TAMSAT), in 8 locations in Egypt for 18 years. Ground stations records (annual and monthly) were considered for comparison. The performance of RFE, GPCC, CPC, and CHIRPS were found to have better at different locations compared to the other datasets. Lately, *Gado, (2023)* published a study that focus on exploring the reliability of 4 commonly used satellites; namely, PERSIANN-CDR, TRMM3B42v7, IMERG-F, GSMaP\_Gauge compared to 23 ground observations stations. GSMaP-Gauge showed a substantial ability in capturing the occurrence and estimating the amount of rainfall.

### II. Sudan

The TRMM 3B42v7 and CHIRPS were evaluated by *Abdelmoneim et al., (2020)* over the Blue Nile Basin in Sudan using daily and monthly records at Khartoum and Eldeim station for the years 1998 – 2007. Both products showed good agreement compared to ground stations observations.

Moreover, TRMM 3B42V7 outperforms CHIRPS in detecting rainfall events. Moreover, [Abd Elhamid et al., \(2020\)](#) assessed the performance of TRMM and RFE rainfall products in using ground gauge based rainfall measurements along the Blue Nile River sub-basin in Sudan for the years 2001– 2016. Both products performed well.

### III. South Sudan

[Basheer & Elagib, \(2019\)](#) explored the performance of GPCC 7.0, CHIRPS, PERSIANN-CDR, ARC2, and MSWEP 2.0 satellite rainfall products. These products were compared to the records of 5 ground stations for the years 1983 – 2010. GPCC 7.0 showed the best performance on monthly and annual scales, followed by CHIRPS. Also, GPCC 7.0 and then PERSIANN-CDR outperforms with regards to detecting the annual rainfall. The monthly variability was detected similarly by GPCC 7.0 and MSWEP 2.0, while ARC2 followed by GPCC 7.0 succeeded in detecting the maximum monthly precipitation.

### IV. Ethiopia

Large number of studies which validated and evaluated the performance of the rainfall satellite datasets were conducted in different Ethiopian regions. Here we focus on the Upper Blue Nile. In Upper Blue Nile region, [Ayehu et al., \(2018\)](#) and [Belete et al., \(2020\)](#) conducted studies in which the performance of CHIRPS, TAMSAT 3, and ARC2 for the period 2000 – 2012, and the CHIRPS, TAMSAT v2 and v3, and TRMM 3B43v7 were assessed respectively. In both studies, CHIRPS exhibited the best performance in rainfall detection regardless of elevation, followed by TAMSAT. ARC2 showed poor performance, while TRMM 3B43v7 performed well over mountainous areas. Moreover, [Abdelwares et al., \(2020\)](#) compared TRMM, CRU, and GPCC datasets to ground stations records, at which the GPCC exhibited to have the closest agreement and best performance with ground readings, followed by TRMM, while CRU showed poor agreement with gauge observations. Lastly, [Lakew et al., \(2020\)](#) evaluated 5 products (CMORPH, TRMM 3B42v7, TMPA, ERA-Interim, GPCC, MSWEP) between 2000 and 2012, in which the MSWEP showed the best performance. Table 2. 4 summarize the findings of the above-mentioned studies.

Table 2. 4 Summary of the performance of satellite precipitation products in Eastern Nile Basin Countries (local scale)

Location	Satellites	Best Performance	Study
Egypt	GSMaP, IMERG, and CHIRPS	CHIRPS	<i>Nashwan et al., (2019)</i>
	ARC2, CHIRPS v2.0, GSMaP (v. 6), TAMSAT (v. 3) and PERSIANN-CCS	Generally GSMaP, and CHIRPS for dry events	<i>Nashwan et al., (2020)</i>
	TRMM, ARC, RFE, Chirps, CMORPH. CPC, CRU, GPCC, GPCP_1DD, GPCP, PERSIANN and TAMSAT	RFE, GPCC, CPC, and CHIRPS	<i>Roushdi, (2020)</i>
	PERSIANN-CDR, TRMM3B42v7, IMERG-F, GSMaP_Gauge	GSMaP_Gauge	<i>Gado, (2023)</i>
Sudan	TRMM 3B42v7 and CHIRPS	TRMM 3B42v7	<i>Abdelmoneim et al., (2020)</i>
	TRMM and RFE	Both	<i>Abd Elhamid et al., (2020)</i>
South Sudan	GPCC 7.0, CHIRPS, PERSIANN-CDR, ARC2, and MSWEP 2.0	Monthly: GPCC 7.0 & CHIRPS Annual: GPCC 7.0 and then PERSIANN-CDR	<i>Basheer &amp; Elagib, (2019)</i>
Ethiopia	CHIRPS, TAMSAT 3, and ARC2	CHIRPS followed by TAMSAT	<i>Ayehu et al., (2018)</i>
	CHIRPS, TAMSAT v2 and v3, and TRMM 3B43v7	CHIRPS followed by TAMSAT, and TRMM for mountainous area	<i>Belete et al., (2020)</i>
	TRMM, CRU, and GPCC	GPCC	<i>Abdelwares et al., (2020)</i>
	CMORPH, TRMM 3B42v7, TMPA, ERA-Interim, GPCC, MSWEP	MSWEP	<i>Akew et al., (2020)</i>

## 2.6 Data Quality

### 2.6.1 Possible problems in the collected rainfall data (satellite and ground station data)

The possible problems of rainfall data arise from cross-system inconsistencies, unstructured data, inconsistent formatting, duplication, inaccuracy and incompleteness due to observer's error and/or meteorological instrument problem in case of manned and automatic stations. Let us see station data quality problems first. There are Outliers, missing, non-numeric representations, and lack of appropriate metadata due to observer error or instrumental source of errors. When it comes to satellite data quality problem, one of the causes is cloud cover, resolution of the satellite data and so on. Therefore, before carrying out any kind of rainfall analysis, the satellite and/or ground observation data need to be checked whether the missing values are there or not, number

of missing values, the outliers and so forth in the time series. That is important for identification of precipitation discontinuity and inconsistency as the non-climatic noises caused by the data impurity which leads to wrong results and conclusion unless it is quality controlled before the analysis (*Brunetti et al., 2006; Informatics et al., 2017; Longobardi & Villani, 2010*).

The challenges to the availability of climate data arise due to scanty and/or deteriorating observation networks and insufficient technical capacities by the National Meteorological and Hydrological Services (NMHS) (*Dinku, 2019*). He suggested that overcoming the challenge would require addressing these issues through blending satellite-based climate data estimates with those sparse ground meteorological station datasets. However, if the raw station data is blended with satellite data without addressing the issues of data quality control, that could be gaps, outliers and any erroneous sets, the quality of the product further decline. Therefore, the reference historical station data should be cleaned from such impurities beforehand (*Amada et al., 2015; Branisavljevi et al., 2009; Climate & Centre, n.d.; Estévez et al., 2022; J A du Plessis, 2021; Vejen et al., 2002*).

## 2.6.2 Rainfall data quality check mechanisms

### 2.6.2.1 Satellite data

The satellite data quality issue is associated to resolution, cloud condition and time steps that the data is collected in. How accurate or inaccurate the satellite data is evaluated with reference to observed station datasets. There are numerous satellite based rainfall data which is recommended to be used after bias correcting the raw data using statistical metrics (*du Plessis, 2021*). The quality control method consists of three consecutive steps: basic, absolute, and relative quality control processes. The latter step compares data from neighboring stations taking into account their proximity, height difference, and correlation, leading to a complete evaluation of each daily value (*Estévez et al., 2022*).

### 2.6.2.2 Ground observation data

The ground stations' data sources referents to both manually performed observations and automatically generated electronic observations from unmanned stations. The collected data may get erroneous in both cases. As a result, quality controlling (QC) is the essential task throughout data processing cycles. To be confident on the data, carrying out the QC activity at the station level as it is real time, is advantageous to avoid ingestion of erroneous data to data archive and potentially deviate the message of the products. Depending on the structure of the National Meteorological and Hydrological Service (NMHS), QC may be performed by a central unit or at the regional level following a consistent, well-defined NMHS-wide process. The important point is that the final QC should be carried out using a uniform procedure, with consistent tools and approaches, prior to final archival. So, the QC tests needed for data that has taken from climate database should be comprehensive, though not exhaustive as it is carried out after ingest, and as such, are often referred to as delayed mode QC. Five types of tests can be used; namely,

constraint tests, consistency tests, Heuristic tests, data provision tests, and statistical tests ([WMO, 2021](#)).

### 2.6.3 Erroneous data correction mechanisms

The missing data can be filled using different techniques. In addition to the missing data, the outlier data trimming with presented lower and upper thresholds is what lead to data correction. There are many statistical precipitation gap filling techniques all over the world. However, for the sake of simplicity, experts prefer the following seven simple techniques practiced in particular case of Ethiopia. These are: Simple arithmetic means (SAM) ([Devi et al., n.d.](#); [Kashani & Dinpashoh, 2014](#); [Zainuri & Muda, 2015](#)) given that the missing values are not greater than 10%, normal ratio method (NRM) ([Zainuri & Muda, 2015](#)), correlation coefficient weighing (CCW) ([Fadhilah et al., 2015](#)), inverse distance weighting (IDW) ([Ahrens, 2006](#)), multiple linear regression (MLR) ([Le, 2020](#)), empirical quantile mapping (EQM) ([Precipitation & Series, 2020](#)), and empirical quantile mapping plus (EQM+) ([Chinasho et al., 2021](#)).

## 3 Material and Methods

### 3.1 General description

The methodology of this study consists of number of steps. Firstly, the different rainfall satellite datasets considered in the study were selected, followed by downloading and correcting this data before analysis. Subsequently, set of techniques were undertaken for the analysis of these rainfall datasets, to finally come up with informative description of the rainfall trends in the Eastern Nile Basin. The study considers the four subbasins of the Eastern Nile Basin; namely, the Blue Nile basin, Baro-Akobo-Sobat basin, Tekeze-Setit-Atbara basin, and Main Nile Basins. However, to follow the physical climatology of the Main Nile and reduce uncertainty in the analysis, the Main Nile sub-basin was further divided into the Upper Main Nile basin and the Lower Main Nile basin. Historical rainfall data of the years 1990 – 2020 was considered for the analysis.

According to the information mentioned in section 2.4 and 2.5, four satellite datasets were selected to conduct rainfall trends analysis in the Eastern Nile Basin. The selection was made based on the spatial coverage, data record length, temporal and spatial resolution of the datasets, the type of data input (calibrated with gauge data or not), as well as the performance of products observed in previous studies for Eastern Nile Basin region and countries. In addition to the 4 satellite/satellite-gauge blended products, GPCC is also considered as it provides gridded data from ground stations with acceptable resolution. The selected products are:

#### **1. Climate Hazards Group InfraRed Precipitation with Station Data (CHIRPS)**

The Climate Hazards Group InfraRed Precipitation with Station (CHIRPS) dataset is a high-resolution rainfall dataset that combines satellite observations blended with ground station data, covering a wide area (50°S - 50°N), with a long record starting from 1981 until now. By integrating multiple data sources, CHIRPS enhances the accuracy and reliability of its rainfall data, to provide reliable precipitation estimates, so as it is widely used in climate research, hydrology, agriculture, and disaster management. CHIRPS provides high-resolution rainfall estimates at a spatial resolution of approximately 0.05 degrees (about 5 km) globally. This fine spatial resolution allows for detailed analysis of precipitation patterns at local and regional scales. Moreover, it offers daily precipitation estimates, and this is valuable for studying short-term weather events, seasonal patterns, and long-term climate trends. The CHIRPS dataset undergoes rigorous validation processes to ensure the accuracy of its precipitation estimates. Number of validation studies were conducted to compare CHIRPS data with ground-based observations and other satellite-derived datasets to assess its performance in capturing actual rainfall patterns.

#### **2. African Rainfall Climatology Version2 (ARC2)**

The African Rainfall Climatology Version2 is a high-resolution gridded rainfall dataset developed specifically for Africa. It provides daily estimates of precipitation at a spatial resolution of 0.1 degrees (approximately 10 km) across the continent. ARC2 combines satellite data, ground station

observations, and numerical weather prediction models to generate rainfall information for various applications, including agriculture, water resource management, and disaster risk reduction in Africa. This dataset also provides a long record (1983 – present) of daily rainfall data.

### **3. Precipitation Estimation from Remotely Sensed Information using Artificial Neural Networks–Climate Data Record (PERSIANN-CDR-CCS)**

Precipitation Estimation from Remotely Sensed Information using Artificial Neural Networks–Climate Data Record (PERSIANN-CDR) Satellite and gauge data is one of the significant products that have been commonly used globally. It allows users to access and download spatiotemporal statistics precipitation data from 1983 up to Present, uses balanced network function classification/approximation procedures to compute an estimate of rainfall rate at about  $0.25^\circ \times 0.25^\circ$  (27 km) pixel resolution. It is a long-term global rainfall dataset that leverages satellite data and machine learning techniques to estimate precipitation on a smallest temporal resolution of daily basis, which covers  $60^\circ\text{S}$  to  $60^\circ\text{N}$  degree, with high resolution and consistency in long-term records. PERSIANN-CDR is widely used for climate studies, hydrological modeling, and monitoring of precipitation trends over extended time periods.

### **4. Tropical Applications of Meteorology using Satellite Data (TAMSAT)**

TAMSAT is a research project that produces high-quality rainfall estimates for tropical regions, with a focus on Africa. The TAMSAT dataset combines satellite data, climate reanalysis products, and ground station observations to generate daily and pentad (5-day) precipitation estimates at a spatial resolution of approximately 4 km over Africa, and a record extending from 1983 until now. TAMSAT data is utilized in various applications; such as famine early warning, drought insurance, agricultural decision support, and climate impact assessments.

### **5. Global Precipitation Climatology Centre (GPCC).**

GPCC is an international initiative that produces global precipitation datasets based on a gridding the rain gauge observations, covering the area  $90^\circ\text{S}$  -  $90^\circ\text{N}$ , with a long record starting from 1891 until present. The GPCC dataset offers monthly and daily precipitation estimates at various spatial resolutions of 0.1 degrees to 0.25 degrees respectively. GPCC data is widely used in climate research, water resource management, and climate impact assessments on a global scale. Table 3. 1 Summary of selected satellites characteristics shows summary of the selected rainfall products' characteristics.

Table 3. 1 Summary of selected satellites characteristics

Dataset	Spatial Resolution	Temporal Resolution	Length of Record	Type of Data
CHIRPS	0.05° (5.5 km)	Daily	1981-present	Satellite and ground data
ARC2	0.1° (11 km)		1983-present	Satellite, ground data, and weather prediction models
PERSIANN-CDR	0.25° (27 km)		1983-present	satellite data and machine learning techniques
TAMAST	0.0375° (4 km)		1983-present	satellite data, climate reanalysis products, and ground data
GPCC	0.25 (27km)		1891 - present	Gridding of ground data

### 3.2 Data acquisition and preprocessing

Daily rainfall data of CHIRPS, ARC2, and TAMSAT products was acquired from the Climate Data Tool (CDT) platform that is based on the R programming language. PERSIANN-CDR rainfall data was acquired from the Center for Hydrometeorology and Remote Sensing (CHRS) website (<https://chrs.web.uci.edu>), also using daily basis. Similarly, the GPCC data was downloaded from NOAA Physical Science Laboratory website (<https://psl.noaa.gov/data/gridded/data.gpcc.html>) in daily temporal resolution. The daily rainfall data of the years between 1990 to 2020 was downloaded using the extents (geographic coordinates or shape file) of the Eastern Nile Basin. During the reprocessing and analysis, the boundaries of the 5 subbasins were considered.

All data was downloaded in NetCDF format as it is the most suitable format for dealing with climate data of long records, due to its ability to analyze large and complex datasets. Moreover, NetCDF files are self-describing, meaning they include metadata along with the actual data.

Simple data quality check was conducted. The downloaded data of the 5 products did not require a lot of reprocessing and correction as it was already reprocessed by the providers. Q/ArcGIS, Climate Data Tool (CDT), as well as R and Python codes were used for the initial presentation and reprocessing of the data; i.e. visualization, clipping to subbasins level, combining of separate daily data into one file for each year, and the conversion to GeoTiff (.tiff) or Comma-separated values (.csv) formats and vice versa. GPCC and PERSIANN-CDR have shown missing (no data) values and false zero records within their daily records. The false zero was corrected using the Climate Data Tool (CDT), while the gap was filled by using either the rainfall average of the previous and next days, or the average of the same day from the available other years in case of many consecutive

missing days. Moreover, PERSIANN-CDR has shown high number of negative values (-99) representing the no data values, especially in the first 10 years. Those values were converted into no data using a Linux code, before filling them using the previously mentioned method.

### 3.3 Tools and software packages

#### 3.3.1 Q/ArcGIS

GIS tools were utilized for the rainfall analysis as it integrates the spatial data with the precipitation records. They were used for data visualization over the 5 subbasins, and thematic maps to display rainfall patterns and distribution across different Eastern Nile Basin regions were prepared at different spatial and temporal scales. Additionally, the Multi-band Zonal Statistics tool of QGIS was used to calculate the statistical characteristics of the historical rainfall of the different 5 products over the study area.

#### 3.3.2 Climate Data Tool (CDT)

The Climate Data Tool (CDT) is an open-source R package developed as part of the Enhancing National Climate Services (ENACTS) initiative by the International Research Institute for Climate and Society (IRI). It is a powerful tool that provides researchers, scientists, and decision-makers with access to a wide range of climate datasets, and allows for analysis and visualization. CDT offers a user-friendly interface and a suite of tools for processing, analyzing, and interpreting climate data, including rainfall datasets. The tool is designed to facilitate the exploration of historical climate information, trends, and variability to support research on climate change, weather patterns, and environmental impacts.

In this study, CDT was used to download (in NetCDF format) and/or analyze the satellite historical rainfall data. Some of the rainfall products data was both downloaded and analyzed using CDT (CHIRPS, ARC2, and TAMSAT), and the rest were downloaded from other sources and then imported to CDT for the analysis. The tool is very powerful in dealing with the NetCDF format files; therefore, it was highly used for combining, splitting, clipping, aggregating, and converting of the different rainfall products' NetCDF data into other formats (GeoTiff (.tiff) and Comma-separated values (.csv)).

The tool also provided an interactive visualization tool for displaying rainfall data in maps, graphs, and time series plots, with customizing the visual representation of data layers, apply color scales, and overlay multiple datasets to compare and analyze rainfall patterns. It was used for visualizing the spatial distribution of rainfall in the shape of maps. As the tool consists of a wide range of statistical and analytical tools for processing data, it assisted in calculating annual and monthly averages, anomalies, seasonal variations, and trends, and in performing spatial analysis using the time series of the different rainfall datasets.

Furthermore, the CDT includes predefined climate indices such as the Standardized Precipitation Index (SPI), Palmer Drought Severity Index (PDSI), and Rainfall Anomaly Index (RAI) that can be

calculated from rainfall data to assess drought conditions, precipitation anomalies, and climate variability. Here it was used for the calculation of Standardized Precipitation Index (SPI) for the different products.

### 3.3.3 Programming languages

Programming languages; R, Python, and Linux were used for performing number of activities as they provide a wide range of tools and libraries that can be used for data analysis and plotting. R was used for producing rainfall spatial distribution maps, as well as operating the CDT tool. Python was used to read rainfall data from CSV format files, perform statistical analysis, and create plots like the box plots of the different satellites' rainfall time series. Moreover, Linux was used for splitting and combining the NetCDF files, as well as filling the missing and correcting the negative values.

### 3.3.4 Easy Fit Software

Easy Fit Software was used to fit the best distribution of the rainfall time series of the different products, including its parameters, and to plot the fitted rainfall distribution.

## 3.4 Rainfall analysis steps

In this study, the CHIRPS rainfall data was selected to be used as a reference for the assessment of the other satellite rainfall products performance, to fill the gap that is caused by the data scarcity problem in the Eastern Nile countries. CHIRPS delivers reliable and complete data up to present, that is blended with ground data, and showed good performance, good precision, and relatively little bias over east Africa compared to ground observations. The historical rainfall records of the five products were analyzed over the five Eastern Nile sub-basins (Baro-Akobo-Sobat, Blue Nile, Tekeze-Setit-Atbara, Upper Main Nile and Lower Main Nile).

The rainfall analysis undertaken in this study consists of set of analysis techniques. Firstly, the spatial distribution over the whole Eastern Nile Basin area was produced to understand the spatio-temporal variations of rainfall, and have initial insights about the trends and changes taking into consideration the observations of the different rainfall products.

For the rest of the analysis, each subbasin was analyzed separately to be able to detect the differences in their satellite observations and rainfall patterns, and to capture the various physical and climate conditions associated with each of them. Firstly, simple statistical analysis was conducted for the daily data to calculate the daily mean and standard deviation over each subbasin (produced from the rainfall values of subbasin cells). This was done using the Multi-band Zonal Statistics tool of QGIS, and the results were presented in GeoPackage format (.gpkg) and Comma-separated values format (.csv). The resultant time series of each rainfall product for each subbasin was considered for the analysis. The historical rainfall analysis included calculating and plotting box plots, scatter plots, rainfall trends, rainfall anomalies, rainfall frequency distribution,

rainfall seasonality, as well as calculating and plotting the Standard Precipitation Index (SPI). Description of these techniques is shown below.

#### 3.4.1 Spatial distribution

Rainfall distribution refers to the spatial and temporal patterns of rainfall in a particular region. This can include the amount of rainfall and the variability of rainfall over time. Different satellite datasets have varying spatial resolutions, which can affect their ability to accurately capture localized rainfall patterns, and the higher resolution datasets may provide more detailed information on rainfall distribution. In this study, the spatial distribution of rainfall over the Eastern Nile Basin was produced using 10 years average, considering the different 5 rainfall products. This was performed using the Climate Data Tool (CDT).

#### 3.4.2 Box plots

Box plots provide a simple yet powerful tool for comparing the performance of different satellite rainfall datasets and identifying patterns or discrepancies in their estimates. They were used to provide graphical representations of the distribution of the different rainfall dataset of each subbasin separately, in the shape of a visual summary of key statistical measures such as the mean, quartiles, and outliers. Annual rainfall (annual sum) data was used for plotting the box plots using a Python code. The plot of each rainfall satellite data consists of a box that represents the interquartile range (IQR) of the data, i.e. the middle 50% of the ranked data, - and it is drawn from the lower quartile value to the upper quartile value, which are the 25<sup>th</sup> until 75<sup>th</sup> percentiles -, with a line inside the box representing the mean. Whiskers extend from the box to show the range of the data (min to max), and any points outside of the whiskers are considered outliers.

The separate box plots of the 5 satellite products were plotted next to each other to be able to compare them. By looking at the means, quartiles, and ranges of the datasets, the differences in the satellites' performance were assessed to determine their accuracy and consistency. Furthermore, the box plots also helped in identifying the outliers in the data, which indicates any errors or inconsistencies in the satellite rainfall estimates. Comparison of the number and distribution of the outliers also give insights into the quality and reliability of the different datasets.

#### 3.4.3 Scatter plots

Scatter plots are graphical representations that provides visual and quantitative measure to assess the relationship between two variables. In the scatter plot, each data point is represented by a point on the graph, with one variable plotted on the x-axis and the other variable plotted on the y-axis. In our case, annual data was used to plot the scatter plots, and used to visualize the correlation and evaluate the performance of each of the rainfall products compared to CHIRPS, in order to identify agreement, biases, or inconsistencies.

By examining the scatter plots, we assessed how well the satellite rainfall estimates match the CHIRPS data. The first metric that has been considered for the analysis is the correlation coefficient (R) and regression line statistical measures, which were calculated to quantify the relationship between the 2 datasets. A high correlation coefficient (close to 1) indicates a strong positive relationship, while a low correlation coefficient suggests a weak or no relationship between the datasets. In other words, a strong positive correlation between the CHIRPS and satellite indicates that the satellite estimates are accurate and reliable compared to CHIRPS. On the other hand, a weak or negative correlation may suggest discrepancies in the satellite rainfall estimates. Moreover, the Bias Ratio (B) has also been used to check the level of agreement between CHIRPS and other products. This metric detects the overestimation or underestimation of rainfall. Having  $B=1$  means there is perfect agreement between the 2 datasets, while having values  $>1$  or  $<1$  indicates an overestimation or underestimation respectively. Another metric that has also been used is the Coefficient of Variation (CV). This metric assesses the dispersion or relative variability of data compared to a reference. Higher values of CV demonstrate greater variability, and thus, poor performance. The last metric for assessing the performance of rainfall products is the Root Mean Square Error (RMSE) that detects the differences and match between each 2 datasets. The lower the RMSE, the higher the match between any dataset compared to the reference (CHIRPS).

#### 3.4.4 Rainfall trend

The rainfall trend plots are used to graphically represent and help to visualize the changes in rainfall patterns over specific time period. In this study, the rainfall trends of the different 5 rainfall products were plotted over the 31 years for each subbasin of the Eastern Nile Basin. The Climate Data Tool (CDT) as well as excel were used for this purpose.

The annual rainfall data (annual sum) were plotted against time to show overall trend in rainfall over time. A trend line was added to visualize the pattern of change. The rainfall trend of each product was plotted in a separate plot for better visualization; however, they were put side by side for comparing, identifying different patterns, and detecting any discrepancies or inconsistencies between them. The trendline in addition to its equation were added to give a quantitative description and comparison of the rainfall trend with its direction.

#### 3.4.5 Rainfall anomalies

The rainfall anomalies plots show the deviation of rainfall from a long-term average or climatology mean. These plots are commonly used in meteorology and climatology to visualize the spatial and temporal variability of rainfall patterns. Annual time scale (rainfall annual sum) was used for the calculation of the anomalies. Firstly, the 31 years average of rainfall is calculated for each dataset of each subbasin. Then, rainfall value of each year from the same time period is subtracted from the long-term average to obtain the anomaly values. Positive anomalies indicate above-average rainfall, while negative anomalies indicate below-average rainfall. The typical color scale was used

to represent the magnitude of anomalies, with warmer blue color indicating positive anomalies and red color indicating negative anomalies. Another presentation of the anomalies can be in the shape of spatial distribution, that can be displayed on a map to show how rainfall patterns vary across different regions.

The anomalies produced from each satellite data of each subbasin were then compared to inspect how well each dataset captures the variability in rainfall patterns. Comparison can also assess in determining which dataset provides more accurate and reliable estimates of rainfall anomalies.

### 3.4.6 Standardized Precipitation Index (SPI)

The Standardized Precipitation Index (SPI) is a widely used index for characterizing meteorological drought on various timescales. There are 1-month, 2-month, 3-month, 6-month and 12-month SPI estimation time scales for different purposes. For example, the 3-months SPI is used for meteorological purposes, 6-month SPI is used for agricultural purposes, while the 12-month SPI is used for hydrological purposes (Bussay et al., 1998; Morid et al., 2006; Szalai and Szinell, 2000). The SPI is obtained by calculating a uniform likelihood for precipitation deficit (see equation (3.1) below) (Patel et al., 2007; McRoberts et al., 2012). Hence, the 12-month SPI is used in this study, as it provides a longer-term view of precipitation conditions and is useful for assessing drought or wet conditions that develop over an entire year.

$$SPI_{ij} = \frac{(X_{ij} - \mu_{ij})}{\alpha_{ij}} \dots \dots \dots (eq. 3.1)$$

Where  $X_{ij}$  is the total rainfall for the  $i^{th}$  month at the  $j^{th}$  period,  $SPI_{ij}$  represents an  $i^{th}$  month at the  $j^{th}$  period, and  $\mu_{ij}$  and  $\alpha_{ij}$  stand for the  $i^{th}$  month's long-term mean and standard deviation, respectively, on the  $j^{th}$  timeframe of the chosen period.

SPI has different output values for classifying drought ranging from -2.0 to 2.0 as shown in Table 3. 2 (Zhen et al., 2018). In this study, the Standardized Precipitation Index (SPI) was plotted using the Climate Data Tool (CDT) and used for measuring droughts in the Eastern Nile basin over the past 31 years, based on the CHIRPS, ARC2, PERSIANN-CDR, TAMSAT and GPCC datasets.

Table 3. 2 Classification of drought based on the distribution of the SPI index (Zhen et al., 2018)

SPI Value	Interpretation
>2.0	Extremely wet
1.5 to 1.99	Severely wet
1.0 to 1.49	Moderately wet
0.99 to -0.99	Near normal
-1.0 to -1.49	Moderately dry
-1.5 to -1.99	Severely dry
<-2.0	Extremely dry

To compare the performance of different satellite rainfall datasets considering SPI, calculations were applied to each dataset and then the resulting SPI values were plotted next to each other. By assessing the degree of agreement between the datasets in terms of the SPI values, the consistency and reliability of the drought classification provided by the different satellite datasets were assessed. This comparison can aid in understanding the strengths and weaknesses of each dataset when it comes to capturing precipitation variability and drought conditions.

#### 3.4.7 Rainfall frequency distribution

The probability and frequency of rainfall data is important to be able to determine the expected rainfall, which is useful to prevent extreme events. The best fit probability distribution of the CHIRPS, ARC2, PERSIANN-CDR, TAMSAT and GPCC datasets for the 5 subbasins was identified using Easy Fit software. It determines the best fit distribution visually by comparing the satellite data and the theoretical (fitted) distribution graphs. This is done using 3 goodness of fit tests; namely, Kolmogorov Smirnov, Anderson Darling, and Chi-squared tests.

#### 3.4.8 Seasonality of rainfall

For this analysis, the 31 years daily rainfall data of the 5 datasets was aggregated into monthly data (monthly sum) for each year. Each month average of the resultant monthly values was then calculated considering the full time period (31 years). The monthly rainfall plots for each dataset of each subbasin were then generated, with time (months) on the X-axis and monthly rainfall on the Y-axis, which provided a visual representation of the rainfall patterns captured by each dataset over time. Comparing the performance of different satellite rainfall datasets using monthly rainfall plots is then used to provide valuable comprehensive understanding of how the different rainfall datasets perform in capturing seasonal or monthly rainfall variations over the Eastern Nile Basin. That is done by assessing the similarities and differences in the magnitude and variability of rainfall between the datasets for each season or month.

Figure 3.1 below illustrates the flowchart for the methodology of this study.

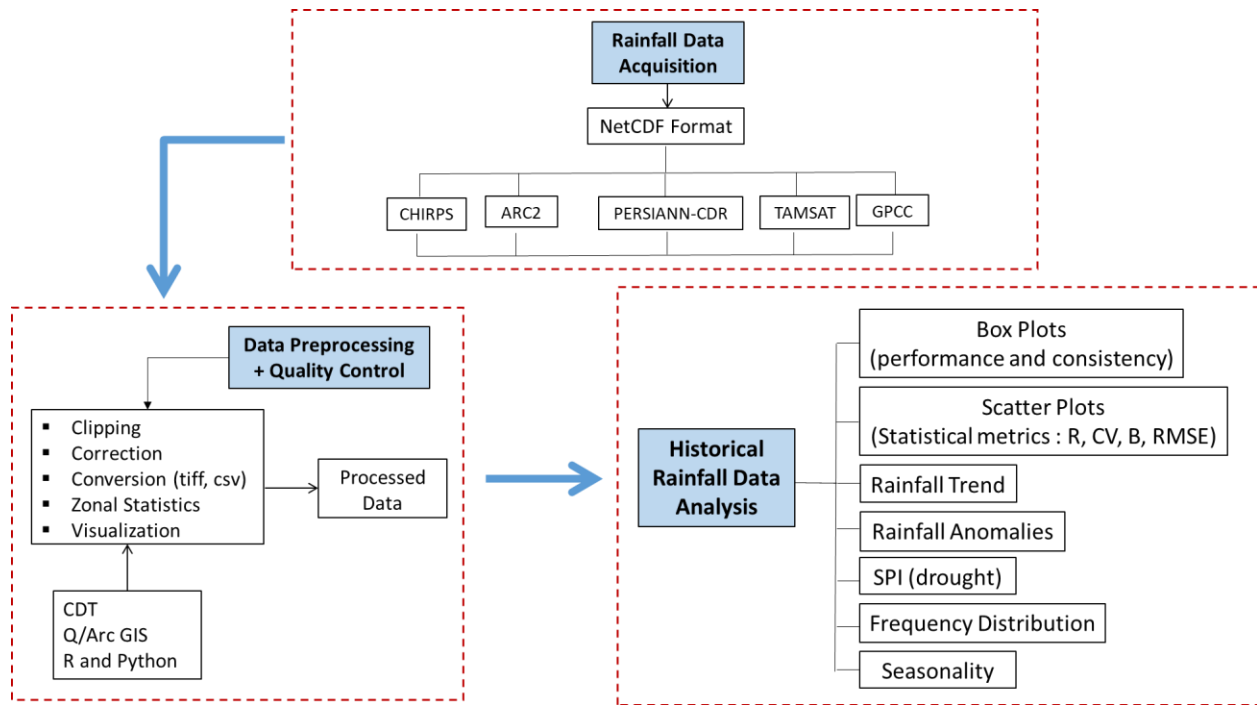


Figure 3.1 Methodology flowchart

## 4 Results and Analysis

### 4.1 General description

In this chapter, the results of the different analysis techniques are described and discussed to come up with comprehensive understanding of the historical rainfall of the Eastern Nile Basin. General overview about the rainfall intensities and distribution over the basin is provided first. That is followed by detailed analysis of each subbasin separately, as the study area consists of various physical and climate conditions.

#### 4.1.1 Rainfall spatial distribution

Figure 4.1 below shows the spatial distribution, as well as the temporal patterns of rainfall over the Eastern Nile Basin area. The graph gives good indication about the rainfall amounts and variability of each subbasin. Generally looking at the estimates of the 5 rainfall products, the basin received amounts of annual rainfall ranging between 0 mm rainfall at the northern part of the basin (north Sudan and Egypt) to around 1500 mm at the south-eastern area of the basin (the highlands of Ethiopia and parts of South Sudan). Blue Nile (BN) and Baro-Akobo-Sobat (BAS) received the highest rainfall intensity; varying between 700 mm to 1500 mm, and 400 mm to 1400 mm respectively, followed by Tekeze-Setit-Atbara (TSA) that received low annual rainfall of 200 mm at its northern part, and high rainfall that reaches up to 1200 mm at the southern part of the subbasin. On the other hand, the Upper and Lower Main Nile received low to very low intensities of rainfall. Annual rainfall of the Upper Main Nile ranged between 0 mm to 250 mm, while the Lower Main Nile showed approximately zero rainfall.

During the 1<sup>st</sup> 10 years of the study period (1990-1999), GPCC and PERSIANN-CDR demonstrated higher annual rainfall intensity compared to the other 3 satellite products (CHIRPS, ARC2, and TAMAT), especially at the south-eastern part of the basin, and that is also similar for the 2<sup>nd</sup> 10 years of the study period. On the other hand, the last 10 years (2011-2020) showed highest rainfall estimates recorded by CHIRPS and TAMSAT, followed by PERSIANN-CDR and GPCC. ARC2 presented the lowest estimation for the annual rainfall over the whole study period.

Comparing the temporal patterns recorded by each rainfall product during the 31 years, the spatial distribution of CHIRPS and TAMSAT data did not show significant change in rainfall over time. GPCC and PERSIANN-CDR showed slightly decreasing rainfall pattern. On the other hand, ARC2 demonstrated rainfall estimate with decreasing pattern between the 1<sup>st</sup> and 2<sup>nd</sup> 10 years, but increasing again between the 2<sup>nd</sup> and 3<sup>rd</sup> 10 years.

The above-mentioned differences can be attributed to the different spatial resolution of the rainfall products, as well as the algorithms used and the assumptions considered for each satellite dataset.

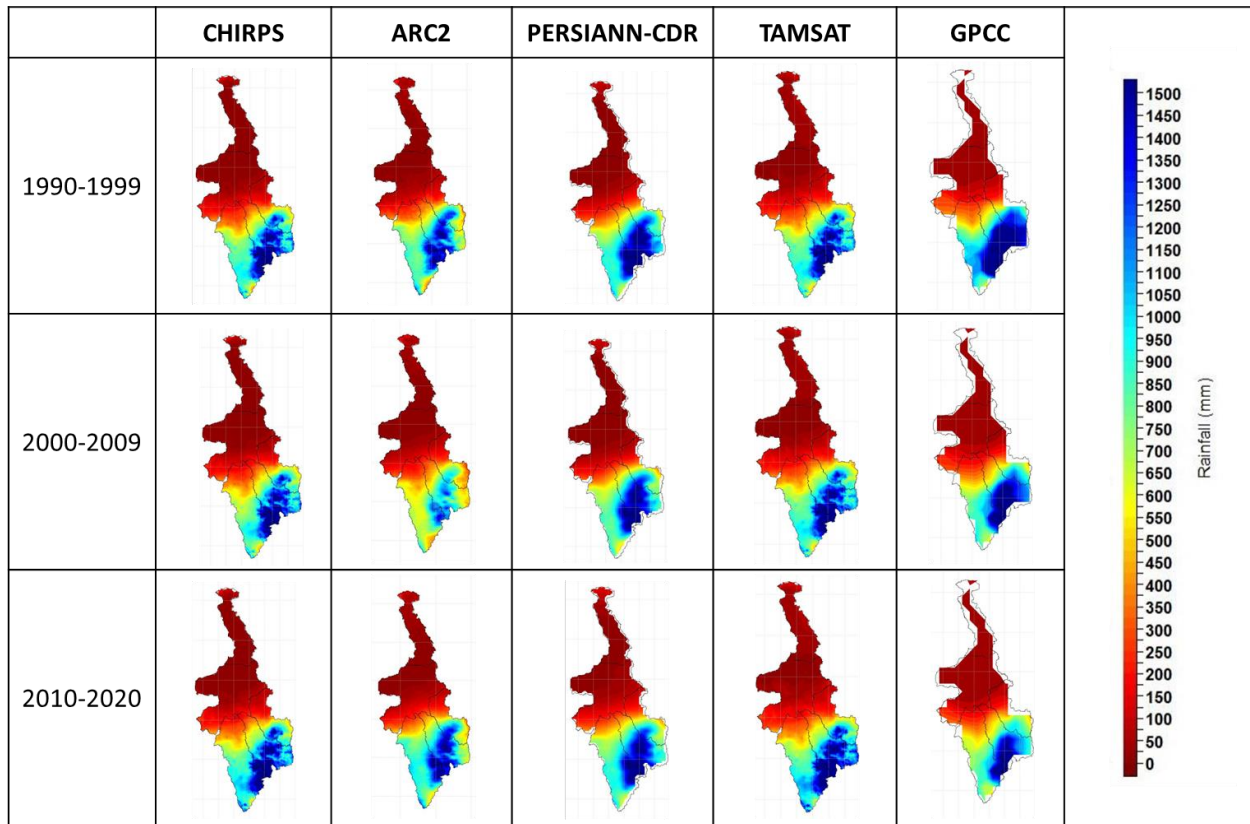


Figure 4.1 Spatial distribution of rainfall over the Eastern Nile Basin

## 4.2 Baro-Akobo-Sobat (BAS)

### 4.2.1 Box Plots

To compare the annual rainfall distribution of BAS subbasin and identify the reliability, consistency, and differences between the rainfall products, we started the analysis by plotting the box plots. Looking at Figure 4.2, the 5 rainfall products showed different distribution of rainfall which demonstrates uncertainty in rainfall estimation. All products showed close values of central tendency (median), except ARC2 that presented lower rainfall. CHIRPS and TAMSAT showed the best performance and highest consistency among the datasets, as they presented low interquartile range (IQR), which means lower variability, with small range of rainfall values (min and max from whisker lines). These are followed by PERSIANN-CDR. Lastly, GPCC and ARC2 demonstrated greater variability, thus, they can be considered unreliable in estimating annual rainfall. All satellites did not show outliers which means low errors or discrepancy.

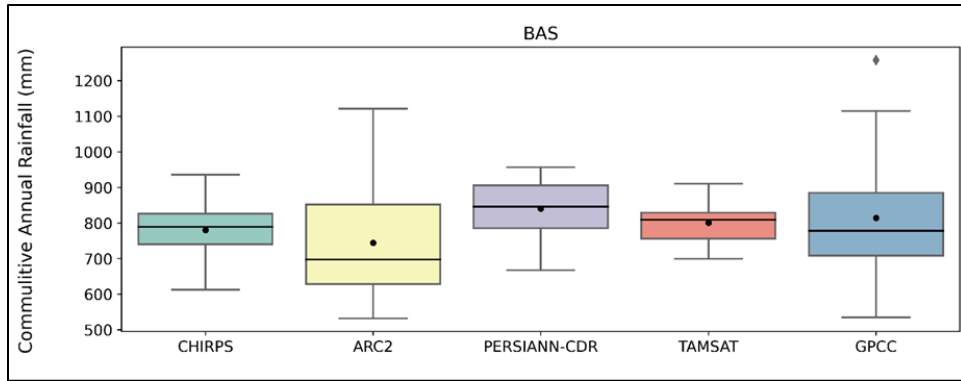
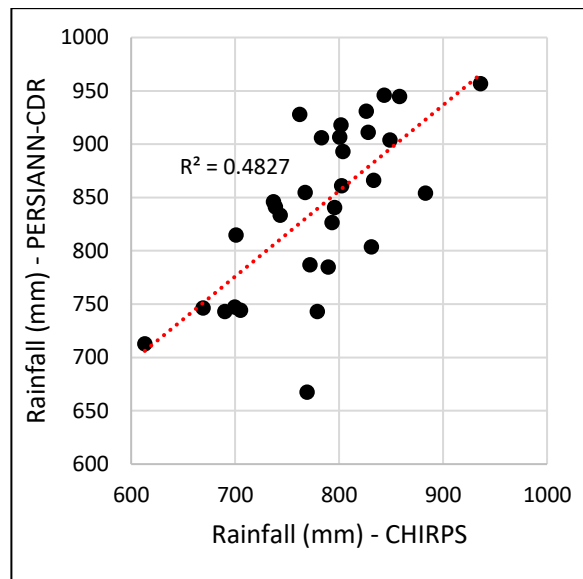
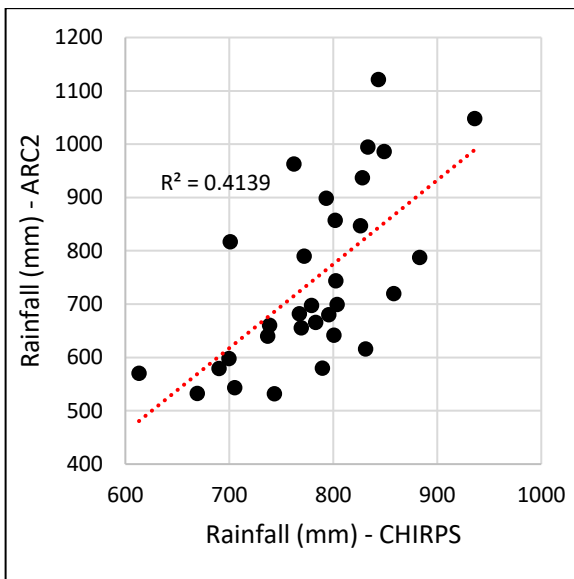


Figure 4.2 Box plots of BAS subbasin

#### 4.2.2 Scatter Plots

As CHIRPS is found to be the best performing rainfall dataset, as well as the information mentioned in section 3.4.3 of this report, it has been considered as a reference to assess the performance of the other rainfall products. Figure 4.3 below show the scatter plots that compare CHIRPS with ARC2, PERSIANN-CDR, TAMSAT, and GPCC, and assess how well the satellite rainfall estimates match the CHIRPS data. Although the coefficient of determination ( $R^2$ ) of TAMSAT = 0.6, which is not considered a good value, it demonstrated the highest fit with CHIRPS, followed by PERSIANN-CDR and ARC2 ( $R^2 = 0.48$  and  $0.41$  respectively). Lastly, GPCC presented very low fit with CHIRPS with  $R^2$  of almost zero.



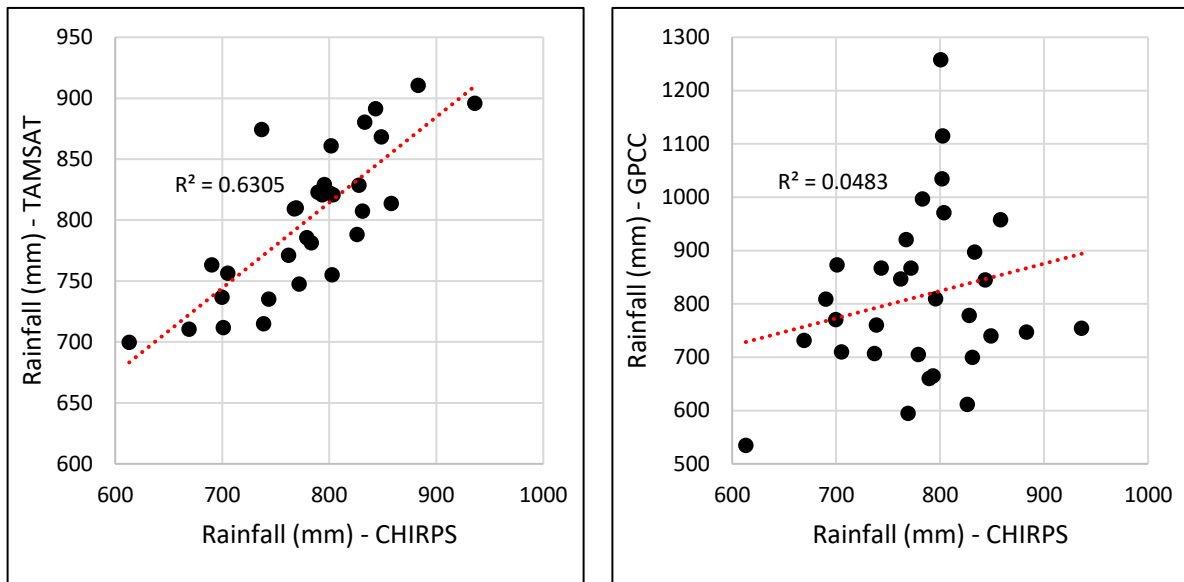


Figure 4.3 Scatter plots of BAS subbasin

Furthermore, the Correlation (R), Bias ratio (B), Coefficient of Variation (CV), and the Root Mean Square Error (RMSE) were also calculated to quantitatively test the performance of ARC2, PERSIANN-CDR, TAMSAT, and GPCC compared to CHIRPS. The results are shown in Table 4.1 below. Looking at R and RMSE, TAMSAT has shown the strongest correlation and match to CHIRPS followed by PERSIANN-CDR and ARC2, while GPCC was found to have the weakest relationship. Moreover, also TAMSAT and PERSIANN-CDR have shown low value of dispersion and relative variability (low CV value), which indicates better performance compared to ARC2 and GPCC (higher CV value). Lastly, the results of the bias ratio demonstrate a very slight overestimation of rainfall recorded by TAMSAT, PERSIANN-CDR, and GPCC, and slight underestimation of rainfall by ARC2 product.

Table 4.1 BAS rainfall products performance tests

	ARC2	PERSIANN-CDR	TAMSAT	GPCC
<b>Correlation (R)</b>	0.64	0.69	0.79	0.22
<b>Bias Ratio (B)</b>	0.95	1.08	1.03	1.04
<b>Coefficient of Determination (CV) %</b>	2.57	1.07	0.86	2.24
<b>Root Mean Square Error (RMSE) mm</b>	133.99	82.25	45.16	156.82

#### 4.2.3 Rainfall Trend

In order to assess the general changes in rainfall over the 31 years of historical rainfall at Baro-Akobo-Sobat, the rainfall trends were plotted using the data of the 5 different rainfall products as illustrated in Figure 4.4. By analyzing the plots, it can be noticed that all rainfall products except

GPCC have indicated increasing rainfall trend over the years between 1990 to 2020. By looking at the slope of the trendlines, CHIRPS, TAMSAT, and PERSIANN-CDR have agreed on the detection of the same direction and amount of rainfall change over the years, i.e., slow positive rainfall increase. However, ARC2 with its steeper trendline slope, captured a generally faster positive rainfall change over the years. Though, it can be observed that ARC2 detected decreasing rainfall during the middle years of study (2000-2009). In Contrast, GPCC demonstrated a fast-decreasing change of rainfall over the years 1990-2020.

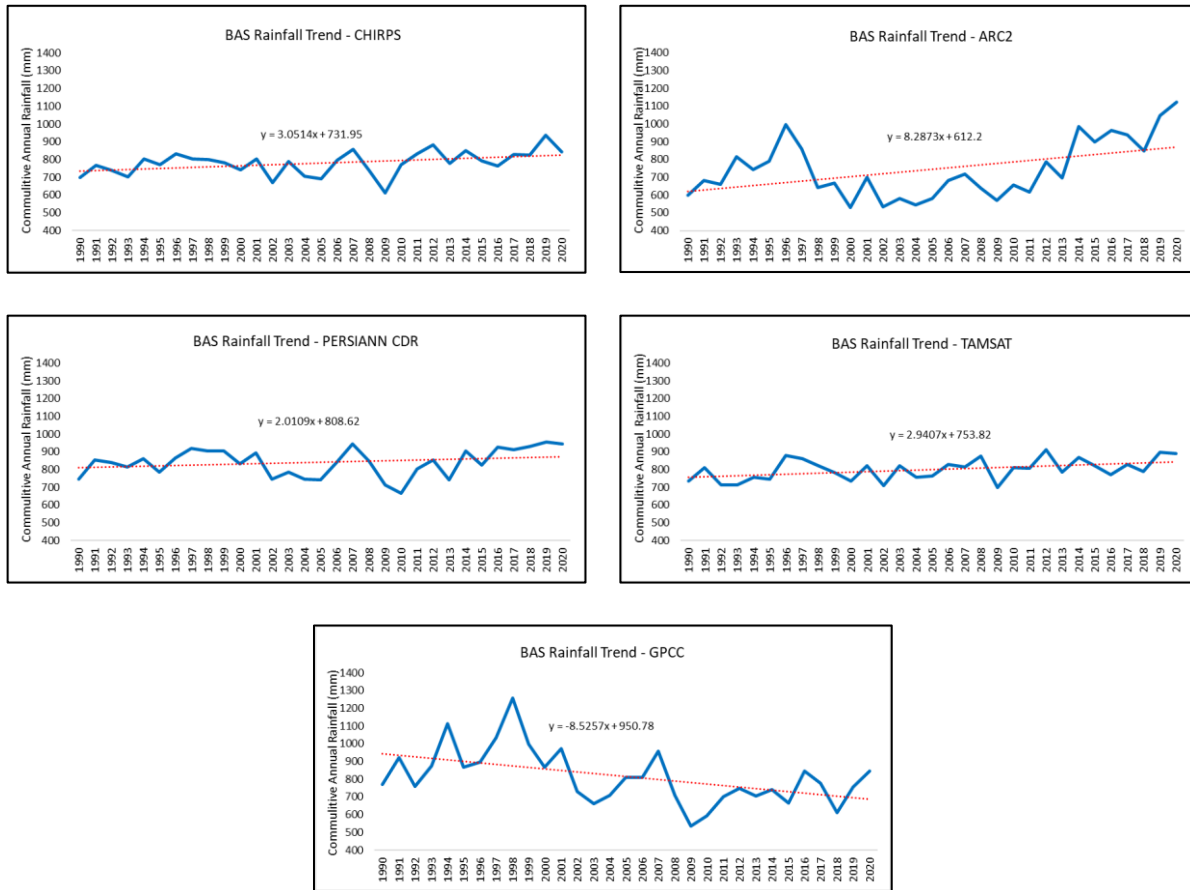


Figure 4.4 Rainfall trends - BAS

#### 4.2.4 Rainfall anomalies

The rainfall anomalies of Baro-Akobo-Sobat illustrate the variation of rainfall compared to the climatology mean for the years 1990 -2020 (see Figure 4.5). Starting with CHIRPS, the year of greatest positive value was 2009, and the year of the lowest value was 2019 compared to the mean. The period from 1990 – 1993 represent the longest consecutive years of rainfall higher than the average, while the last years of 2017 – 2020 represent the longest continuous low rainfall period. With regards to ARC2, the lowest rainfall record compared to the mean was in 2020. The period from 1998 – 2012 represents the longest continuous period with high rainfall, while 2014 – 2020 show lower rainfall than the mean. PERSIANN-CDR and TAMSAT recorded the highest

rainfall in 2010 and 2009 respectively, and the lowest rainfall record in 2012 and 2019 respectively. For both satellites, the period with consecutive higher rainfall than average was in the middle of the study under consideration, while the longest continuous dry years were recorded in the last years. Lastly, GPCC showed different pattern, having continuous years of low rainfall between 1990 – 2001, and higher rainfall for the remaining period (2009 - 2019).

To conclude, anomalies are showing approximately similar patterns but with different intensity, except ARC2 and GPCC. all rainfall products agreed on detecting lower rainfall than average during the last 5 years, except GPCC which showed the opposite. The number of the below-average years is 15, which means a frequency of 48%.

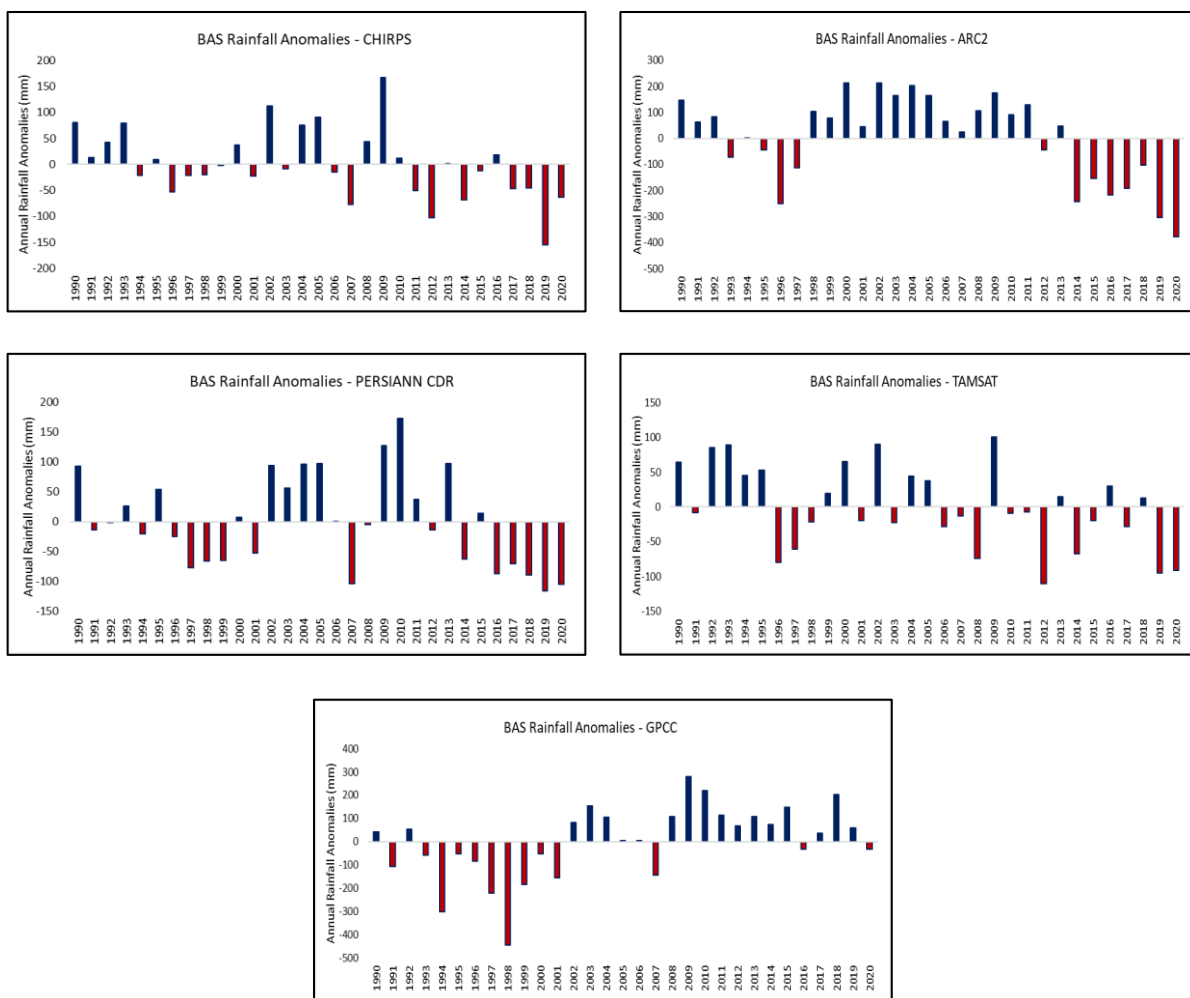


Figure 4.5 Rainfall anomalies - BAS

#### 4.2.5 Standardized Precipitation Index (SPI)

Looking at Figure 4.6 below, and considering table 3.1 of this report, the meteorological drought of Baro-Akobo-Sobat over the period 1990 – 2020 can be classified using the SPI value. CHIRPS, TAMSAT, and PERSIANN-CDR are showing approximately similar pattern, with the longest wet

period at the end of the study period (2015 – 2020), ranging between moderately to extremely wet, with one extremely dry year (2019) recorded by TAMSAT. The driest years are 2009 – 2011, and the most wet years are 2007 – 2008 and 2019 – 2020. On the other hand, ARC2 and GPCC showed different patterns. ARC2 demonstrated long moderately dry period between 2000 – 2010, followed by moderately to extremely wet years until the end of the study period. GPCC showed opposite results, with long near normal to extremely wet period in 1990 – 2002, and extremely to moderately dry period in 2009 – 2020.

Generally, most of the satellites recorded the period between 2002 – 2007 as dry with different intensities (moderately to severely), and the last five years 2016 – 2020 as moderately to extremely wet.

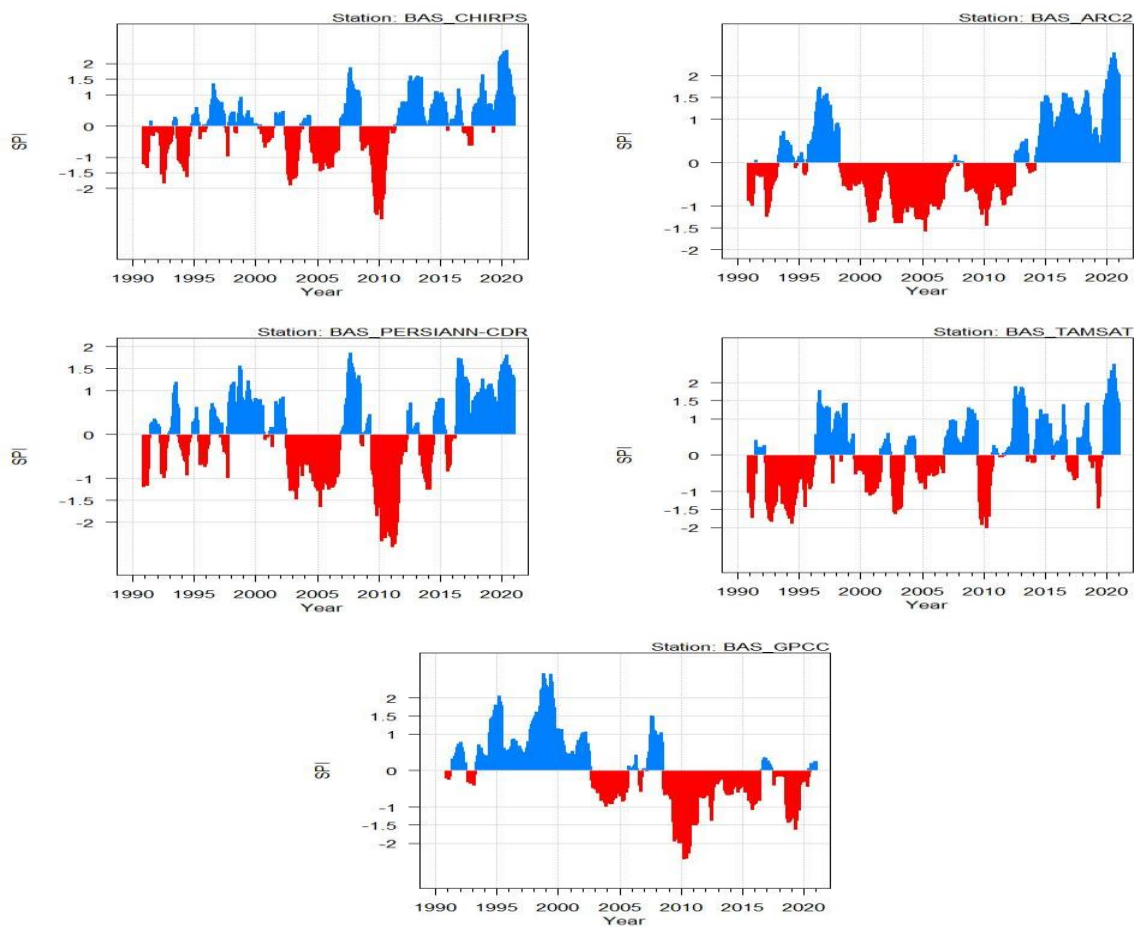


Figure 4.6 Standardized Precipitation Index (SPI) - BAS

#### 4.2.6 Rainfall frequency distribution

In Baro-Akobo-Sobat, the rainfall captured by the different products during the years 1990-2020 was found to follow different frequency distributions as shown in Figure 4.7. CHIRPS and TAMSAT followed the Log-logistic 3P and the Logistic distributions respectively, with symmetric shape, and the most common rainfall intensity (peak of the curves) aligning with the climatology mean (800

mm). The other datasets have shown more skewed distribution curves. ARC2 and GPCC presented negative skewness of curves following Log-Pearson 3 and Frechet 3P distributions, with more frequency of the high rainfall intensities. Also, both of them underestimated the climatology mean. On the other hand, PERSIANN-CDR followed Johnson SB distribution with more frequency of the low rainfall values (positive skewness). All rainfall datasets have not shown long tails, indicating lower frequency of extreme events.

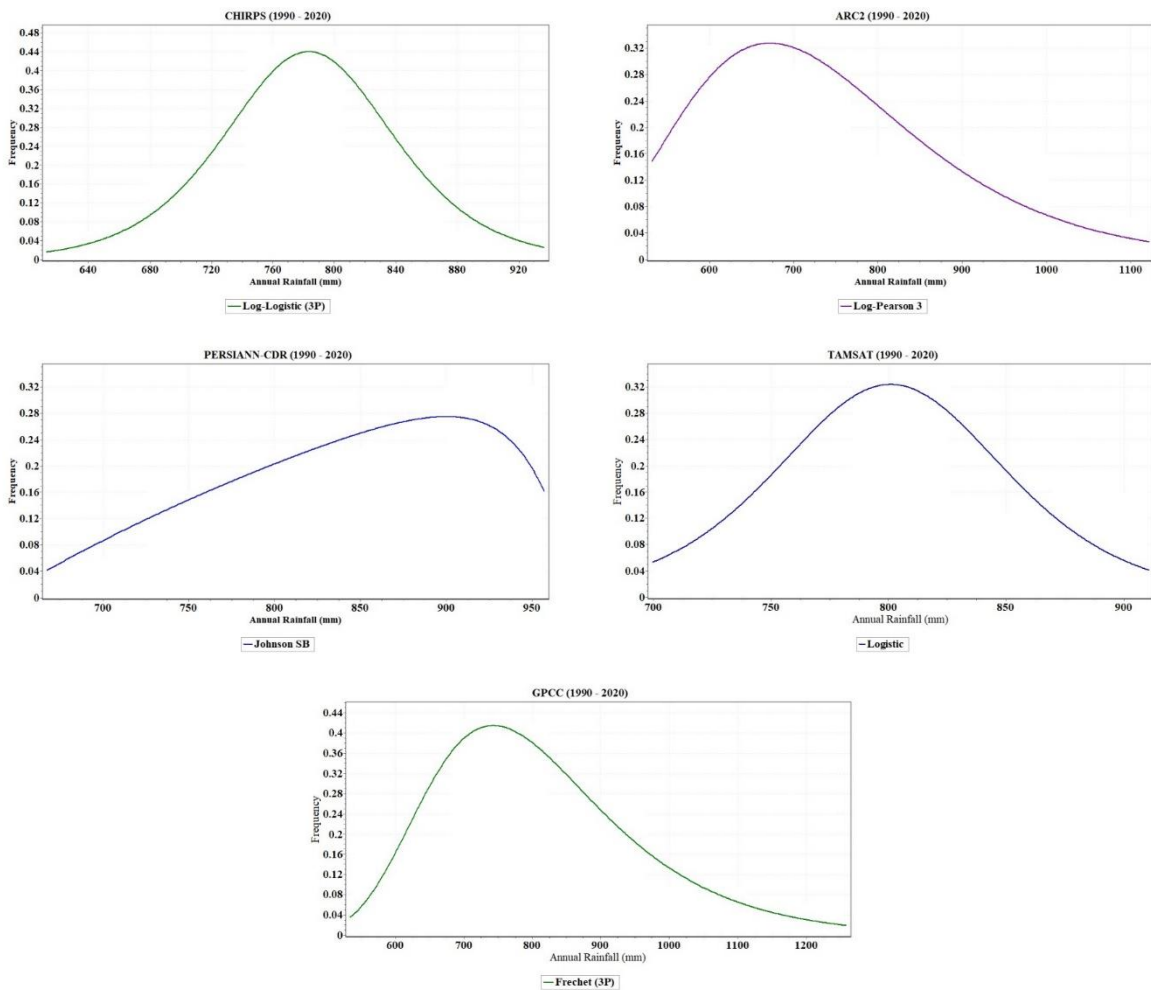


Figure 4.7 Rainfall distribution - BAS

#### 4.2.7 Seasonality of rainfall

In this section, the five rainfall products detection of the rainfall seasonality of Baro-Akobo-Sobat is compared. From Figure 4.8, it can be noticed that all datasets agreed on the continuation of rainfall in the subbasin from March up to November, with July and August having the highest monthly rainfall (around 160 mm). The main rainy season is from June to October. Agreement also noticed in the estimated amount of the monthly rainfall along the year between all products except ARC2 that demonstrated lower estimates especially during the peak season (June, July, August, September) with more than 40 mm less rainfall.

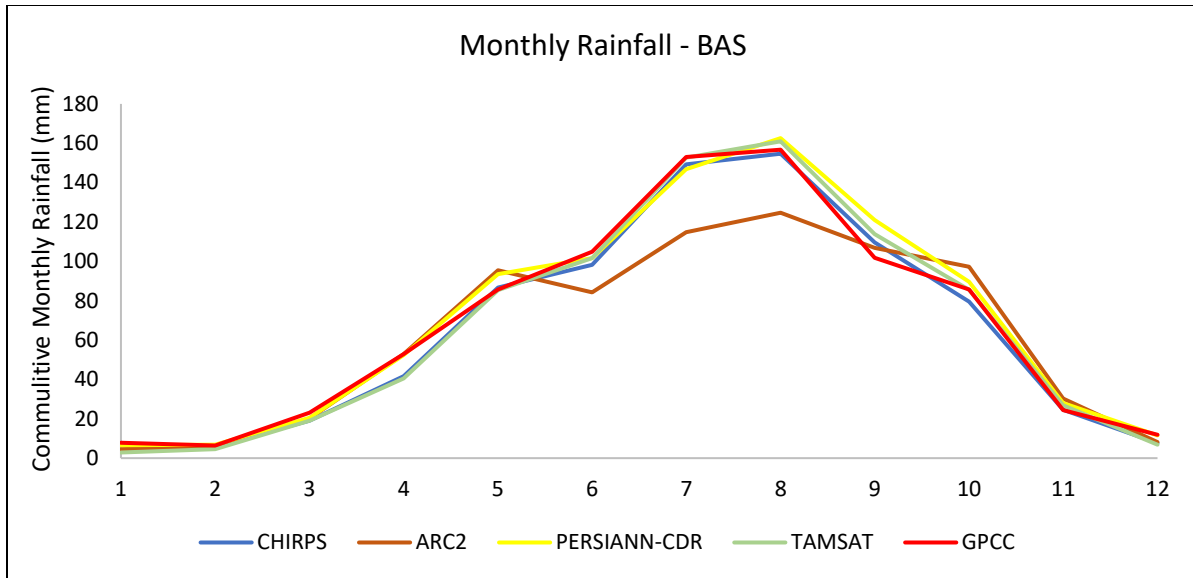


Figure 4.8 Monthly rainfall - BAS

### 4.3 Blue Nile (BN)

#### 4.3.1 Box Plots

Comparing the annual rainfall distribution and variability over the Blue Nile, Figure 4.9 **Error! Reference source not found.** shows that CHIRPS followed by TAMSAT represent the best performance rainfall products with similar rainfall estimate (median) and low variability (low IQR). This means they are more reliable and consistent in estimating the annual rainfall. PERSIANN-CDR also showed low variability, but higher annual rainfall. The highest variability was observed by GPCC and ARC2 datasets. It can be noticed that this result is similar to BAS results.

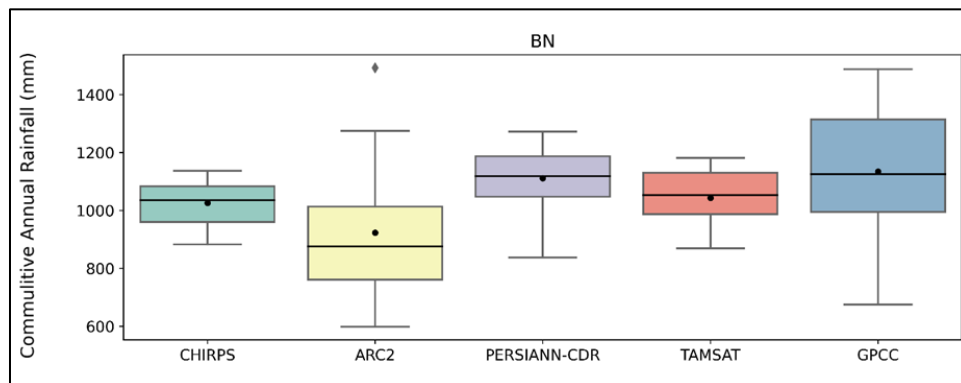


Figure 4.9 Box plots - BN

#### 4.3.2 Scatter Plots

In the Blue Nile, CHIRPS has also been used as a reference to compare the performance of other rainfall datasets. Figure 4.10 below shows the scatter plots that assess how well ARC2, PERSIANN-CDR, TAMSAT, and GPCC rainfall estimates match the CHIRPS data. TAMSAT demonstrated better

fit with CHIRPS having coefficient of determination ( $R^2$ ) = 0.6, followed by PERSIANN-CDR ( $R^2$  = 0.54). However, these  $R^2$  values are not considered high. On the other hand, ARC2 and GPCC provided low fit with CHIRPS with  $R^2$  of 0.34 and 0.18 respectively.

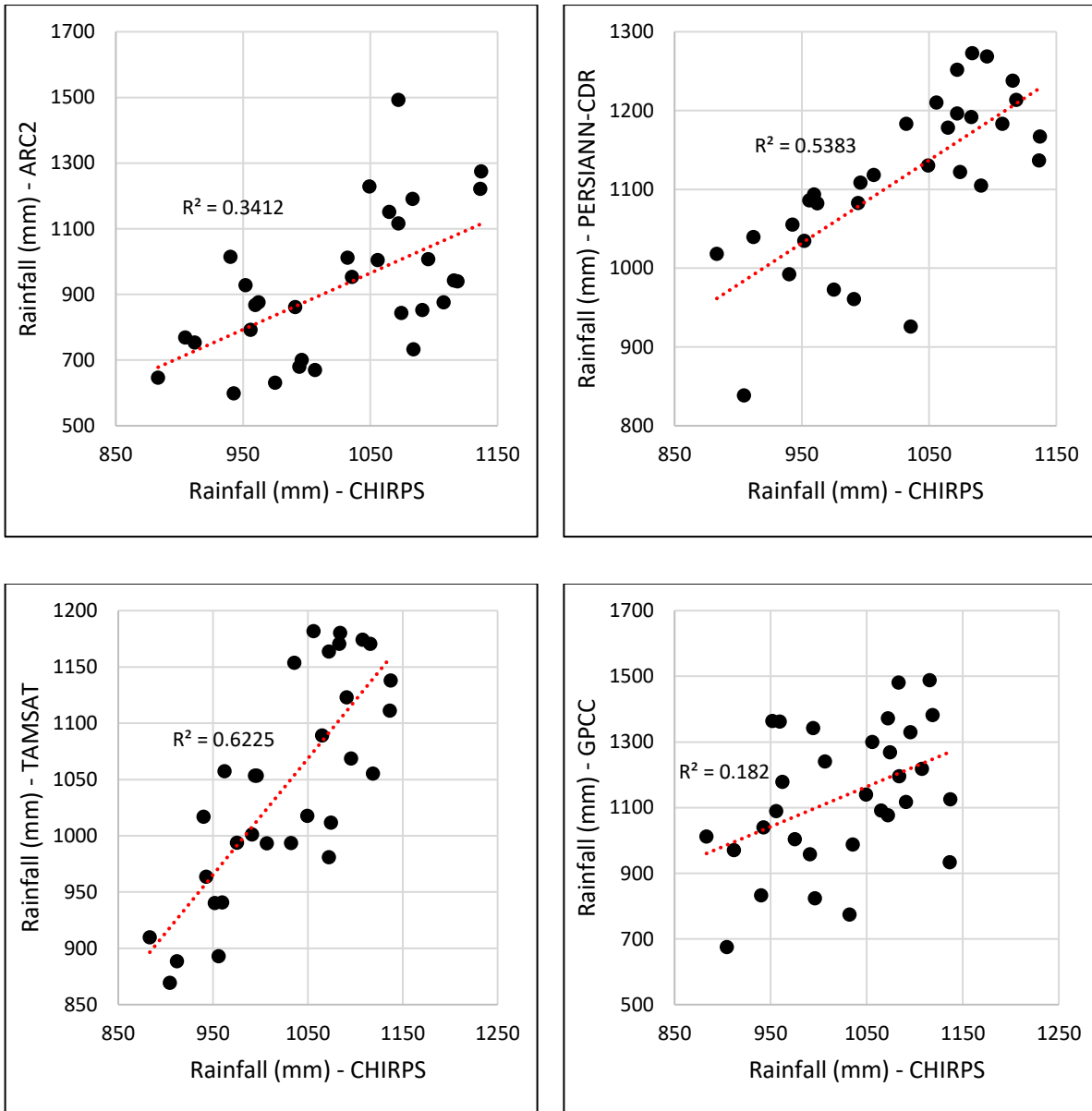


Figure 4.10 Scatter plots - BN

From Table 4. 2 below, TAMSAT and PERSIANN-CDR represent a strong match with CHIRPS with the highest correlation ( $R$ ) and the lowest RMSE. Relatively, ARC2 and GPCC recorded lower fit with CHIRPS. TAMSAT and PERSIANN-CDR have also shown low value of relative variability (low CV), which indicates better performance compared to ARC2 and GPCC (higher CV value). Lastly, the results of the bias ratio demonstrate good agreement of TAMSAT and PERSIANN-CDR with

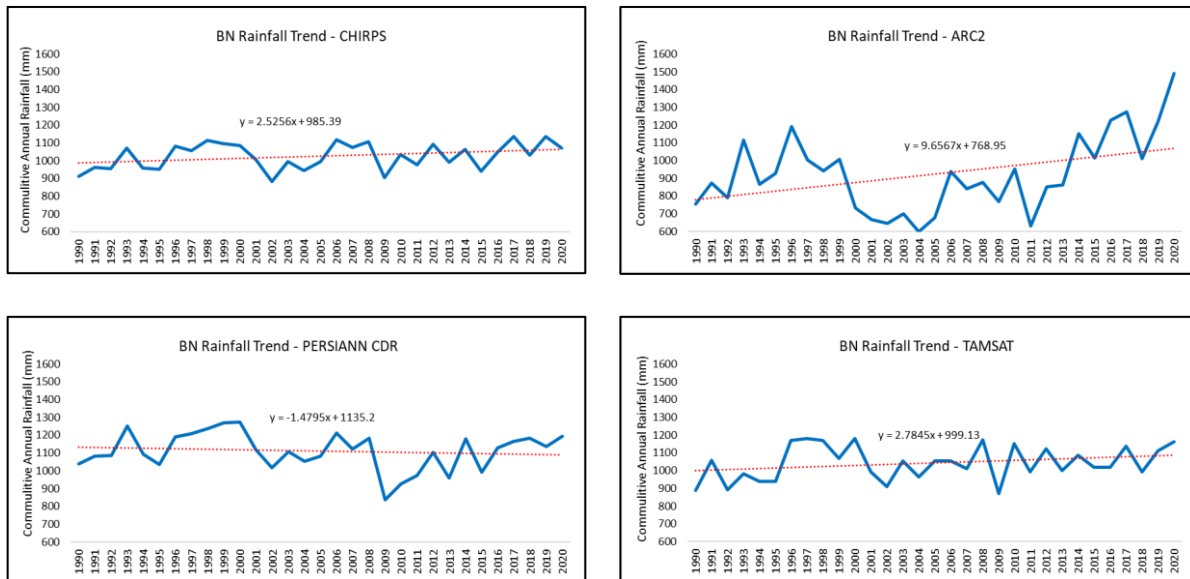
CHIRPS, while showing overestimation and underestimation of rainfall recorded by GPCC and ARC2 respectively.

Table 4. 2 BN rainfall products performance tests

	ARC2	PERSIANN-CDR	TAMSAT	GPCC
<b>Correlation (R)</b>	0.58	0.73	0.79	0.43
<b>Bias Ratio (B)</b>	0.90	1.08	1.02	1.11
<b>Coefficient of Determination (CV) %</b>	3.27	1.32	1.29	2.59
<b>Root Mean Square Error (RMSE) mm</b>	206.7	110.8	60.6	216.1

### 4.3.3 Rainfall Trend

Rainfall trends for the years 1990 -2020 were also plotted for the Blue Nile considering the 5 rainfall products. Looking at Figure 4.11, CHIRPS and TAMSAT have shown a similar rainfall trend with positive mild slope of trendlines which indicates slow increasing trend of rainfall. ARC2 also detected an increasing rainfall trend, but faster than the previous 2 satellites (it also shows decreasing rainfall in the middle years and rising rainfall afterwards). This result is similar to the previous subbasin (BAS). On the other hand, both PERSIANN-CDR and GPCC demonstrated decreasing rainfall over the 31 years. However, GPCC have shown faster negative change in rainfall compared to PERSIANN-CDR which have a minor decrease of rainfall detected from the almost flat rainfall trend.



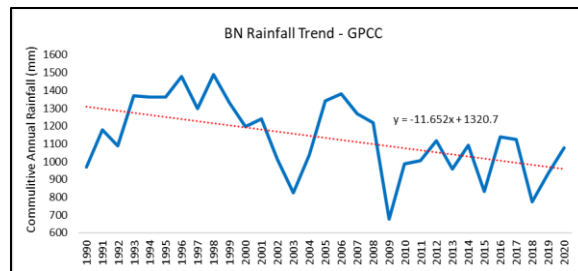


Figure 4.11 Rainfall trends - BN

#### 4.3.4 Rainfall anomalies

The Blue Nile is subjected to some differences in the results of the rainfall anomalies recorded by the different satellites (see Figure 4.12). For CHIRPS, the longest consecutive years with positive rainfall anomalies from 2001 to 2005, while the longest consecutive negative rainfall anomalies are from 1996 to 2000 as well as from 2016 to 2020, which shows the presence of no droughts and occurrence of droughts respectively. The greatest above-average rainfall anomaly occurred in 2002 and highest negative rainfall anomaly occurred in 2019. For ARC2, the longest positive consecutive rainfall anomalies occurred from 2000 to 2010 and the longest negative rainfall anomalies occurred from 2014 to 2020. The greatest below-average rainfall anomaly occurred in 2020. Moreover, PERSIANN-CDR shows that longest period with above-average rainfall was between 2009 – 2013, while the longest consecutive years of below-average rainfall were recorded between 1996 and 2001. The years 2000 and 2009 received the lowest and the highest rainfall compared to average. TAMSAT have shown the longest consecutive positive rainfall anomalies from 1990 to 1995, followed by the longest consecutive negative rainfall anomaly occurred between 1996 to 2000. The greatest above-average rainfall occurred in 2009 and greatest below-average recorded in 2000, 2008 and 2020. Lastly for GPCC, the longest negative and positive consecutive rainfall anomalies were from 1993 to 2001 and 2009 to 2015 respectively.

In conclusion, all satellites recorded the highest rainfall in 2009. Also, all of them agreed on the longest consecutive years of low rainfall from 2001 – 2009, and from 2016 – 2020. However, GPCC showed higher rainfall than average during the last years opposite to the rest of products. The number of the below-average years ranges between 11 and 14 (frequency = 35% - 45%).

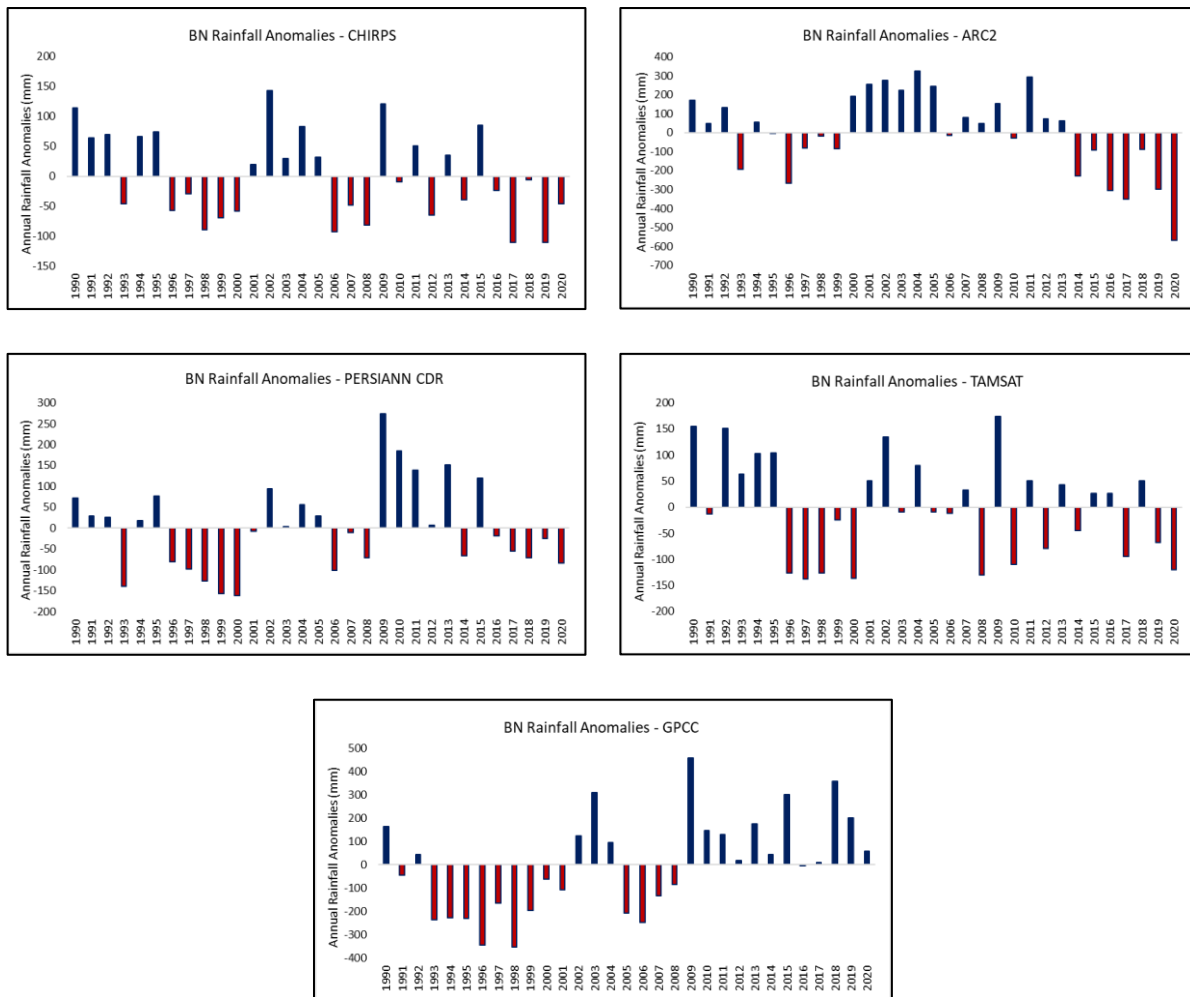


Figure 4.12 Rainfall anomalies - BN

#### 4.3.5 Standardized Precipitation Index (SPI)

Looking at Figure 4.13 below, and considering table 3.1 of this report, the meteorological drought of the Blue Nile over the period 1990 – 2020 can be classified using the SPI values. All satellites showed similar pattern of SPI for the Blue Nile. The first 4 years can be classified as near normal to moderately dry. That is followed by a near normal to severely wet period until 1998. The longest dry period is from 1999 to 2013 (moderately dry), followed by a severely to extremely wet years up to 2020. The years 2005 and 2010 can be considered the driest years, while 2019 and 2020 represent the wettest years over the study period.

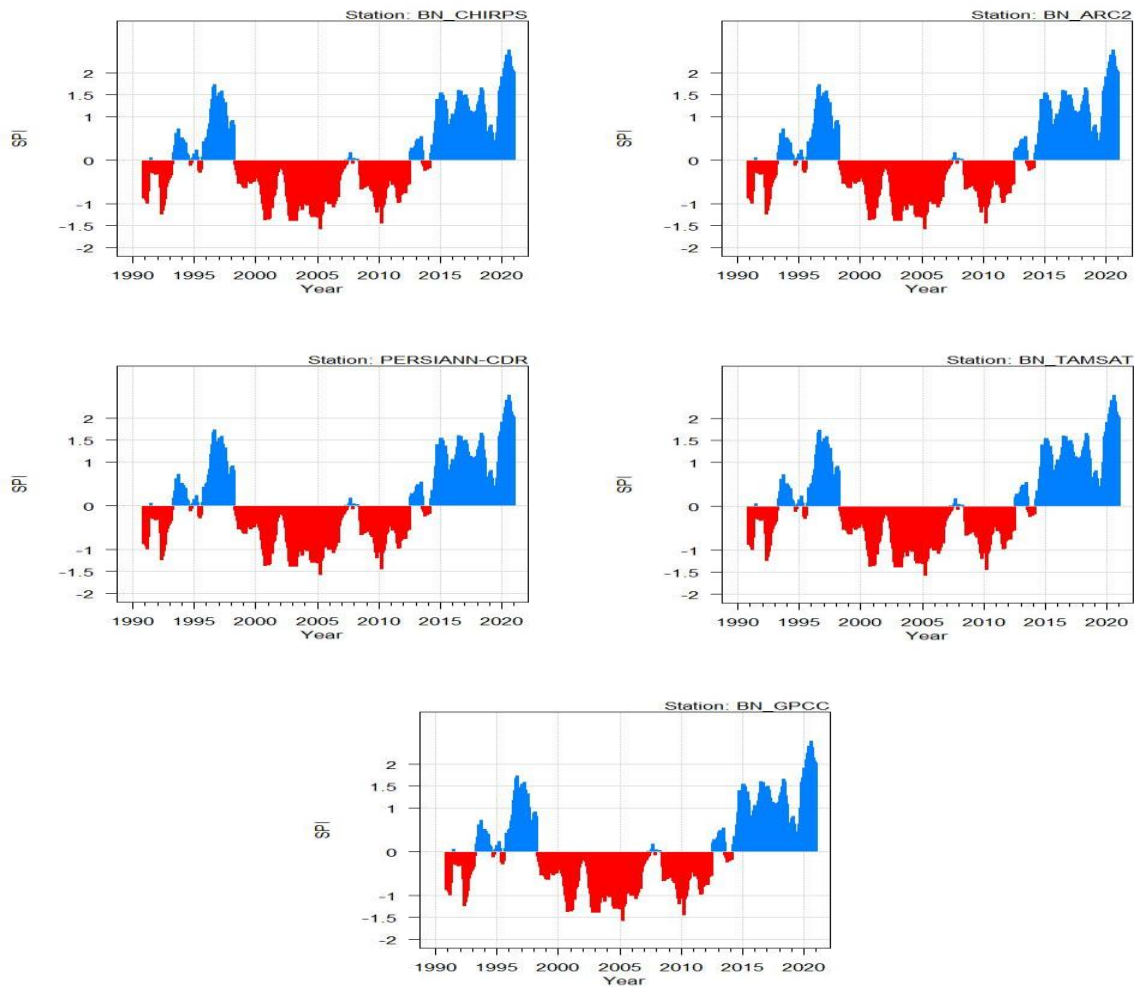


Figure 4.13 Standardized Precipitation Index (SPI) - BN

#### 4.3.6 Rainfall frequency distribution

In the Blue Nile, the different products also show significant differences regarding the frequency distribution of rainfall during the years 1990 – 2020 (see Figure 4.14). Looking at the most frequent rainfall value, CHIRPS and ARC2 underestimated the climatology mean (1000-1100 mm), and the other 3 products managed to detect it. CHIRPS, PERSIANN-CDR, and TAMSAT have shown a negative skewed distributions (more frequent of high values) following Weibul, Gen. Extreme Value and Gumbel distributions respectively. On the other hand, ARC2 followed the Gen. Extreme Value distribution with higher frequency for the lower rainfall values. Lastly, GPCC demonstrated a symmetric distribution (Log-Logistic). All rainfall datasets have not shown long tails, indicating lower frequency of extreme events.

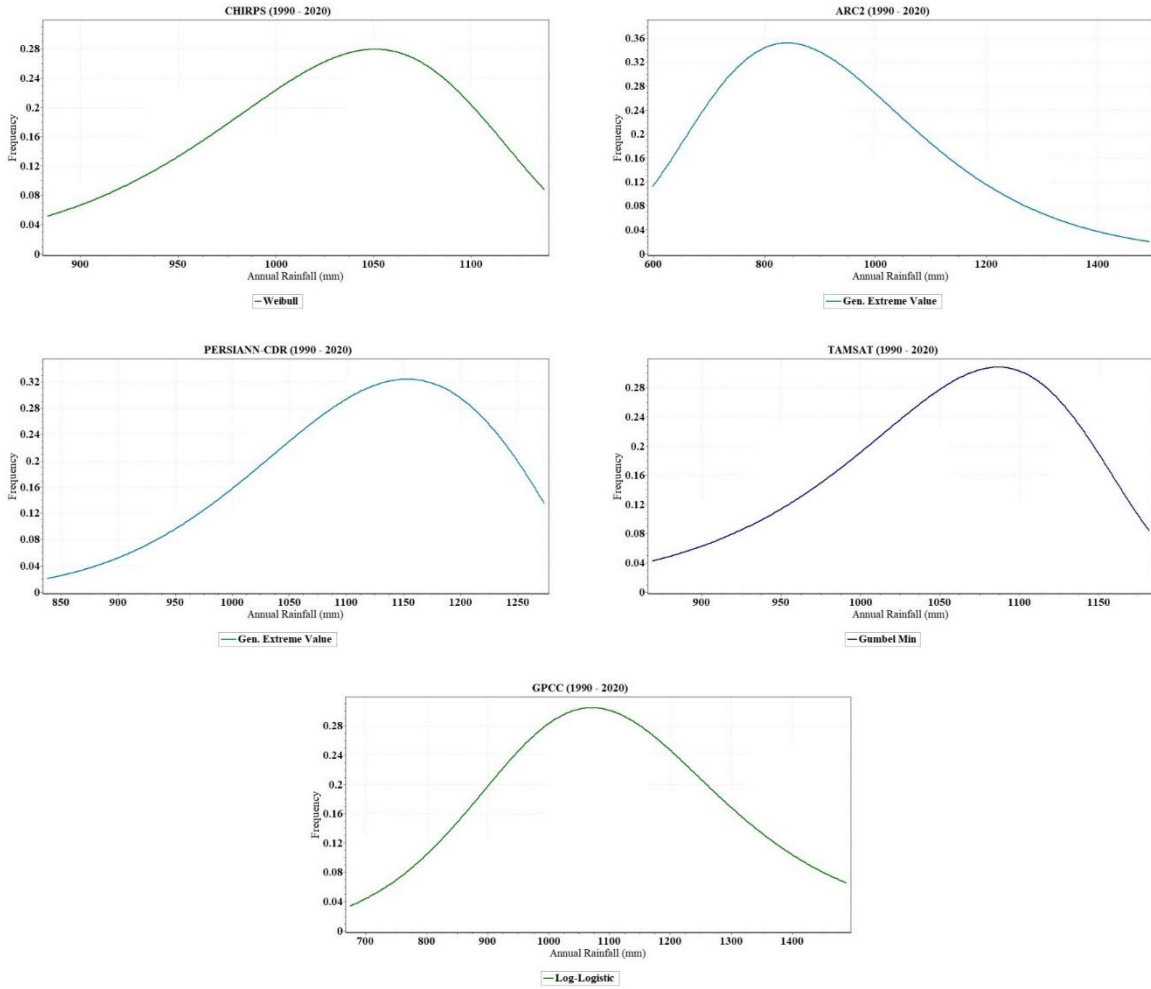


Figure 4.14 Rainfall distribution - BN

#### 4.3.7 Seasonality of rainfall

In the Blue Nile, also long rainy months are observed as shown in Figure 4.15 below. The different satellites agreed on recording similar performance of the monthly rainfall starting from low intensities in April (40 mm), increasing gradually until reaching the peaks during July and August (250 mm), and decreasing gradually again to lower rainfall in October and November. However, CHIRPS recorded slightly lower amounts of monthly rainfall, and ARC2 has shown the lowest estimates of peaks (50 mm less).

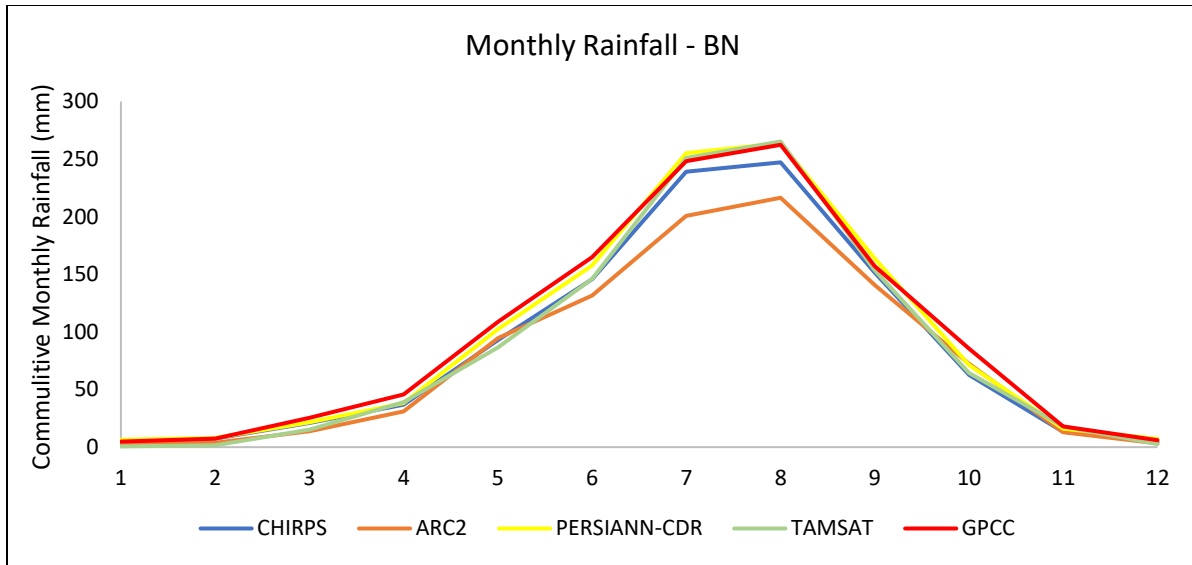


Figure 4.15 Monthly rainfall - BN

#### 4.4 Tekeze-Setit-Atbara

##### 4.4.1 Box Plots

Regarding the annual rainfall distribution over the TSA subbasin (see Figure 4.16), also CHIRPS and TAMSAT showed the best performance and highest consistency. They demonstrated low variability, with similar central tendency (median) that indicates similar rainfall estimate. The variability of PERSIANN-CDR and GPCC are also not high, however, they estimated higher and lower rainfall respectively. ARC2 is considered unreliable as it showed high IQR (rainfall variability).

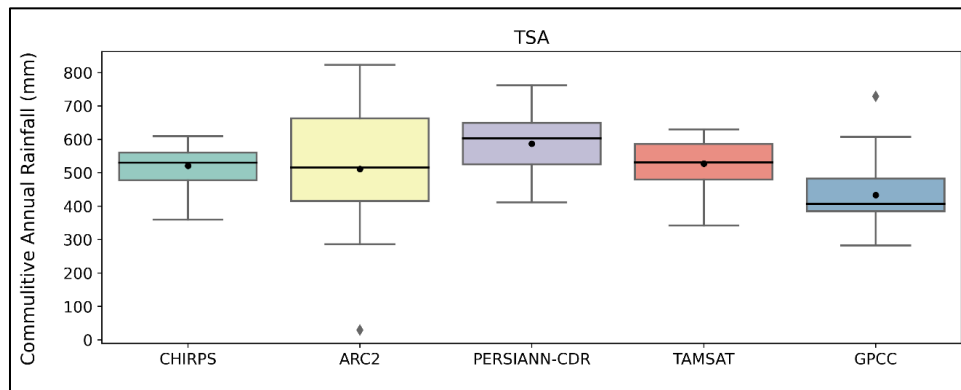


Figure 4.16 Box plots - TSA

##### 4.4.2 Scatter Plots

Figure 4.17 below show the scatter plots that assess how well ARC2, PERSIANN-CDR, TAMSAT, and GPCC rainfall estimates match the CHIRPS data at Tekeze-Setit-Atbara. TAMSAT demonstrated the

highest fit with CHIRPS having coefficient of determination ( $R^2$ ) = 0.73, followed by PERSIANN-CDR ( $R^2$  = 0.64). ARC2 and GPCC provided low fit with CHIRPS with  $R^2$  of 0.3.

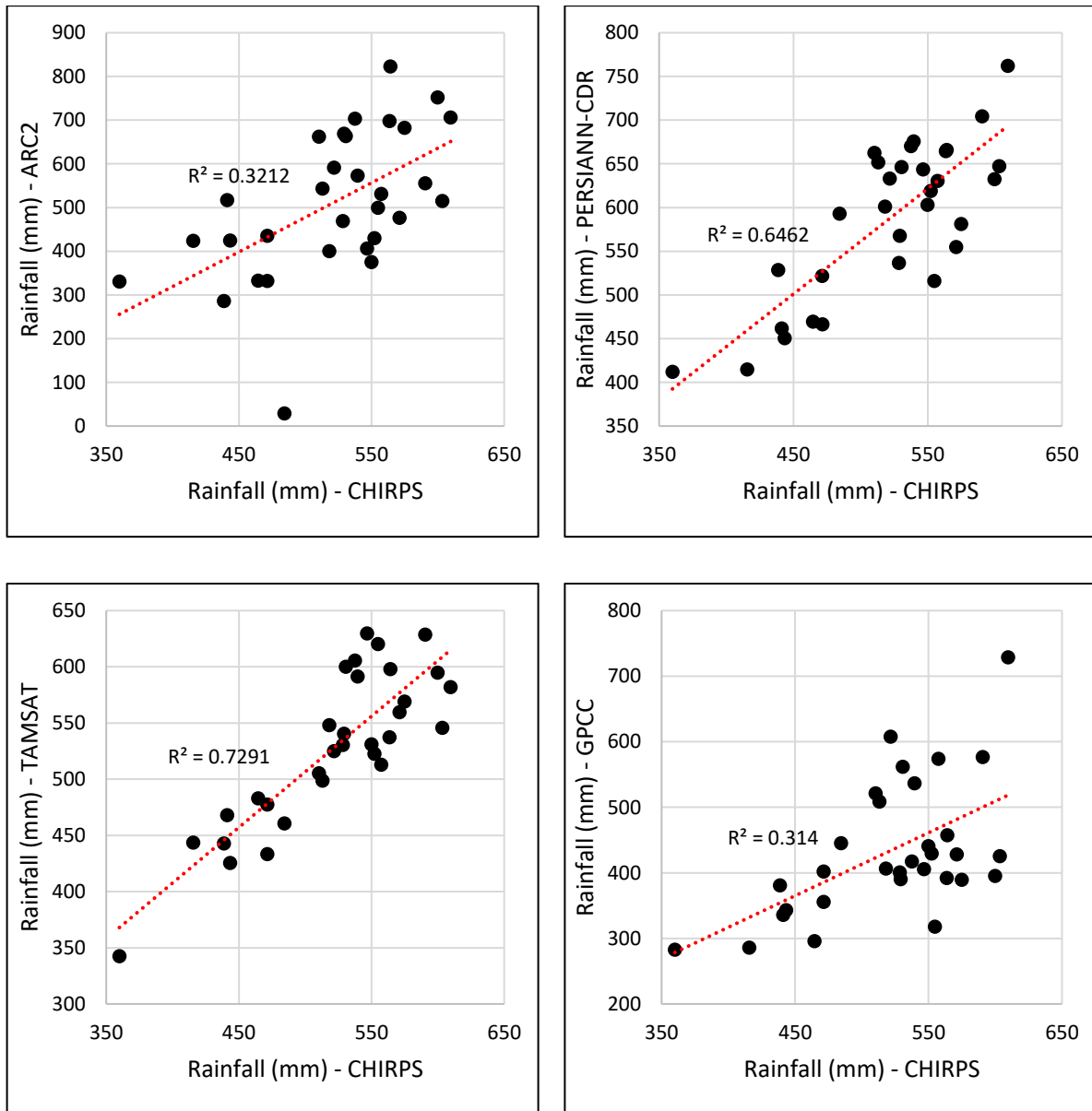


Figure 4.17 Scatter plots - TSA

Using the performance metrics in Table 4. 3 below, TAMSAT and PERSIANN-CDR represent the strongest correlation with CHIRPS (highest R and the lowest RMSE), indicating the best performance. On the other hand, ARC2 and GPCC were found to have weaker match with CHIRPS, thus, poor performance. TAMSAT and PERSIANN-CDR have also shown lower value of coefficient of variation (CV), which indicates better performance compared to ARC2 and GPCC (higher CV value).

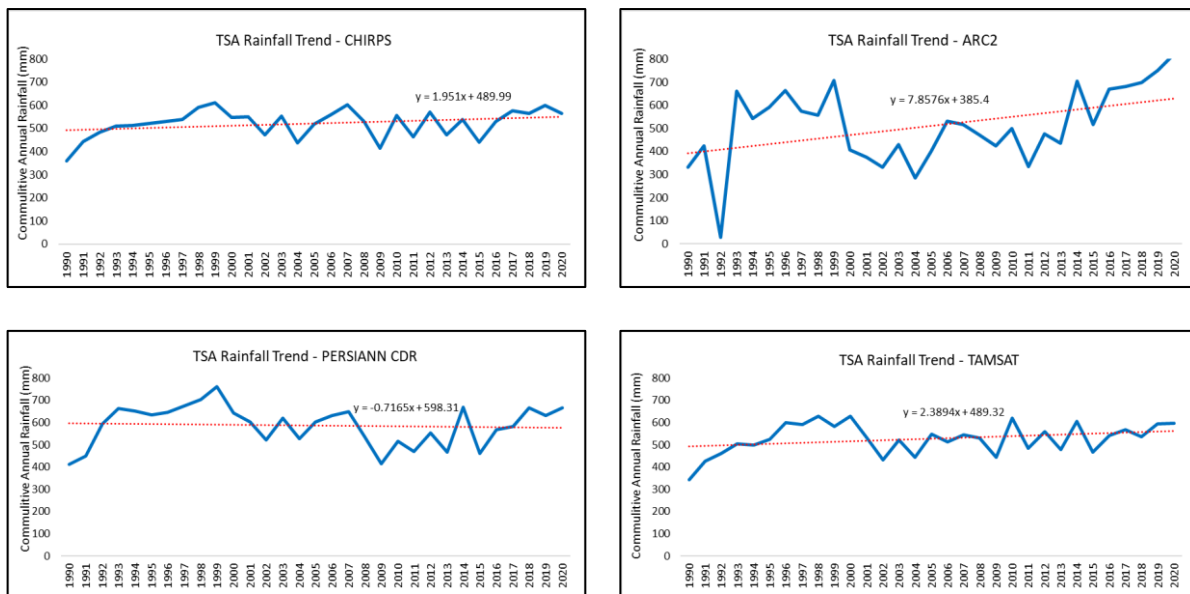
Lastly, the results of the bias ratio demonstrate high agreement of TAMSAT and CHIRPS, and slight overestimation of rainfall recorded by PERSIANN-CDR. In contrast, GPCC and ARC2 were found to underestimate the rainfall amounts.

Table 4. 3 TSA rainfall products performance tests

	ARC2	PERSIANN-CDR	TAMSAT	GPCC
<b>Correlation (R)</b>	0.57	0.80	0.85	0.56
<b>Bias Ratio (B)</b>	0.98	1.13	1.01	0.83
<b>Coefficient of Determination (CV) %</b>	2.85	1.33	1.14	2.06
<b>Root Mean Square Error (RMSE) mm</b>	139.5	84.7	35.9	121

#### 4.4.3 Rainfall Trend

Historical rainfall data of Tekeze-Setit-Atbara subbasin shows uncertainty in detecting the rainfall trends over the years 1990 – 2020 in terms of direction and rate of change. Looking at Figure 4.18, it can be noticed that both CHIRPS and TAMSAT presented positive change of rainfall over the years, with slightly faster increase observed by TAMSAT. On the other hand, ARC2 detected a rapid increase of rainfall between 1990 – 2020 (steeper positive slope of trendline). In contrast, GPCC recorded a decreasing rainfall change over the years. Lastly, PERSIANN-CDR has shown almost a flat rainfall trend which indicates minor or no change of rainfall.



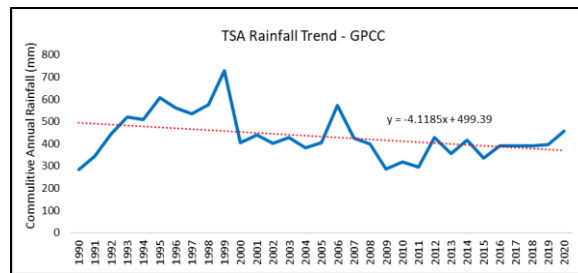
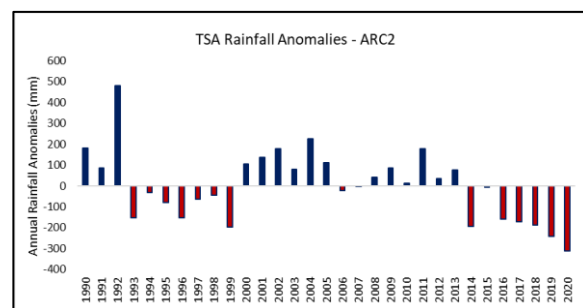
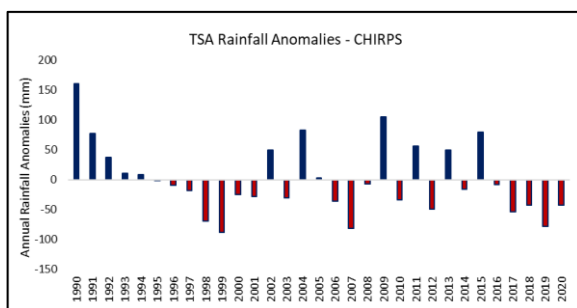


Figure 4.18 Rainfall trends - TSA

#### 4.4.4 Rainfall anomalies

Figure 4.19 illustrates the rainfall anomalies of Tekeze-Setit-Atbara. CHIRPS shows that the maximum positive rainfall compared to average occurred in 1990 and the maximum negative rainfall compared to average occurred in 1999. It also recorded consecutive above-average rainfall years between 1990 – 1995, followed by below average rainfall between 1996 – 2001, and 2017 - 2020. For ARC2, the greatest positive and negative rainfall anomalies occurred in 1992 and 2020 respectively. The longest consecutive years of above-average rainfall were from 2000 -2005 and 1993 – 1999, while the longest below-average years of rainfall were from 2014 to 2020. For PERSIAN CDR the longest negative consecutive rainfall anomalies occurred from 1992 to 2001, and the longest positive consecutive rainfall anomalies occurred from 2008 to 2013. The greatest below-average and above-average rainfall were recorded in 1999 and 2019, which indicates the extreme events occurrence. For TAMSAT, the maximum positive rainfall anomaly occurred in 1990 and the maximum negative rainfall anomaly was recorded in 2000. This satellite shows continuous above-average rainfall between 1990 and 1995, followed by below-average rainfall from 1996 to 2000. GPCC shows different pattern during the last years indicating continuous positive anomalies between 2007 and 2019, with dry years between 1992 and 1999. The driest year was 1999.

To summarize, CHIRPS, PERSIANN, and TAMSAT are showing similar pattern of anomalies approximately. All rainfall products agreed on detecting long below-average rainfall period between 1994 – 2001, with above-average rainfall between 1990 and 1993. Also, all products except GPCC recorded low rainfall during the last 4 years. The number of the below-average years is 15 – 18 (frequency = 45% - 58%).



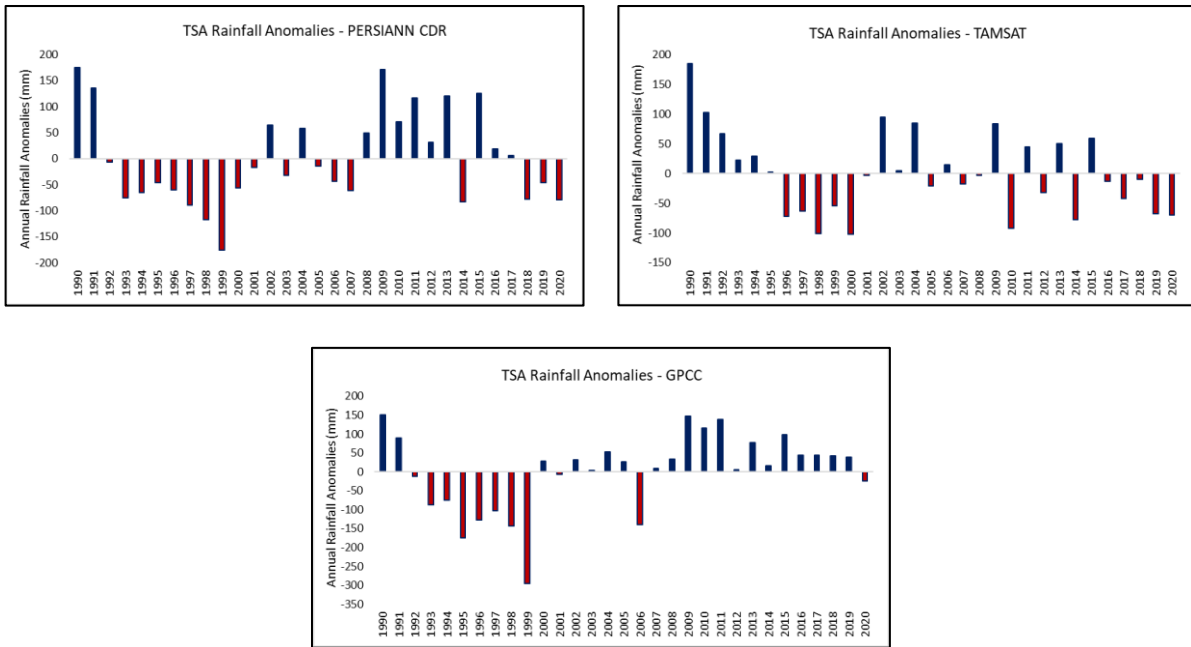
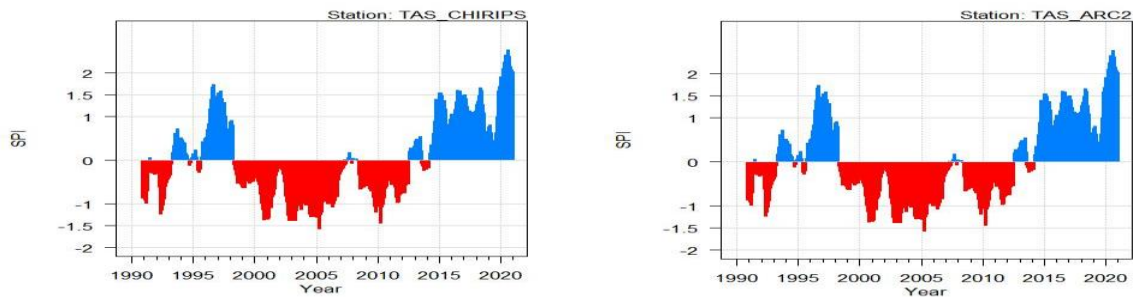


Figure 4.19 Rainfall anomalies - TSA

#### 4.4.5 Standardized Precipitation Index (SPI)

Looking at Figure 4.13 below, and considering table 3.1 of this report, the meteorological drought of Tekeze-Setit-Atbara over the period 1990 – 2020 can be classified using the SPI values. Tekeze-Setit- Atbara demonstrated similar SPI pattern to Blue Nile. The first 4 years can be classified as near normal to moderately dry, followed by near normal to severely wet period until 1998. The longest dry period is from 1999 to 2013 (moderately dry), followed by a severely to extremely wet years up to 2020. The years 2005 and 2010 are the driest years, while 2019 and 2020 represent the wettest years.



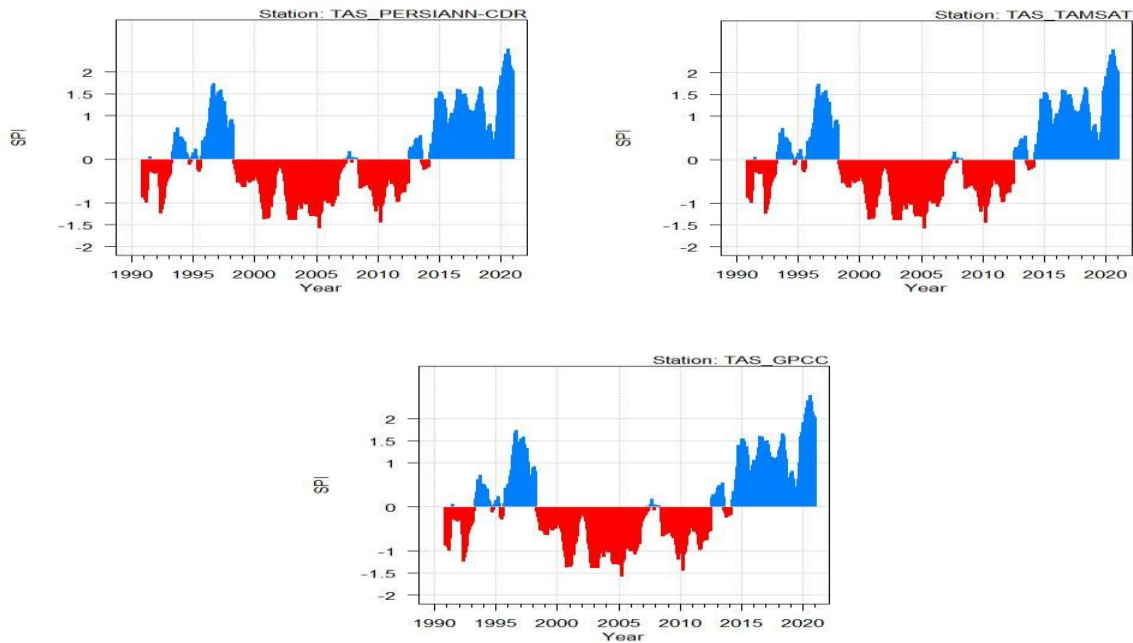
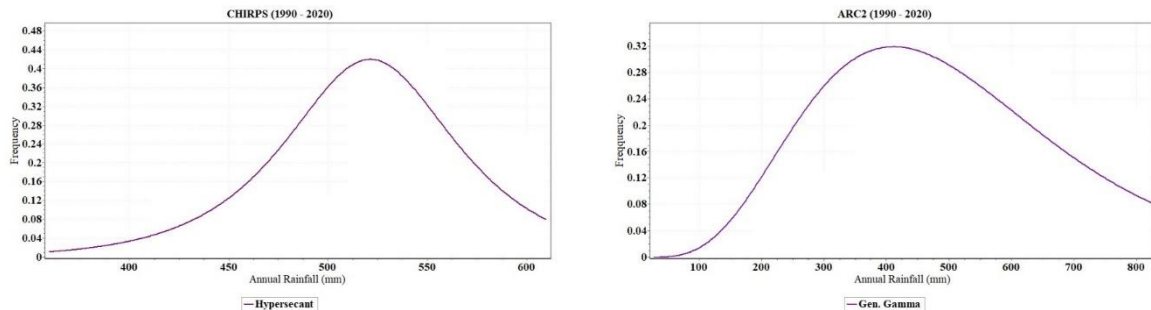


Figure 4.20 Standardized precipitation Index (SPI) - TSA

#### 4.4.6 Rainfall frequency distribution

Regarding the rainfall frequency distribution in Tekeze-Setit-Atbara, also some differences can be observed. The most frequent rainfall recorded by CHIRPS and TAMSAT aligns with the climatology mean of the basin, following Hypersecant and the Gen. Extreme Value distributions respectively. Both satellites show a negative skewed distribution curves that indicates greater frequency for the high rainfall amounts. On the other hand, ARC2, PERSIANN-CDR, and GPCC could not detect the climatology mean accurately, following the Gen. Gamma, Gumbel Min, and Burr frequency distributions respectively. PERSIANN-CDR demonstrated higher frequency for the high rainfall, while GPCC showed the opposite, and ARC2 tended to distribute more symmetrically. All rainfall datasets have not shown long tails, indicating lower frequency of extreme events.



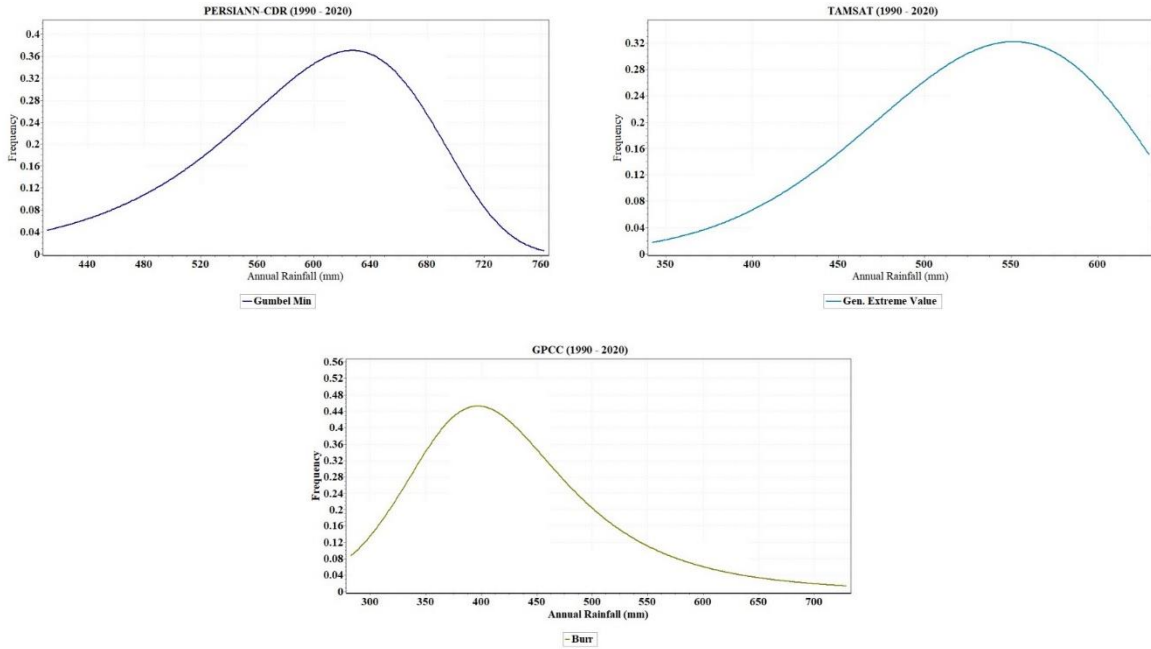


Figure 4.21 Rainfall distribution - TSA

#### 4.4.7 Seasonality of rainfall

The performance of the monthly rainfall of Tekeze-Setit-Atbara is approximately similar to Baro-Akobo-Sobat (see Figure 4.22). Rainfall starts from late March or beginning of April with low amounts (20 mm), increases gradually until it reaches the peak during July and August (190 mm), and decreasing again until October. The different rainfall products have shown matching results in capturing the seasonality, however, differences in the monthly rainfall were observed. GPCC demonstrated the lowest monthly rainfall records along the year.

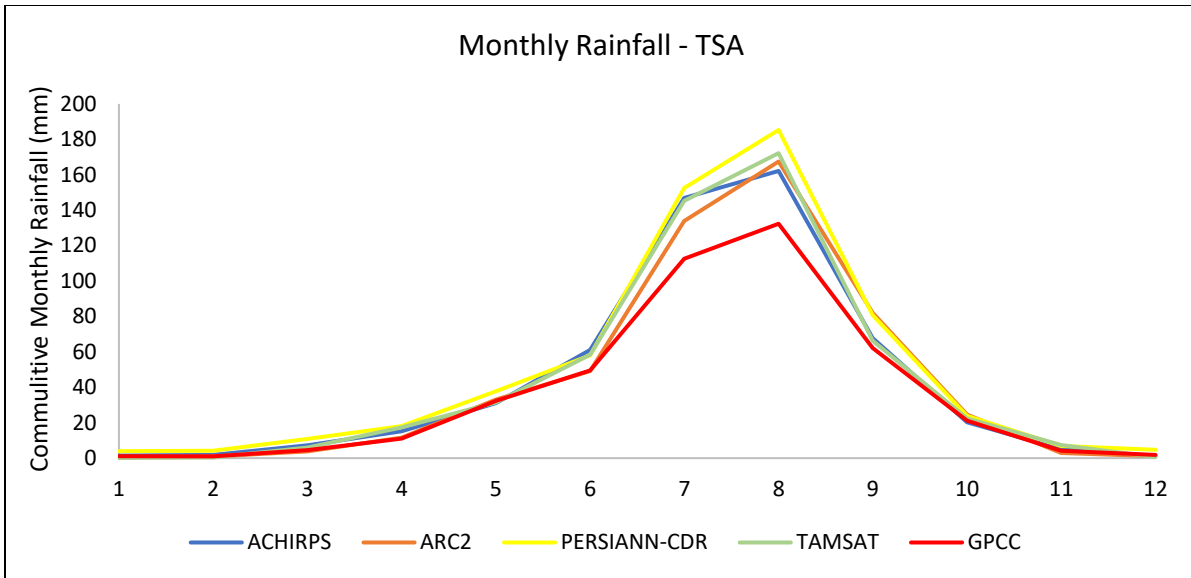


Figure 4.22 Monthly rainfall - TSA

## 4.5 Upper Main Nile

### 4.5.1 Box Plots

Looking at Figure 4.23, similar to the previous subbasins, CHIRPS and TAMSAT have shown the highest consistency and reliability in estimating annual rainfall over the Upper Main Nile. Their good performance is proved by their low variability (IQR). GPCC also show low spreading with lower rainfall estimate (median). It also showed few outliers among the data. Lastly, ARC2 and PERSIANN-CDR demonstrated relatively higher variability with few number of outliers.

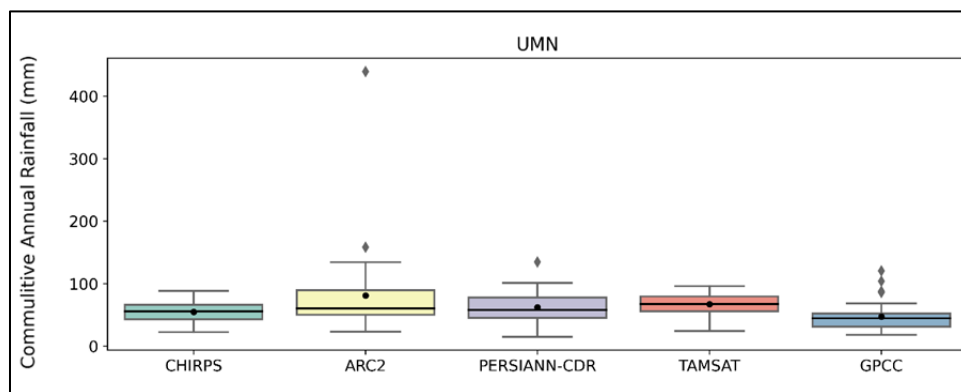


Figure 4.23 Box plots of Upper Main Nile subbasin

### 4.5.2 Scatter Plots

From Figure 4.24 below that shows the scatter plots of the Upper Main Nile, similar result to the previous subbasins can be observed, showing that TAMSAT and PERSIANN-CDR represent the rainfall products with the highest fit with CHIRPS having coefficient of determination ( $R^2$ ) of  $> 0.8$ . ARC2 and GPCC also provided low fit with CHIRPS with  $R^2$  of 0.1 and 0.3 respectively.

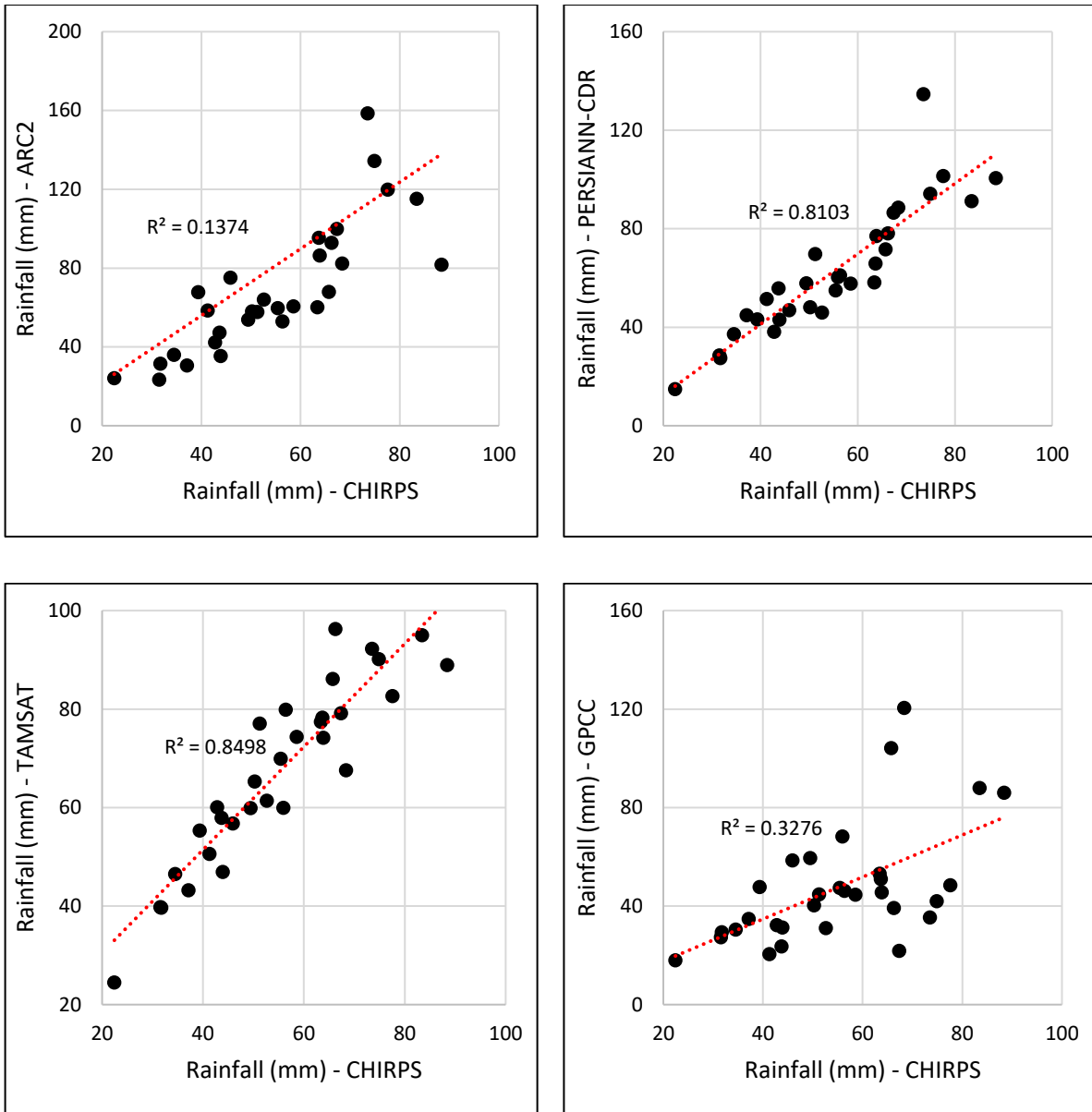


Figure 4.24 Scatter plots of UMN subbasin

By using the performance metrics in Table 4. 4 below and looking at correlation (R) and RMSE, TAMSAT and PERSIANN-CDR were found to have the strongest correlation with CHIRPS, representing the best performance. Conversely, ARC2 and GPCC have weaker correlation with CHIRPS and higher RMSE, thus, poor performance. TAMSAT and PERSIANN-CDR have also shown lower relative variability (low CV), which demonstrates better performance compared to ARC2 and GPCC (higher CV). The bias ratio (B) indicates high overestimation of rainfall recorded by ARC2, and low overestimation by TAMSAT and PERSIANN-CDR. In contrast, GPCC was found to underestimate the rainfall amounts.

Table 4. 4 UMN rainfall products performance tests

	ARC2	PERSIANN-CDR	TAMSAT	GPCC
<b>Correlation (R)</b>	0.37	0.90	0.92	0.57
<b>Bias Ratio (B)</b>	1.48	1.14	1.22	0.86
<b>Coefficient of Determination (CV) %</b>	3.09	1.39	0.93	1.72
<b>Root Mean Square Error (RMSE) mm</b>	73.3	15	14	21

### 4.5.3 Rainfall Trend

The rainfall trend plots of the Upper Main Nile indicate low change in rainfall over the years 1990-2020 as illustrated in Figure 4.25 below. CHIRPS, TAMSAT, and PERSIANN-CDR recorded an increasing trend of rainfall, with faster change observed by the later. On the other hand, GPCC indicated decreasing rainfall, and ARC2 demonstrated almost no change in rainfall.

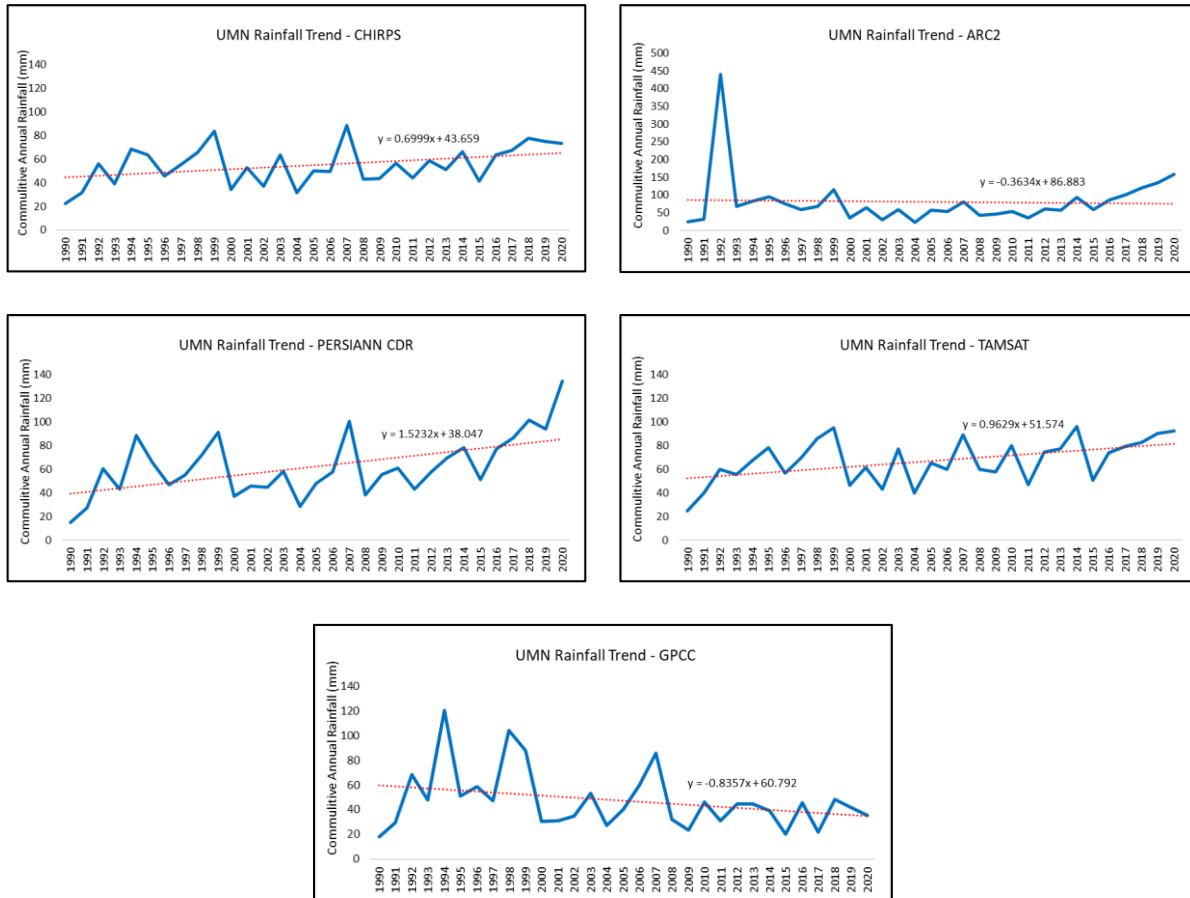


Figure 4.25 Rainfall trends - UMN

#### 4.5.4 Rainfall anomalies

Figure 4.26 illustrates the rainfall anomalies of the Upper Main Nile. It can be noticed that CHIRPS, PERSIANN-CDR, and TAMSAT have shown similar pattern. They detected the longest period of above-average years between 1990 – 1994, 2000 – 2007, and 1990 – 2005 respectively. Moreover, they agreed on recording similar consecutive below-average years between 2019 – 2020. CHIRPS and PERSIANN-CDR recorded the lowest value of rainfall in 2007, while TAMSAT recorded 2014 as the driest year compared to average. 1990 show high rainfall value for the 3 satellites. Coming to ARC2, it shows a very low rainfall in the year 1992, and long consecutive period of above-average rainfall between 2000 and 2015. On the other hand, GPCC performed in a different way, showing long period of below-average rainfall between 1992 to 1999, with 2014 having the lowest value, and long period of above-average rainfall from 2008 – 2020. Generally, the number of below-average years is 11 – 14, with frequency of 35% - 45%.

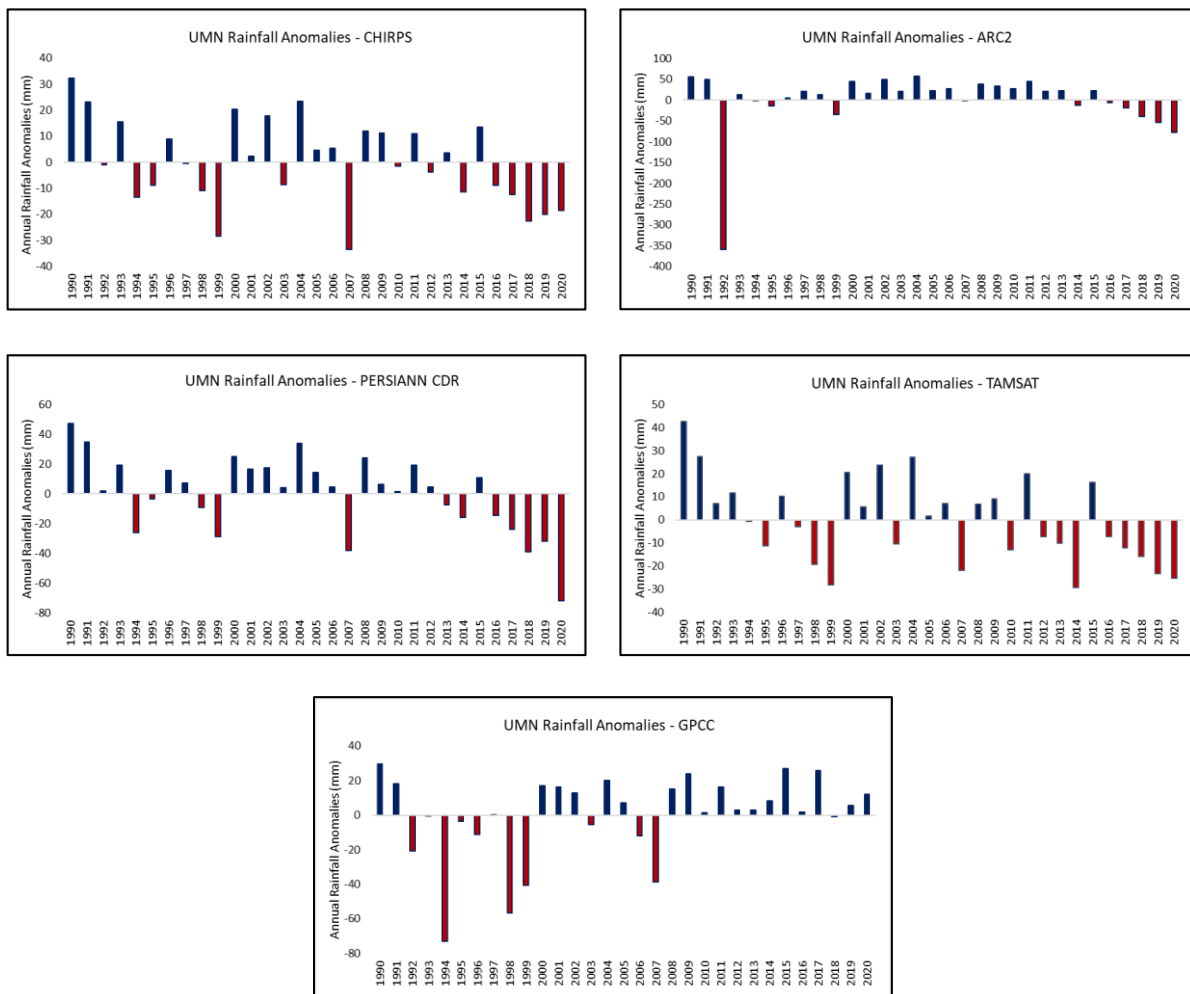


Figure 4.26 Rainfall anomalies - UMN

#### 4.5.5 Standardized Precipitation Index (SPI)

Figure 4.13 show the SPI plots of the Upper Main Nile, that can be used with table 3.1 of this report to classify the meteorological drought over the period 1990 – 2020. In the Upper Main Nile, all satellites generally showed similar pattern of SPI, with few variations recorded by CHIRPS. It can be noticed that the longest dry period is between 1998 to 2012, which can be classified as near normal to moderately dry. That is followed by the longest wet period between 2014 to 2020, ranging from moderately to extremely wet. The years 2005 and 2020 can be considered the driest and wettest years respectively.

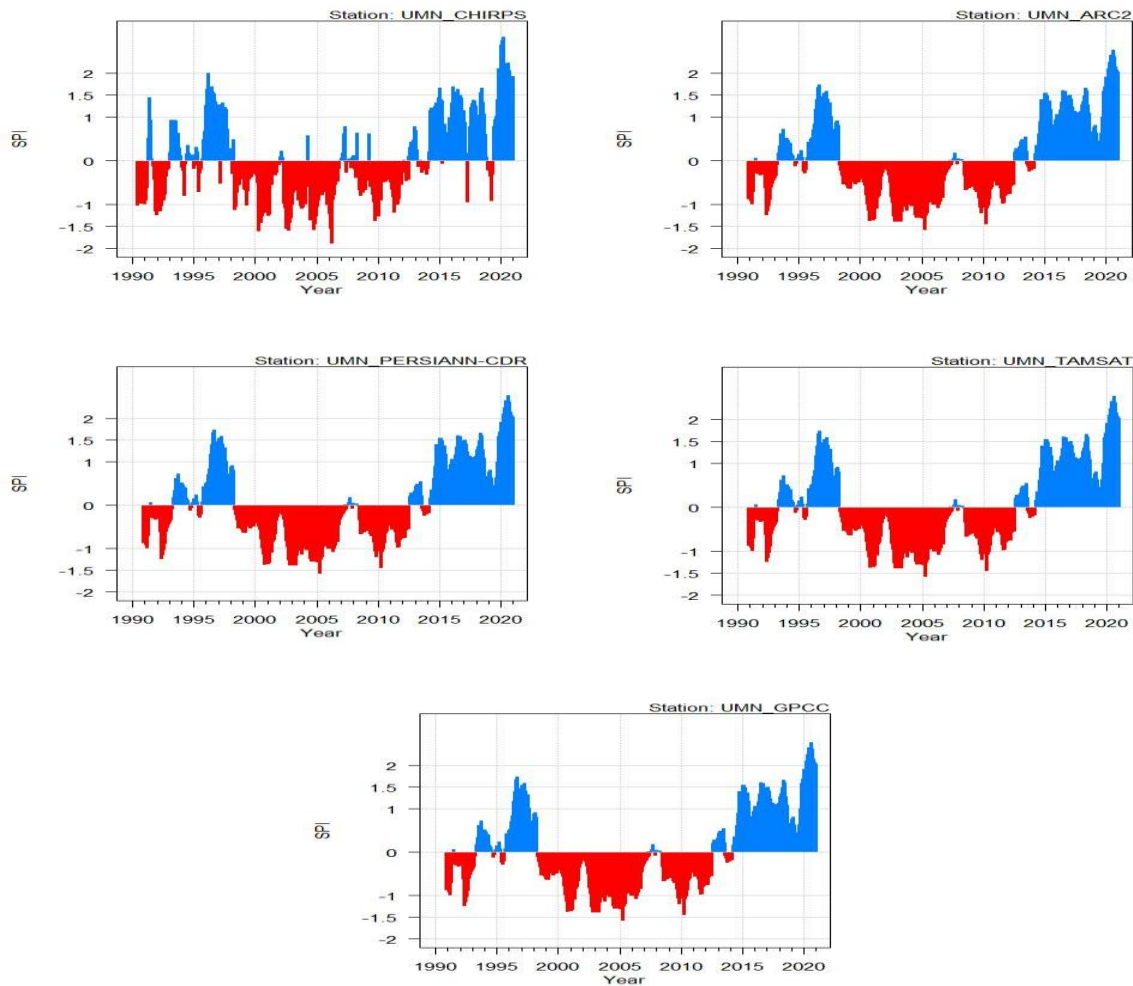


Figure 4.27 Standardized Precipitation Index (SPI) - UMN

#### 4.5.6 Rainfall frequency distribution

Uncertainty can be observed with regards to the rainfall frequency distribution in the Upper Main Nile subbasin. ARC2, PERSIANN-CDR, and GPCC follow a positive skewed curves with higher frequency of the low rainfall intensities, following Rayleigh, Inv. Gaussian, and Weibull distributions respectively. CHIRPS followed Beta distribution with symmetric curve, and TAMSAT

followed the Log-Persons 3 distribution with negative skewness (high frequency the high rainfall intensities). All rainfall products showed most common rainfall values that align with the climatology mean, except TAMSAT, which overestimated it.

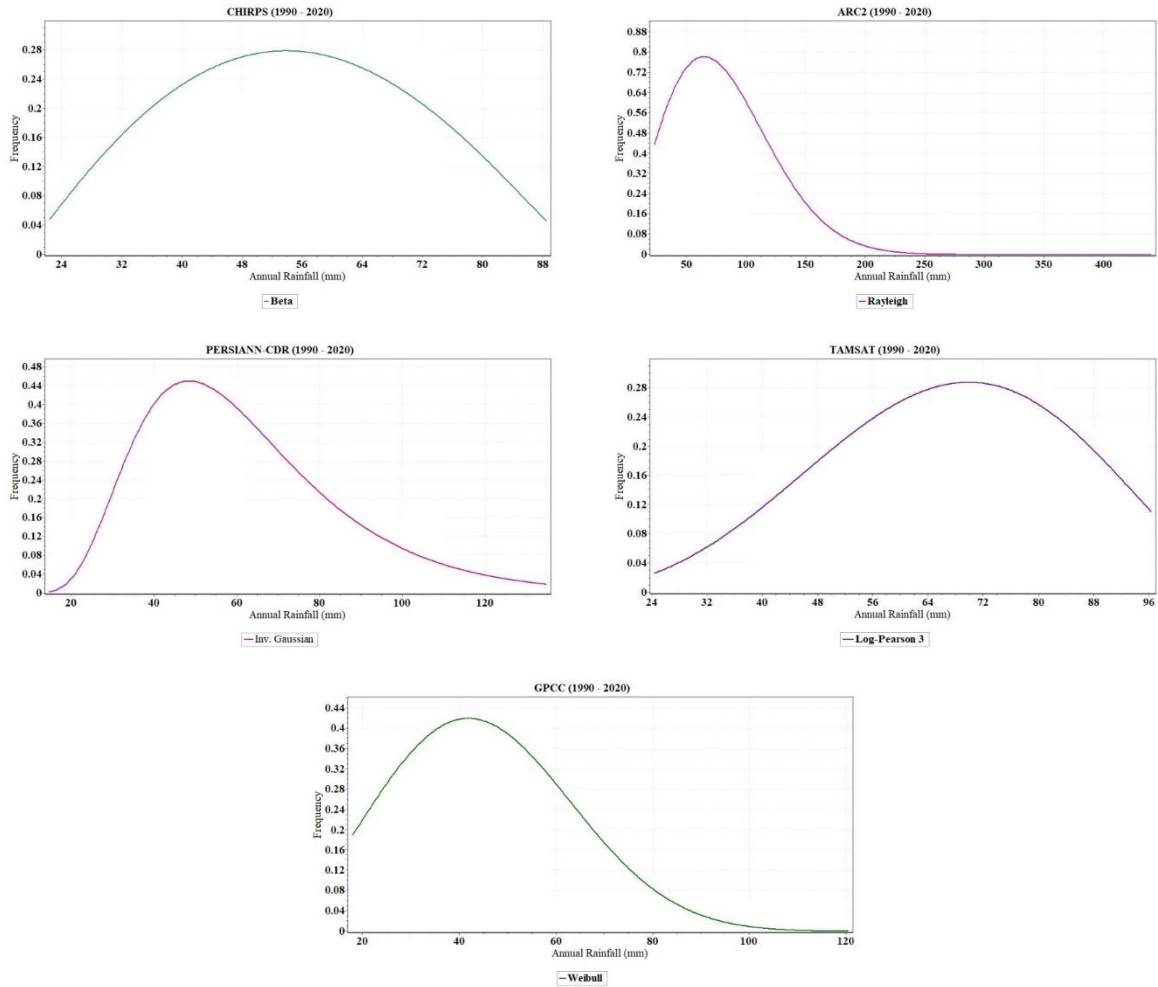


Figure 4.28 Rainfall distribution - UMN

#### 4.5.7 Seasonality of rainfall

Figure 4.29 shows the monthly rainfall of the Upper Main Nile. Generally, the subbasin receives low amounts of rainfall (max is 30 mm), and this may cause uncertainty in estimating the monthly records. As a result, there are differences in the amount of the monthly rainfall captured by the different satellites during the rainy months of July and August (ranges between 15 to 30 mm). In this subbasin, the GPCC recorded the lowest estimate of the monthly rainfall.

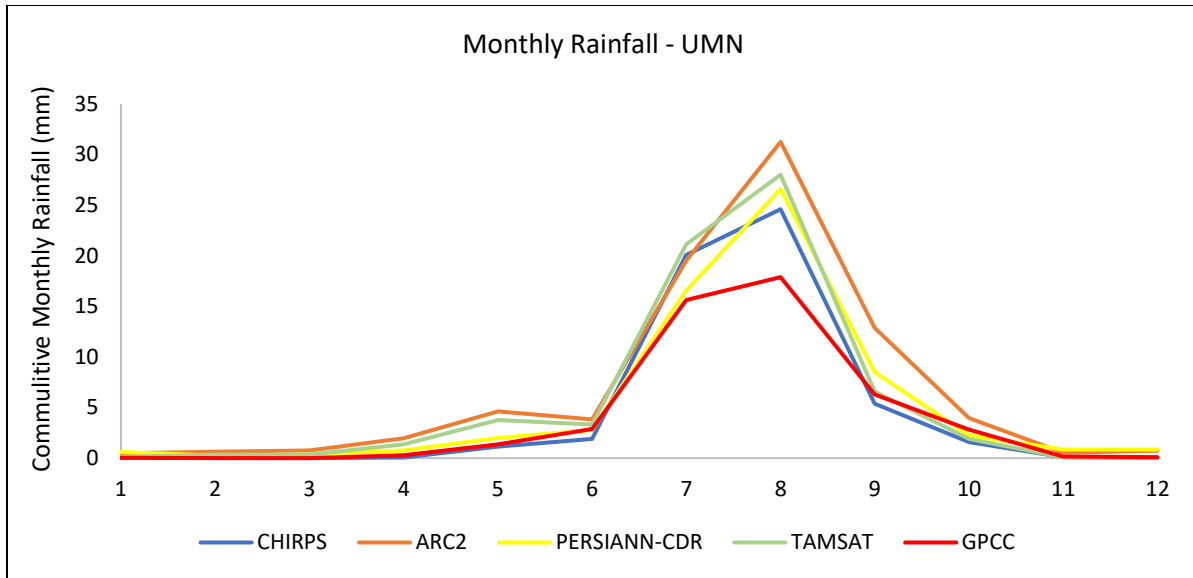


Figure 4.29 Monthly rainfall - UMN

## 4.6 Lower Main Nile

### 4.6.1 Box Plots

The Lower Main Nile presented high uncertainty in the annual rainfall distribution as shown in Figure 4.30. The small IQR of CHIRPS and GPCC indicates that they are the best performing satellites showing low variability, and similar rainfall estimates. The remaining 3 datasets (ARC2, PERSIANN-CDR, and TAMSAT) have shown high spreading of the data. This means they are uncertain and less reliable in estimating annual rainfall.

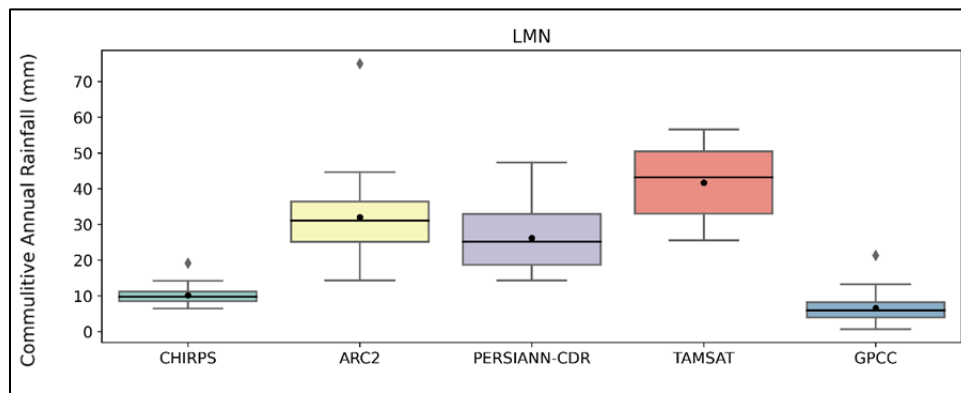


Figure 4.30 Box plots - LMN

### 4.6.2 Scatter Plots

From Figure 4.31 below that shows the scatter plots of the Lower Main Nile, all datasets have shown poor match with CHIRPS rainfall data.

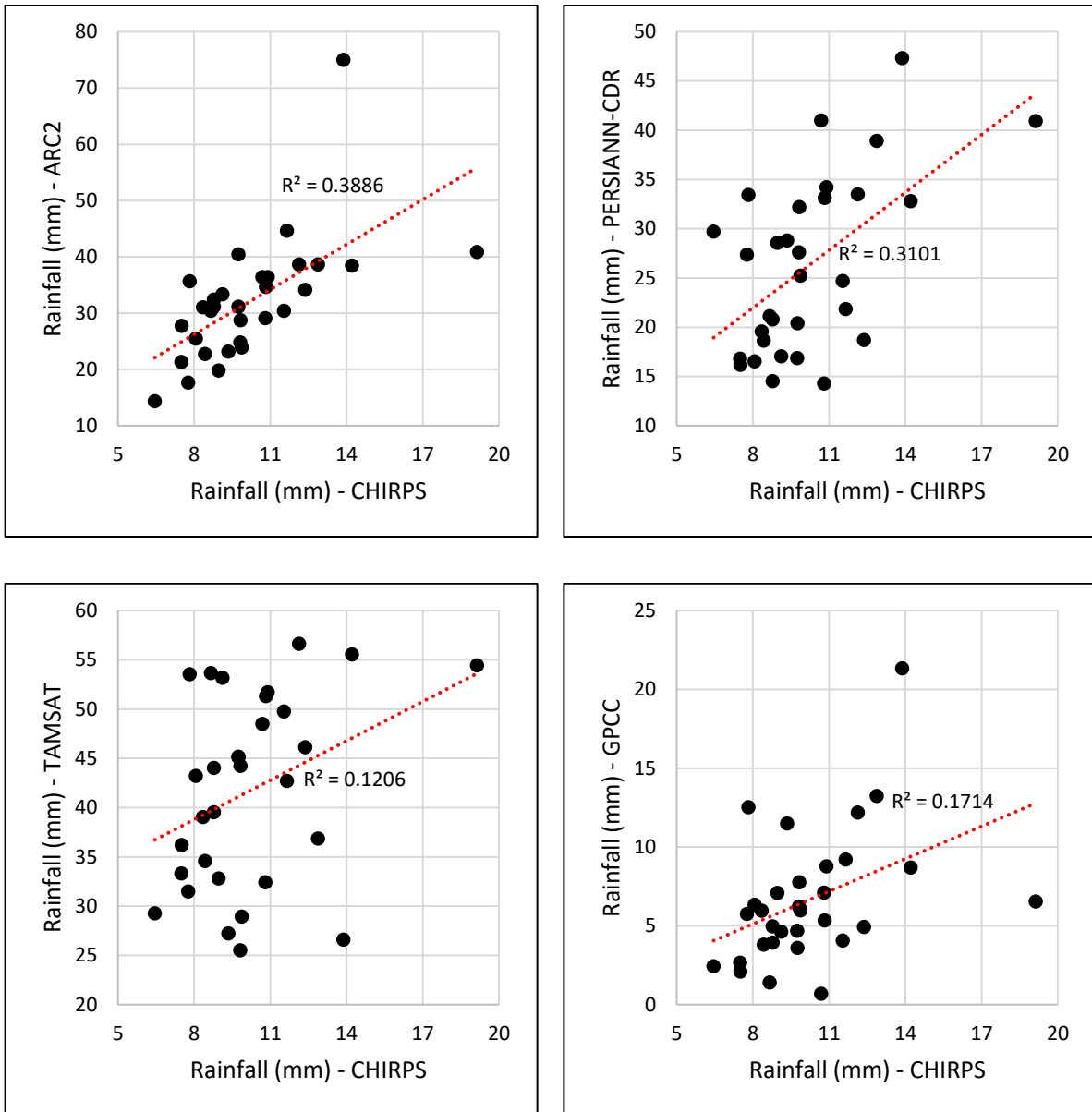


Figure 4.31 Scatter plots - LMN

However, by using the performance metrics in Table 4. 5, values of the correlation (R) and RMSE of TAMSAT and PERSIANN-CDR indicate stronger correlation with CHIRPS, representing the best performance satellites. On the other hand, GPCC followed by ARC2 show weaker correlation with CHIRPS and higher RMSE, thus, poor performance. ARC2 was found to have the highest relative variability compared to the other products. The bias ratio (B) indicates overestimation of rainfall recorded by ARC2, PERSIANN-CDR, and TAMSAT, and underestimation of rainfall observed by GPCC.

Table 4. 5 LMN rainfall products performance tests

	ARC2	PERSIANN-CDR	TAMSAT	GPCC
<b>Correlation (R)</b>	0.37	0.90	0.92	0.57
<b>Bias Ratio (B)</b>	1.48	1.14	1.22	0.86
<b>Coefficient of Determination (CV) %</b>	3.09	1.39	0.93	1.72
<b>Root Mean Square Error (RMSE) mm</b>	73.3	15	14	21

#### 4.6.3 Rainfall Trend

Looking at Figure 4.32, the Lower Main Nile can be categorized by no change or a slightly increasing rainfall over the 31 years under consideration. CHIRPS and GPCC agreed on detecting flat trend, which means no change of rainfall amounts, while ARC2, PERSIANN-CDR, and TAMSAT recorded a slow increase in rainfall between 1990-2020.



Figure 4.32 Rainfall trends – LMN

#### 4.6.4 Rainfall anomalies

Regarding the rainfall anomalies of the Lower Main Nile (see Figure 4.33), All satellites agreed on capturing consecutive years of below-average rainfall during the last 5 years, except TAMSAT

that recorded high rainfall compared to average in 2020. For CHIRPS, the longest consecutive above and below-average rainfall periods were 2005 – 2011, and 2016 – 2020 respectively, with 2016 as the driest year. ARC2 shows dry years from 1991 to 1996, followed by equal or above-average period between 1997 – 2012, and another dry period compared to average between 2016 and 2020, with 2020 as the driest year relatively. The longest above-average rainfall period detected by PERSIANN-CDR was from 2001 – 2009, followed by drier continuous years in 2010 – 2020. TAMSAT showed variation in the pattern with the longest wetter period 1999 – 2003, and the longest drier years in 2014 to 2019. Lastly, the anomalies of GPCC recorded a long above-average rainfall period between 1998 – 2012, and 2020 recorded the greatest below-average rainfall year. All satellites show dry period compared to average during the last 3 to 6 years. The number of below-average years ranges between 9 to 16, , with frequency of below-average years= 29% - 51% (high uncertainty).

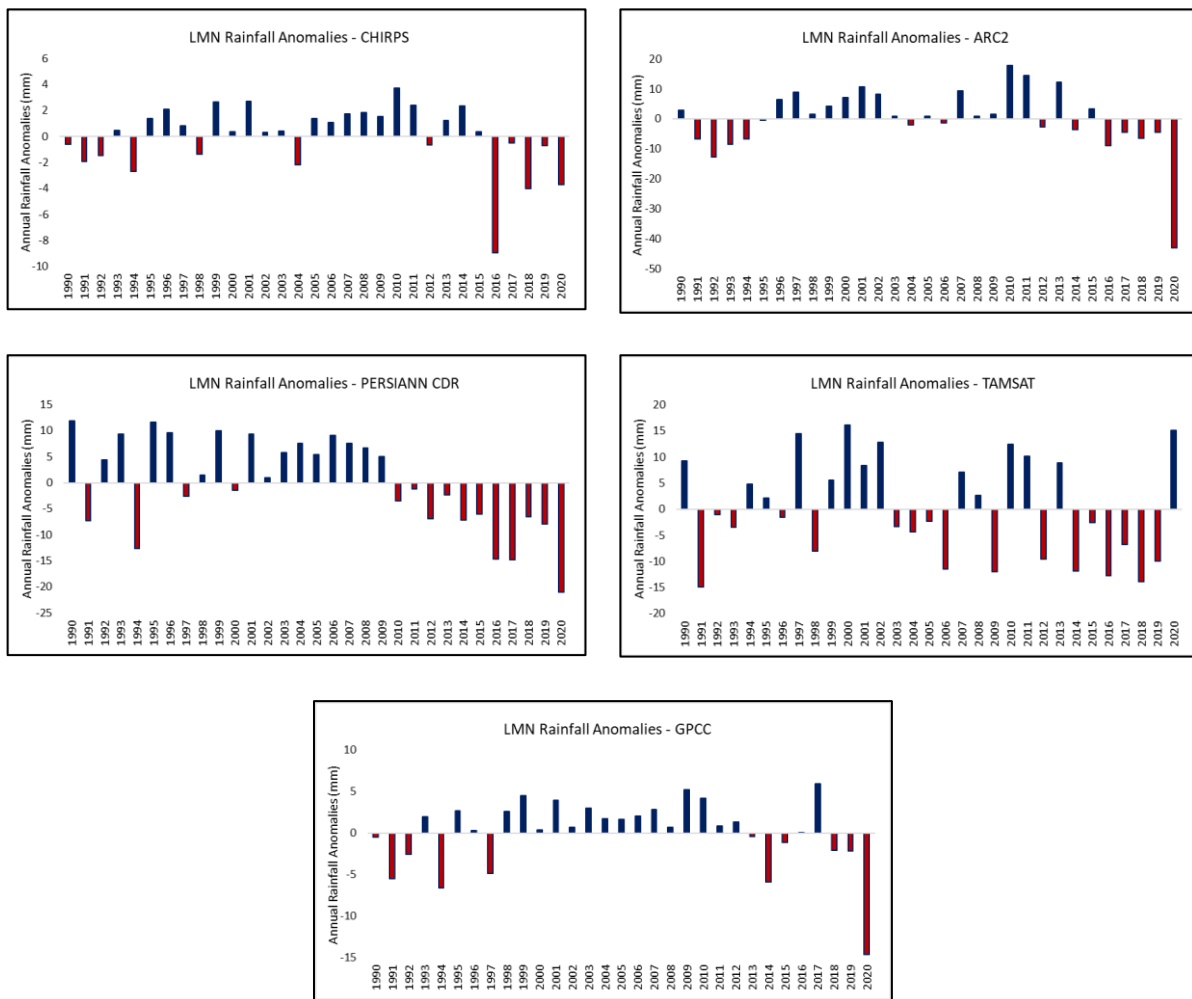


Figure 4.33 Rainfall anomalies - LMN

#### 4.6.5 Standardized Precipitation Index (SPI)

Figure 4.34 show the SPI plots of the Lower Main Nile, that can be used with table 3.1 of this report to classify the meteorological drought over the period 1990 – 2020. CHIRPS, TAMSAT, and GPCP recorded the same pattern of SPI, with the longest wet period from 2013 to 2020 (moderately to extremely wet). It can be noticed that 2010 and 2020 are the driest and wettest years respectively. On the other hand, ARC2 and PERSIANN-CDR showed similar SPI to each other, with the longest near normal to moderately dry period from 1998 to 2012, followed by the longest moderately to extremely wet period from 2013 to 2020.

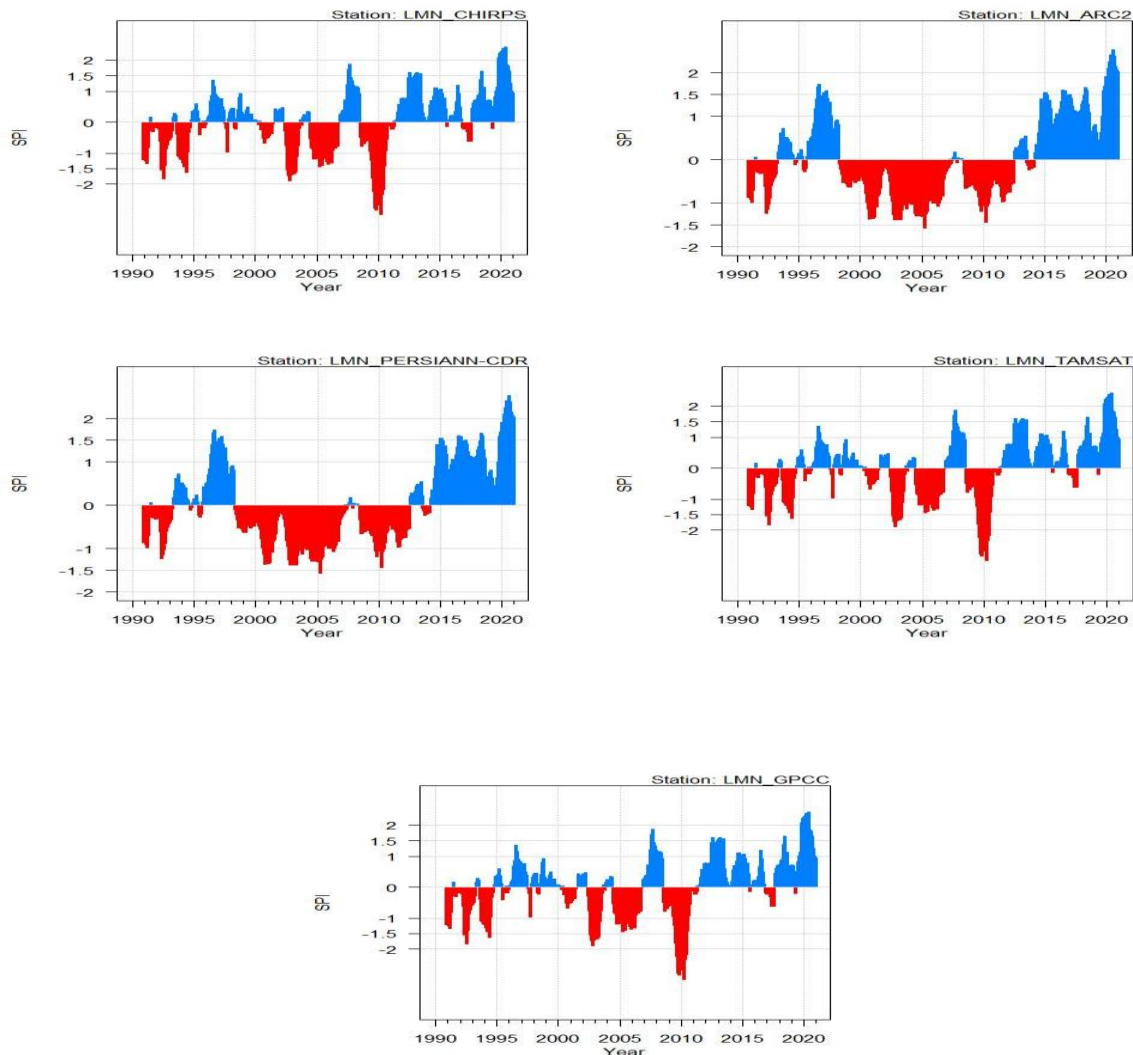


Figure 4.34 Standardized Precipitation Index (SPI) - LMN

#### 4.6.6 Rainfall frequency distribution

In the Lower Main Nile subbasin, CHIRPS, ARC2, PERSIANN-CDR, and GPCP have shown higher frequency for the low rainfall values (positive skewness), following the Pert, Logistic, Burr 4P, and Rice frequency distributions respectively. On the other hand, TAMSAT demonstrated higher

frequency for the high rainfall values following Pert distribution with negative skewness. Only CHIRPS and GPCC managed to align with the climatology mean of rainfall (peak of curves or most frequent rainfall). The other 3 products overestimated rainfall.

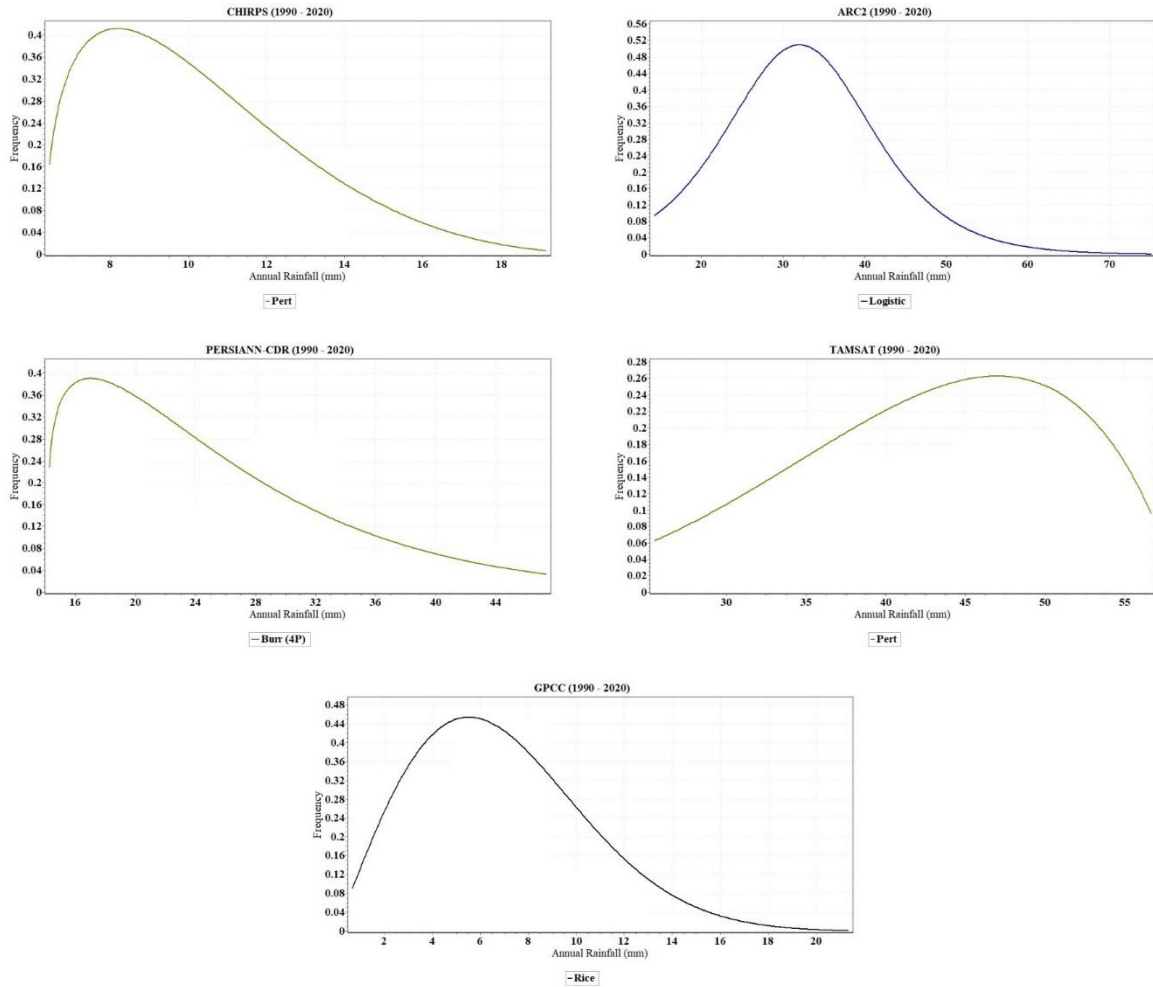


Figure 4.35 Rainfall distribution - LMN

#### 4.6.7 Seasonality of rainfall

The different rainfall products failed in detecting the seasonality of rainfall in the Lower Main Nile (see Figure 4.36), and that can be attributed to the very low values of rainfall that the subbasin receives. Although the subbasin is generally dry almost all of the year, some of the northern parts receive rain during January and February, and high uncertainty can be noticed in the satellites' estimations.

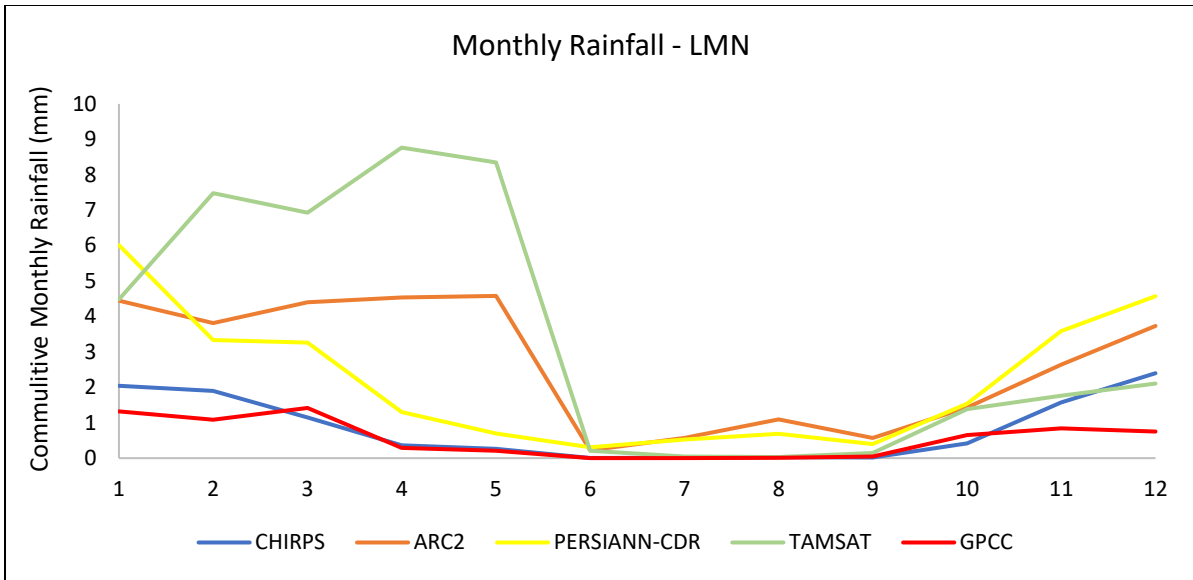


Figure 4.36 Monthly rainfall - LMN

## 5 Conclusion

Historical rainfall data for the Eastern Nile Basin with its four subbasins; Blue Nile, Baro-Akobo-Sobat, Tekeze-Setit-Atbara, and the Main Nile, was analyzed to understand the rainfall trends in the region, which plays a major role in water resources management and development. The years 1990 – 2020 were considered for analyzing the rainfall patterns and distribution. Due to the limitation on the availability and the uncertainty in the ground observation data, rainfall data was acquired from 5 open-source rainfall satellite products; namely, CHIRPS, ARC2, PERSIANN-CDR, TAMSAT, and GPCC. The selection of the five datasets among the available products was based on literature review according to their performance, the spatial and temporal resolution, the spatial coverage, and the data record length. Data quality check and correction was performed for the downloaded data before the analysis.

On the analysis, CHIRPS was taken as a reference for comparison as it showed the best performance compared to ground observations over East Africa according to literature and applications. This can be attributed to the fact that CHIRPS is blended and correlated with station data to improve its quality. Different statistical and spatial techniques were conducted to analyze the historical rainfall data. Those techniques included producing the spatial distribution maps for the whole Eastern Nile Basin to understand the spatio-temporal distribution of rainfall, and have initial insights about the trends and changes taking into consideration the observations of the different rainfall products. The basin was found to receive amounts of annual rainfall ranging between 0 mm rainfall at the northern part of the basin (north Sudan and Egypt) to around 1500 mm at the south-eastern area of the basin (the highlands of Ethiopia and parts of South Sudan). Blue Nile and Baro-Akobo-Sobat received the highest rainfall intensity (700 mm to 1500 mm and 400 mm to 1400 mm respectively), followed by Tekeze-Setit-Atbara (200 mm to 1200 mm), with low to very low rainfall at the Upper and Lower Main Nile (0 mm to 250 mm). Differences were observed when comparing the spatial distribution maps of the 5 products considering 10-year average of rainfall. From 1990 – 2010, GPCC and PERSIANN-CDR demonstrated higher annual rainfall intensity compared to the other 3 satellite products, while in 2011 – 2020, CHIRPS and TAMSAT showed the highest estimation. ARC2 presented the lowest estimation for the study period. This can be attributed to the spatial resolution of the rainfall products, the algorithms used and the assumptions considered for each satellite dataset.

In Baro-Akobo-Sobat, the rainfall products were found to follow different distributions. CHIRPS and TAMSAT showed the best performance and highest consistency among the datasets, and ARC2 was found to have the worst performance. Considering the statistical metrics, TAMSAT has shown the strongest correlation and match to CHIRPS. All rainfall products have indicated increasing rainfall trend over the years between 1990 to 2020, with different rate of change, except GPCC that showed a fast-decreasing trend. Generally, most of the satellites recorded the

period between 2002 – 2007 as dry with different intensities (moderately to severely), and the last five years 2016 – 2020 as moderately to extremely wet, considering the SPI.

The rainfall data of the 5 products in the Blue Nile also followed different distributions. Similar results to Baro-Akobo-Sobat were observed in the Blue Nile, as CHIRPS followed by TAMSAT also represent the best performance datasets. However, GPCC recorded the lowest performance. Satellites have shown uncertainty in observing the rainfall trend. PERSIANN-CDR and GPCC observed decreasing trend of rainfall, in contrast to CHIRPS, TAMSAT. Moreover, SPI shows that the longest dry period is from 1999 to 2013 (moderately dry), followed by the longest severely to extremely wet years up to 2020.

In Tekeze-Setit-Atbara subbasin, the rainfall distribution of satellites show that they performed similar to the previous subbasins, having CHIRPS and TAMSAT as the best performance and highest consistency products, and ARC2 as the lowest. However, the statistical metrics show that PERSIANN-CDR performed better than TAMSAT compared to CHIRPS. About the trend, 3 out of the 5 products show rising rainfall trend (CHIRPS, TAMSAT, and ARC2), opposite to PERSIANN-CDR and GPCC. Additionally, similar to Blue Nile, SPI shows that the longest dry period is from 1999 to 2013 (moderately dry), followed by the longest severely to extremely wet years up to 2020.

Over the Upper Main Nile, there is uncertainty in evaluating the performance of the satellites. CHIRPS followed by TAMSAT and GPCC can be considered as the best performing satellites considering the rainfall distribution. However, by looking at the statistical metrics, PERSIANN-CDR performed better than GPCC. In both cases, ARC2 did not perform well. Three out of the satellites recorded an increasing trend of rainfall with different rates. Furthermore, according to SPI, the longest dry period is between 1998 to 2012 (near normal to moderately dry), followed by the longest wet period between 2014 to 2020 (moderately to extremely wet).

Lastly, the Lower Main Nile presented high variability in the annual rainfall distribution of the 5 rainfall products. CHIRPS and GPCC were found to be the best performing products considering their distribution. Nevertheless, the statistical metrics have shown uncertainties in evaluating the best performing satellite, but generally ranking the GPCC performance to be the third. This high uncertainty in the Lower Main Nile can be attributed to the zero to very low rainfall amounts that it receives, which makes it difficult for the satellites and algorithms to detect and develop accurate estimations. This subbasin can be considered to have no change or a slightly increasing rainfall over the 31 years according to the satellites' records. According to SPI, the longest wet period was recorded from 2013 to 2020 (moderately to extremely wet), while the longest dry period was found to be between 1998 – 2011 (near normal to moderately dry).

In conclusion, generally CHIRPS and TAMSAT can be classified as the best performing satellite rainfall datasets over the Blue Nile, Baro-Akobo-Sobat, Tekeze-Setit-Atbara, and the Upper Main Nile. For the Lower Main Nile, there is uncertainty in ranking the performance of the satellites,

but CHIRPS and GPCC can be considered the best. Focusing on the results of the best performing satellites, the study has demonstrated that the Eastern Nile Basin have shown an increasing rainfall trend with different rates over the period 1990 – 2020. Satellite agreed on recording the period 2000 - 2010 as the longest dry period, and the period 2015 – 2020 as the longest wet period according to SPI.

The results of this study provide important inputs for all water resources management related sectors, and can be used by the different stakeholders, and policy makers for research, as well as for to informing decision-making process.

## 6 Recommendations

The following points are recommended as continuation for this study:

- Expand the analysis to focus on smaller regions to understand the localized variations in rainfall patterns and trends, considering factors such as topography, land use, and climate variability.
- Further work is recommended for assessing the performance of GPCC to understand the uncertainty of its observations.
- Conduct further research to assess the impacts of changing rainfall patterns on various sectors, such as agriculture, water resources, environment, and socio-economic conditions, to inform adaptation strategies.
- Explore the attribution of the observed changes in historical rainfall trends to natural variability versus human-induced climate change, using advanced statistical methods and climate models.
- Encourage collaboration and data sharing among researchers, meteorological agencies, and policymakers within the ENB to enhance the availability and accessibility of rainfall data for research and decision-making purposes.

## 7 References List

- Abd Elhamid, A. M. I., Eltahan, A. M. H., Mohamed, L. M. E., & Hamouda, I. A. (2020). Assessment of the two satellite-based precipitation products TRMM and RFE rainfall records using ground based measurements. *Alexandria Engineering Journal*, 59(2), 1049–1058. <https://doi.org/10.1016/j.aej.2020.03.035>
- Abd Ellah, R. G. (2020). Water resources in Egypt and their challenges, Lake Nasser case study. *Egyptian Journal of Aquatic Research*, 46(1), 1–12. <https://doi.org/10.1016/j.ejar.2020.03.001>
- Abdelmoneim, H., Soliman, M. R., & Moghazy, H. M. (2020). Evaluation of TRMM 3B42V7 and CHIRPS Satellite Precipitation Products as an Input for Hydrological Model over Eastern Nile Basin. *Earth Systems and Environment*, 4(4), 685–698. <https://doi.org/10.1007/s41748-020-00185-3>
- Abdelwares, M., Lelieveld, J., Zittis, G., Haggag, M., & Wagdy, A. (2020). A comparison of gridded datasets of precipitation and temperature over the Eastern Nile Basin region. *Euro-Mediterranean Journal for Environmental Integration*, 5(1), 1–16. <https://doi.org/10.1007/s41207-019-0140-y>
- Adler, R. F., Huffman, G. J., Chang, A., Ferraro, R., Xie, P. P., Janowiak, J., Rudolf, B., Schneider, U., Curtis, S., Bolvin, D., Gruber, A., Susskind, J., Arkin, P., & Nelkin, E. (2003). The version-2 global precipitation climatology project (GPCP) monthly precipitation analysis (1979-present). *Journal of Hydrometeorology*, 4(6), 1147–1167. [https://doi.org/10.1175/1525-7541\(2003\)004<1147:TVGPCP>2.0.CO;2](https://doi.org/10.1175/1525-7541(2003)004<1147:TVGPCP>2.0.CO;2)
- Ahrens, B. (2006). *Distance in spatial interpolation of daily rain gauge data*. 2005, 197–208.
- Amada, A. H., Rakawa, O. A., & Atagai, A. Y. (2015). *An Automated Quality Control Method for Daily Rain-gauge Data*. December 2011.
- Arsano, Y., & Tamrat, I. (2005). Ethiopia and the Eastern Nile Basin. *Aquatic Sciences*, 67(1), 15–27. <https://doi.org/10.1007/s00027-004-0766-x>
- Asfaw, A., Simane, B., Hassen, A., & Bantider, A. (2018). Variability and time series trend analysis of rainfall and temperature in northcentral Ethiopia: A case study in Woleka sub-basin. *Weather and Climate Extremes*, 19(June 2017), 29–41. <https://doi.org/10.1016/j.wace.2017.12.002>
- Awange, J. L., Ferreira, V. G., Forootan, E., Khandu, Andam-Akorful, S. A., Agutu, N. O., & He, X. F. (2016). Uncertainties in remotely sensed precipitation data over Africa. *International Journal of Climatology*, 36(1), 303–323. <https://doi.org/10.1002/joc.4346>

- Awulachew, S. B., McCartney, M., Steenhuis, T. S., & Ahmed, A. A. (2009). *A review of hydrology, sediment and water resource use in the Blue Nile Basin*.
- Ayehu, G. T., Tadesse, T., Gessesse, B., & Dinku, T. (2018). Validation of new satellite rainfall products over the Upper Blue Nile Basin, Ethiopia. *Atmospheric Measurement Techniques*, 11(4), 1921–1936. <https://doi.org/10.5194/amt-11-1921-2018>
- Basheer, M., & Elagib, N. A. (2019). Performance of satellite-based and GPCC 7.0 rainfall products in an extremely data-scarce country in the Nile Basin. *Atmospheric Research*, 215, 128–140. <https://doi.org/10.1016/j.atmosres.2018.08.028>
- Becker, A., Finger, P., Meyer-Christoffer, A., Rudolf, B., Schamm, K., Schneider, U., & Ziese, M. (2013). A description of the global land-surface precipitation data products of the Global Precipitation Climatology Centre with sample applications including centennial (trend) analysis from 1901-present. *Earth System Science Data*, 5(1), 71–99. <https://doi.org/10.5194/essd-5-71-2013>
- Belay zerga, Getaneh, G. (2016). Climate Change in Ethiopia Variability, Impact, Mitigation, and Adaptation. *Journal of Social Science and Humanities Research* 1., 2(4), 66–84. <https://doi.org/10.13140/RG.2.2.16782.46408>
- Belete, M., Deng, J., Wang, K., Zhou, M., Zhu, E., Shifaw, E., & Bayissa, Y. (2020). Evaluation of satellite rainfall products for modeling water yield over the source region of Blue Nile Basin. *Science of the Total Environment*, 708, 134834. <https://doi.org/10.1016/j.scitotenv.2019.134834>
- Beyene, T., Lettenmaier, D. P., & Kabat, P. (2010). Hydrologic impacts of climate change on the Nile River Basin: Implications of the 2007 IPCC scenarios. *Climatic Change*, 100(3), 433–461. <https://doi.org/10.1007/s10584-009-9693-0>
- Branisavljevi, N., Prodanovi, D., Arsi, M., Simi, Z., & Borota, J. (2009). *Hydro-Meteorological Data Quality Assurance and Improvement*. 3(1), 228–249.
- Brunetti, M., Maugeri, M., Monti, F., & Nanni, T. (2006). *TEMPERATURE AND PRECIPITATION VARIABILITY IN ITALY IN THE LAST TWO CENTURIES FROM HOMOGENISED INSTRUMENTAL TIME*. 381(January), 345–381. <https://doi.org/10.1002/joc.1251>
- Cattani, E., Merino, A., & Levizzani, V. (2016). Evaluation of monthly satellite-derived precipitation products over East Africa. *Journal of Hydrometeorology*, 17(10), 2555–2573. <https://doi.org/10.1175/JHM-D-15-0042.1>
- Chinasho, A., Bedadi, B., Lemma, T., Tana, T., Hordofa, T., & Elias, B. (2021). *Evaluation of Seven Gap-Filling Techniques for Daily Station-Based Rainfall Datasets in South Ethiopia*. 2021.

- Climate, A., & Centre, P. (n.d.). *Assessment of Africa 's Climatic Records and Recording Networks Including Strategic for Rescuing of Climatic Data United Nations Economic Commission for Africa*.
- Conway, D. (2005). From headwater tributaries to international river: Observing and adapting to climate variability and change in the Nile basin. *Global Environmental Change*, 15(2), 99–114. <https://doi.org/10.1016/j.gloenvcha.2005.01.003>
- Cooper, P. J. M., & Coe, R. (2011). Assessing and addressing climate-induced risk in sub-Saharan rainfed agriculture. *Experimental Agriculture*, 47(2), 179–184. <https://doi.org/10.1017/S0014479711000019>
- Dee, D. P., Uppala, S. M., Simmons, A. J., Berrisford, P., Poli, P., Kobayashi, S., Andrae, U., Balmaseda, M. A., Balsamo, G., Bauer, P., Bechtold, P., Beljaars, A. C. M., van de Berg, L., Bidlot, J., Bormann, N., Delsol, C., Dragani, R., Fuentes, M., Geer, A. J., ... Vitart, F. (2011). The ERA-Interim reanalysis: Configuration and performance of the data assimilation system. *Quarterly Journal of the Royal Meteorological Society*, 137(656), 553–597. <https://doi.org/10.1002/qj.828>
- Devi, U., Shekhar, M. S., Singh, G. P., Rao, N. N., & Bhatt, U. S. (n.d.). *Methodological application of Quantile Mapping to generate precipitation data over Northwest Himalaya*. 0–2. <https://doi.org/10.1002/joc.6008>
- Dinku, T. (2019). *Challenges with availability and quality of climate data in Africa*. January. <https://doi.org/10.1016/B978-0-12-815998-9.00007-5>
- Dinku, T., Ceccato, P., & Connor, S. J. (2011). Challenges of satellite rainfall estimation over mountainous and arid parts of east africa. *International Journal of Remote Sensing*, 32(21), 5965–5979. <https://doi.org/10.1080/01431161.2010.499381>
- Di Baldassarre, G., Elshamy, M., van Griensven, A., Soliman, E., Kigobe, M., Ndomba, P., ... & Uhlenbrook, S. (2011). *Future hydrology and climate in the river Nile basin: a review*. *Hydrological Sciences Journal–Journal des Sciences Hydrologiques*, 56(2), 199–211.
- Eastern Nile Technical Regional Office (2006). *Project Preparation: Flood Preparedness and Early Warning, Technical Background Paper. Volume 1: Main Report. ENTRO*.
- Edoardo B.; Claire C.; Nicolas S. G.; Osei Kwadwo, Victor O. K. (2023). *Rising from the Depths: Water Security and Fragility in South Sudan*. © Washington, DC: World Bank. <http://hdl.handle.net/10986/38379> License: CC BY 3.0 IGO.”
- Edossa, A., Bekele, A., & Debella, H. J. (2021). *Diet preferences of common warthogs (Phacochoerus africanus) in Gassi and Haro Aba Diko controlled hunting areas, Western*

- Ethiopia*. *Global Ecology and Conservation*, 29, e01722.
- El-Sayed, E., Ragab, M., Abd El-Ati, a., & Fawzy, S. (2022). The Economic Impacts of Drought Mitigation Mechanisms in the Northwestern Coast of Egypt. *المجلة المصرية للاقتصاد الزراعي*, 440–420 ,(2)32. <https://doi.org/10.21608/meae.2022.136912.1054>
- El-sheikh, M., Saleh, H., Mostafa, H., & Kheireldin, K. (2017). The Nile Flow Changes regarding the Expected Changes of Climate. *Ninth Conference of Sustainable Environmental Development, April*.
- El-Tom Hamad, O., & El-Battahani, A. (2005). Sudan and the Nile Basin. *Aquatic Sciences*, 67(1), 28–41. <https://doi.org/10.1007/s00027-004-0767-9>
- Elshamy, M. E., Seierstad, I. A., & Sorteberg, A. (2009). Impacts of climate change on Blue Nile flows using bias-corrected GCM scenarios. *Hydrology and Earth System Sciences*, 13(5), 551–565. <https://doi.org/10.5194/hess-13-551-2009>
- Estévez, J., Llabrés, A., Carmen, B. M., Castillo, C., Penélope, A., Marín, G., Kirchner, R., & Rodríguez, R. (2022). A quality control procedure for long - term series of daily precipitation data in a semiarid environment. *Theoretical and Applied Climatology*, 1029–1041. <https://doi.org/10.1007/s00704-022-04089-2>
- Fadhilah, N., Radi, A., Zakaria, R., & Azman, M. A. Bin. (2015). *Estimation of missing rainfall data using spatial interpolation and imputation methods*. February. <https://doi.org/10.1063/1.4907423>
- Feidas, H., Lagouvardos, K., Kotroni, V., & Cartalis, C. (2005). Application of three satellite techniques in support of precipitation forecasts of a NWP model. *International Journal of Remote Sensing*, 26(24), 5393–5417. <https://doi.org/10.1080/01431160500273551>
- Gehne, M., Hamill, T. M., Kiladis, G. N., & Trenberth, K. E. (2016). Comparison of global precipitation estimates across a range of temporal and spatial scales. *Journal of Climate*, 29(21), 7773–7795. <https://doi.org/10.1175/JCLI-D-15-0618.1>
- Habib, E., Elsaadani, M., & Haile, A. T. (2012). Climatology-Focused evaluation of CMORPH and TMPA satellite rainfall products over the Nile Basin. *Journal of Applied Meteorology and Climatology*, 51(12), 2105–2121. <https://doi.org/10.1175/JAMC-D-11-0252.1>
- Habib, E., Haile, A. T., Tian, Y., & Joyce, R. J. (2012). Evaluation of the high-resolution CMORPH satellite rainfall product using dense rain gauge observations and radar-based estimates. *Journal of Hydrometeorology*, 13(6), 1784–1798. <https://doi.org/10.1175/JHM-D-12-017.1>
- Hamouda, M. A., Nour El-Din, M. M., & Moursy, F. I. (2009). Vulnerability assessment of water resources systems in the Eastern Nile Basin. *Water Resources Management*, 23(13), 2697–

2725. <https://doi.org/10.1007/s11269-009-9404-7>

Harris, I., Osborn, T. J., Jones, P., & Lister, D. (2020). Version 4 of the CRU TS monthly high-resolution gridded multivariate climate dataset. *Scientific Data*, 7(1), 1–18. <https://doi.org/10.1038/s41597-020-0453-3>

Herold, N., Behrangi, A., & Alexander, L. V. (2017). Large uncertainties in observed daily precipitation extremes over land. *Journal of Geophysical Research*, 122(2), 668–681. <https://doi.org/10.1002/2016JD025842>

Huffman, G. J., Adler, R. F., Morrissey, M. M., Bolvin, D. T., Curtis, S., Joyce, R., McGavock, B., & Susskind, J. (2001). Global precipitation at one-degree daily resolution from multisatellite observations. *Journal of Hydrometeorology*, 2(1), 36–50. [https://doi.org/10.1175/1525-7541\(2001\)002<0036:GPAODD>2.0.CO;2](https://doi.org/10.1175/1525-7541(2001)002<0036:GPAODD>2.0.CO;2)

Informatics, E., Informatics, E., & Informatics, E. (2017). *Multidecadal Trends and Interannual Variability of Rainfall as Observed from Five Lowland Stations at Mt. Kilimanjaro, Tanzania*. 349–361. <https://doi.org/10.1175/JHM-D-16-0062.1>

J A du Plessis, J. K. K. (2021). *Applicability of CHIRPS - based satellite rainfall estimates for South Africa*. 63(3), 43–54.

Kashani, M. H., & Dinpashoh, Y. (2014). *Evaluation of efficiency of different estimation methods for missing climatological data*. January 2011. <https://doi.org/10.1007/s00477-011-0536-y>

Katsanos, D., Retalis, A., & Michaelides, S. (2016). Validation of a high-resolution precipitation database (CHIRPS) over Cyprus for a 30-year period. *Atmospheric Research*, 169, 459–464. <https://doi.org/10.1016/j.atmosres.2015.05.015>

Kidd, C., & Huffman, G. (2011). Global precipitation measurement. *Meteorological Applications*, 18(3), 334–353. <https://doi.org/10.1002/met.284>

Kim, U., & Kaluarachchi, J. J. (2009). Climate change impacts on water resources in the upper Blue Nile River Basin, Ethiopia. *Journal of the American Water Resources Association*, 45(6), 1361–1378. <https://doi.org/10.1111/j.1752-1688.2009.00369.x>

Kimani, M. W., Hoedjes, J. C. B., & Su, Z. (2017). An assessment of satellite-derived rainfall products relative to ground observations over East Africa. *Remote Sensing*, 9(5), 1–21. <https://doi.org/10.3390/rs9050430>

Lakew, H. B., Moges, S. A., & Asfaw, D. H. (2020). Hydrological performance evaluation of multiple satellite precipitation products in the upper Blue Nile basin, Ethiopia. *Journal of Hydrology: Regional Studies*, 27(January), 100664. <https://doi.org/10.1016/j.ejrh.2020.100664>

- Le, M. (2020). *SF Journal of Environmental and Earth Science Techniques of Filling Missing Values of Daily and Monthly Rain Fall Data : A Review*.
- Liu, Z., Ostrenga, D., Teng, W., & Kempler, S. (2012). Tropical rainfall measuring mission (TRMM) precipitation data and services for research and applications. *Bulletin of the American Meteorological Society*, 93(9), 1317–1325. <https://doi.org/10.1175/BAMS-D-11-00152.1>
- Longobardi, A., & Villani, P. (2010). *Trend analysis of annual and seasonal rainfall time series in the Mediterranean area*. 1546(August 2009), 1538–1546. <https://doi.org/10.1002/joc.2001>
- Letcher, T. (Ed.). (2021). *Climate change: observed impacts on planet Earth*.
- Mekawi, A. (2010). *Flood propagation of the Blue Nile in he Sudan using Muskingum routing*. Nile Basin Water Science & Engineering Journal, 3(1), 39-50.
- Merid, F. (2005). *National Nile Basin water quality monitoring baseline report for Ethiopia*. Nile Basin Initiative Transboundary Environmental Action Project, Accessed online February 30, 2006.
- Mohamed, M. A., El Afandi, G. S., & El-Mahdy, M. E. S. (2022). *Impact of climate change on rainfall variability in the Blue Nile basin*. Alexandria Engineering Journal, 61(4), 3265-3275.
- Mohamed, M.A., El Afandi, G.S. and El-Mahdy, M.E.S., 2022. *Impact of climate change on rainfall variability in the Blue Nile basin*. Alexandria Engineering Journal, 61(4), pp.3265-3275.
- Mojwok, O. M, (2013) *the current status, functions, challenges and needs of South Sudan Meteorological Department (SSMD), Juba*.
- Macharia, D., Fankhauser, K., Selker, J. S., Neff, J. C., & Thomas, E. A. (2022). Validation and Intercomparison of Satellite-Based Rainfall Products over Africa with TAHMO In Situ Rainfall Observations. *Journal of Hydrometeorology*, 23(7), 1131–1154. <https://doi.org/10.1175/JHM-D-21-0161.1>
- Michelson, D. B. (2004). Systematic correction of precipitation gauge observations using analyzed meteorological variables. *Journal of Hydrology*, 290(3–4), 161–177. <https://doi.org/10.1016/j.jhydrol.2003.10.005>
- Mohamed, M. A., El Afandi, G. S., & El-Mahdy, M. E. S. (2022). *Impact of climate change on rainfall variability in the Blue Nile basin*. Alexandria Engineering Journal, 61(4), 3265–3275. <https://doi.org/10.1016/j.aej.2021.08.056>
- Nashwan, M. S., Shahid, S., Dewan, A., Ismail, T., & Alias, N. (2020). Performance of five high resolution satellite-based precipitation products in arid region of Egypt: An evaluation. *Atmospheric Research*, 236, 104809. <https://doi.org/10.1016/j.atmosres.2019.104809>

- Nashwan, M. S., Shahid, S., & Wang, X. (2019). Assessment of satellite-based precipitation measurement products over the hot desert climate of Egypt. *Remote Sensing*, *11*(5). <https://doi.org/10.3390/rs11050555>
- Novella, N. S., & Thiaw, W. M. (2013). African rainfall climatology version 2 for famine early warning systems. *Journal of Applied Meteorology and Climatology*, *52*(3), 588–606. <https://doi.org/10.1175/JAMC-D-11-0238.1>
- Onyutha, C., Tabari, H., Taye, M. T., Nyandwaro, G. N., & Willems, P. (2016). Analyses of rainfall trends in the Nile River Basin. *Journal of Hydro-Environment Research*, *13*, 36–51. <https://doi.org/10.1016/j.jher.2015.09.002>
- Onyutha, C., & Willems, P. (2015). Spatial and temporal variability of rainfall in the Nile Basin. *Hydrology and Earth System Sciences*, *19*(5), 2227–2246. <https://doi.org/10.5194/hess-19-2227-2015>
- Pfeifroth, U., Mueller, R., & Ahrens, B. (2013). Evaluation of satellite-based and reanalysis precipitation data in the tropical pacific. *Journal of Applied Meteorology and Climatology*, *52*(3), 634–644. <https://doi.org/10.1175/JAMC-D-12-049.1>
- Precipitation, D., & Series, T. (2020). *A Quantile Mapping Method to Fill in Discontinued Daily Precipitation Time Series*. 1–13.
- Sarojini, B. B., Stott, P. A., & Black, E. (2016). Detection and attribution of human influence on regional precipitation. *Nature Climate Change*, *6*(7), 669–675. <https://doi.org/10.1038/nclimate2976>
- Setegn, S. G., Rayner, D., Melesse, A. M., Dargahi, B., & Srinivasan, R. (2011). Impact of climate change on the hydroclimatology of Lake Tana Basin, Ethiopia. *Water Resources Research*, *47*(4), 1–13. <https://doi.org/10.1029/2010WR009248>
- Soliman, Eman S.A.; Sayed, M.A.; Jeuland, M. (2009). *Impact Assessment of Future Climate Change for the Blue Nile Basin, Using a RCM Nested in a GCM*. 369(1), 1689–1699. <http://dx.doi.org/10.1016/j.jsames.2011.03.003><https://doi.org/10.1016/j.gr.2017.08.001><http://dx.doi.org/10.1016/j.precamres.2014.12.018><http://dx.doi.org/10.1016/j.precamres.2011.08.005><http://dx.doi.org/10.1080/00206814.2014.902757><http://dx.doi.org/10.1016/j.jher.2015.09.002>
- Sun, Q., Miao, C., Duan, Q., Ashouri, H., Sorooshian, S., & Hsu, K. L. (2018). A Review of Global Precipitation Data Sets: Data Sources, Estimation, and Intercomparisons. *Reviews of Geophysics*, *56*(1), 79–107. <https://doi.org/10.1002/2017RG000574>
- Taye, M. T., & Willems, P. (2012). Temporal variability of hydroclimatic extremes in the Blue Nile

- basin. *Water Resources Research*, 48(3), 1–13. <https://doi.org/10.1029/2011WR011466>
- Uppala, S. M., Kållberg, P. W., Simmons, A. J., Andrae, U., da Costa Bechtold, V., Fiorino, M., Gibson, J. K., Haseler, J., Hernandez, A., Kelly, G. A., Li, X., Onogi, K., Saarinen, S., Sokka, N., Allan, R. P., Andersson, E., Arpe, K., Balmaseda, M. A., Beljaars, A. C. M., ... Woollen, J. (2005). The ERA-40 re-analysis. *Quarterly Journal of the Royal Meteorological Society*, 131(612), 2961–3012. <https://doi.org/10.1256/qj.04.176>
- Vejen, F., Jacobsson, C., & Fredriksson, U. (2002). *Quality Control of*.
- WMO. (2021). *Guidelines on Surface Station Data Quality Control and Quality Assurance for Climate Applications 2021* (Issue 1269).
- Yitayew, M., & Melesse, A. M. (2011). Nile River Basin. *Nile River Basin, January 2011*. <https://doi.org/10.1007/978-94-007-0689-7>
- Zainuri, N. A., & Muda, N. (2015). *A Comparison of Various Imputation Methods for Missing Values in Air Quality Data A Comparison of Various Imputation Methods for Missing Values in Air Quality Data*. June.
- Zhang, Q., Körnich, H., & Holmgren, K. (2013). How well do reanalyses represent the southern African precipitation? *Climate Dynamics*, 40(3–4), 951–962. <https://doi.org/10.1007/s00382-012-1423-z>
- Zhenyun, H., Hu, Q., Zhang, C., & Qingxiang, L. (2016). Evaluation of reanalysis, spatially interpolated and satellite remotely sensed precipitation data sets in central Asia. *Journal of Geophysical Research Atmospheres*, 121(June), 5648–5663. <https://doi.org/10.1002/2016JD024781>.Received